PHUGOID DAMPING CONTROL

THESIS

Nicolas J. Schindeler, Lieutenant, USAF

AFIT/GE/ENG/01M-19

DEPARTMENT OF THE AIR FORCE
AIR UNIVERSITY

AIR FORCE INSTITUTE OF TECHNOLOGY

Wright-Patterson Air Force Base, Ohio

The views expressed in this thesis are those of the author and do not reflect the official policy or position of the United States Air Force, Department of Defense, or the U. S. Government.

AFIT/GE/ENG/01M-19

PHUGOID DAMPING CONTROL

THESIS

Presented to the Faculty

Department of Electrical and Computer Engineering

Graduate School of Engineering and Management

Air Force Institute of Technology

Air University

Air Education and Training Command

In Partial Fulfillment of the Requirements for the

Degree of Master of Science in Electrical Engineering

Nicolas J. Schindeler, B.S.E.E.

Lieutenant, USAF

March 2001

AFIT/GE/ENG/01M-19

PHUGOID DAMPING CONTROL

Nicolas J. Schindeler, B.S.E.E.
Lieutenant, USAF

Approved:

M. Pachter	6 March, 2001
Meir Pachter (Chairman)	Date
Peter S. Maybeck	6 Mar 2001
Peter S. Maybeck (Member)	Date
David R. Jacques	6 MAR 0
David R. Jacques (Member)	Date
Juan R. Vasquez	6 Mar 01
Juan R. Vasquez (Member)	Date

ACKNOWLEDGMENTS

I would like to express my sincere appreciation to my faculty advisor, Dr. Meir Pachter, for his guidance and support throughout the course of this thesis effort. His insight and experience is certainly appreciated. I feel fortunate to have chosen him as an advisor.

I would also like to thank the members of my thesis committee for their work proofreading and suggesting improvements in this thesis. Their judgment and comments were valuable in improving the research effort.

Thanks must also be extended to my wife for her version of steadfast support: recurrent kicks to the posterior. Sometimes such things actually work.

Finally, thanks to classmates Daryl Burnette and Thao Nguyen for the support throughout the AFIT experience. Yes, Thao, you are the man.

Nicolas J. Schindeler

TABLE OF CONTENTS

LIST OF FIGURES

Page

LIST OF TABLES

Page

ABSTRACT

A novel phugoid damping control design methodology is developed, based on the use of wind axes and a point-mass aircraft model. The state variables are air speed, flight path angle, and heading angle, the control variables are thrust setting, angle of attack, bank angle, and sideslip angle, and the command signals are airspeed, flight path angle, and heading angle or heading rate. All the variables and parameters are nondimensionalized. A multivariable set point controller is developed which consists of: (i) a trim calculation-based nonlinear feed-forward control computer; thus, given a commanded new trim state (air speed, flight path angle, and yaw rate), the required trim thrust setting and trim angle of attack, bank angle, and sideslip angle inputs are determined, and, (ii) a small signal linear feedback regulator; the equations of motion linearized about the trim condition of wings level, and constant altitude flight, which simplifies the dynamics to allow separation between the lateral and longitudinal control channels, are used, and a small-signal linear multivariable regulator is designed. The linear compensator also entails integral action. Thus, the controller consists of a strongly nonlinear feed-forward module and a linear small signal compensator. The novel proposed multivariable nonlinear set point controller encompasses full three-axes autopilot functions. Moreover, this controller is used as a tracking controller, a.k.a. a "phugoid damping" controller, provided that the bandwidth of the command signal is substantially less than the bandwidth of the closed loop flight control system. The phugoid damping controller's performance is examined in extensive simulations and its wide operational envelope is demonstrated.

NOMENCLATURE

a_T	Tail Lift Curve Slope
a_W	Wing Lift Curve Slope
AR	Aspect Ratio
b	Wing Span
C_D	Drag Coefficient
C_L	Lift Coefficient
C_{D0}	Zero-Lift Drag Coefficient
D	Drag
e	Error Signal
f_s	Sampling Frequency
F	Side Force
g	Acceleration of Gravity
K	Parabolic Drag Polar Constant
K_I	Controller Gain Matrix – Integral Part
K_P	Controller Gain Matrix – Proportional Part
$K_{\bullet,\bullet}$	Controller Gain
L	Lift
m	Mass
$\overline{q}$	Dynamic Pressure
S_T	Vertical Tail Surface Area
S_W	Wing Surface Area
t	Time
t_s	Settling Time
T	Thrust
V	Velocity
z	Integrator Charge
α	Angle of Attack
β	Sideslip Angle
γ	Flight Path Angle
ρ	Air Density
τ	Directional Control Channel's Time Constant (specified)
μ	Thrust (Normalized)
ϕ	Bank Angle
ϕ_D	Disturbance Bank Angle
ψ	Heading Angle
$\overline{\omega}$	Yaw Rate at Trim
ω_n	Phugoid Natural Frequency
ω_{n_L}	Lateral Control Channel's Natural Frequency (Specified)
ω_{n_P}	Longitudinal Control Channel's Natural Frequency (Specified)
ξ	Phugoid Damping Ratio

ξ_L Lateral Control Channel's Damping Ratio (Specified)

ξ_P Longitudinal Control Channel's Damping Ratio (Specified)

PHUGOID DAMPING CONTROL

1. INTRODUCTION

Phugoid damping control entails the design of compensators for the control of the aircraft's slow states. Thus, in the pitch channel, one controls the airspeed and flight path angle. In the directional channel, the heading angle is controlled. When one's attention is confined to the regulation function, one then refers to autopilots, viz., altitude-hold, Mach-hold, and heading-hold autopilots. Traditionally, automatic pilots have been used extensively in missiles and in aircraft to decrease pilot workload and improve flight safety. It is envisioned that, in the future, complex outer-loop flight control systems will be used increasingly in the control of emerging Uninhabited Combat Air Vehicles (UCAVs). Thus, the challenge is to increase the operational envelope of autopilots, and also increase the bandwidth of the command signals that outer-loop tracking controllers, a.k.a. "phugoid damping" controllers, can successfully handle, thus endowing UCAVs with high performance autonomous flight control systems.

Model based control design is standard practice in aerospace. Conventional autopilot design, as espoused e.g., in [1], is almost exclusively based on a linear plant model derived from a linearization of the 6 DOF (Degrees Of Freedom) aircraft equations of motion. One acknowledges the inherently slow time scale of the autopilot controlled variables by using a nested control loop structure. The inner loops consist of the SAS (Stability Augmentation System) and CAS (Control Augmentation System), whereas the autopilot is relegated to the outer loop. Typically, control loops for aircraft control

systems are designed from the "inside out". That is, the first step is the design of an inner-loop stability augmentation system (SAS), including actuator dynamics. From there, the design moves progressively toward more complex outer-loops: control augmentation system (CAS), and altitude/Mach/heading –hold autopilots.

The standard autopilot is a linear compensator, augmented with gain scheduling [3]. Conventional autopilots have performed well over many decades. At the same time, the operational envelope of conventional autopilots is somewhat limited, viz., the linear control design envisages small perturbations in the states, low amplitude set point changes, and slowly varying set point settings. Thus, in World War II, the autopilot controlled V1 cruise missile was downed by RAF pilots by exploiting the V1 autopilot's limited operational envelope. They tipped the V1 over with their wingtips [2,10]. Also, autopilot "upsets" have been reported in recent times [4,6].

In the present paper, the model-based design of the autopilot / outer loop controller hinges on a point-mass model of the aircraft dynamics. The low order dynamics exclusively encompass the states relevant to autopilot design. The "fast" inner loop states are the control variables.

The novel approach to outer-loop controller design pursued in this thesis is as follows: Directly design the outer loop controller employing a low-order, slow-dynamics, albeit nonlinear model. It is hypothesized that such an approach would simplify the outer-loop controller design and help better capture the nonlinear characteristics of the air vehicle. The latter is, in part, conducive to a "full envelope" controller, thus obviating the need for gain scheduling. Although this approach does not

include the "fast" dynamics in the outer-loop controller's design, ensuring that sufficient "phase margin" exists in the outer-loop compensates for this deficiency.

There is reason to believe that ab initio using a low order plant model is the right approach to outer loop controller / autopilot design. Moreover, using the right plant model, a nonlinear, trim solution-based controller naturally suggests itself. Hence, a high quality outer loop controller / autopilot with an expanded operational envelope is realized.

Specifically, in this paper, a novel phugoid damping control design method is developed, based on the use of wind axes and a point-mass aircraft model. The state variables are air speed, flight path angle, and heading angle, the control variables are thrust setting, angle of attack, bank angle, and sideslip angle, and the command (reference) signals are airspeed, flight path angle, and heading angle or heading rate. All variables and parameters are nondimensionalized. A multivariable set point controller is developed which consists of: (i) A trim calculation-based nonlinear feed-forward control computer; thus, given a commanded new trim state (air speed, flight path angle, and yaw rate), the required trim thrust setting, angle of attack, roll angle, and sideslip angle inputs are determined, and, (ii) a small signal linear feedback multivariable regulator. The equations of motion are linearized about the trim condition of wings level, constant altitude flight, which simplifies the dynamics to allow separation between the lateral and longitudinal control channels. The linear compensator also entails integral action. Thus, the controller consists of a strongly nonlinear feed-forward module and a linear small-signal multivariable tracking controller. The novel proposed multivariable set point controller encompasses full three-axes autopilot functions. Moreover, this controller is

used as a tracking controller, provided that the bandwidth of the command signal is substantially less than the bandwidth of the closed-loop flight control system, and we then refer to the phugoid damping controller. It is envisaged that the latter will receive inputs from a higher level supervisory control module, thus affording UCAVs a high degree of control autonomy.

The paper is organized as follows. In Chapter 2, the aircraft model is introduced. The aircraft parameters are representative of an F-16 class aircraft flying at 200 m/s at 20,000 ft, and are given in Table 1. Chapter 2 also introduces the wind axes used in the design, the nonlinear equations of motion, and the nondimensionalization used to simplify the dynamics. The required aircraft trim control settings for a commanded trim state are derived in Chapter 3. In Chapter 4, the equations of motion are linearized about the trim state. These linearized equations of motion and, in particular, the trim condition of wings level, constant altitude flight, with trim speed equal to initial speed, simplify the dynamics and allow decoupling between the lateral and longitudinal control channels. These results are used in Chapter 5 to design small signal linear multivariable regulators for the two control channels. The linear compensators also entail integral action. Thus, the controller consists of a strongly nonlinear feed-forward module and a linear multivariable small-signal compensator. Chapter 6 addresses issues impacting the operational envelope of the controller. The novel multivariable set point controller encompasses full three-axes autopilot functions. Moreover, this controller is used as a dynamic phugoid damping controller, provided that the bandwidth of the command signal is substantially less than the bandwidth of the closed loop flight control system. Chapter 7 presents the results of extensive simulations for the phugoid damping controller's

performance evaluation. The wide operational envelope of the controller is demonstrated. Concluding remarks are made in Chapter 8.

2. WIND AXES AND EQUATIONS OF MOTION

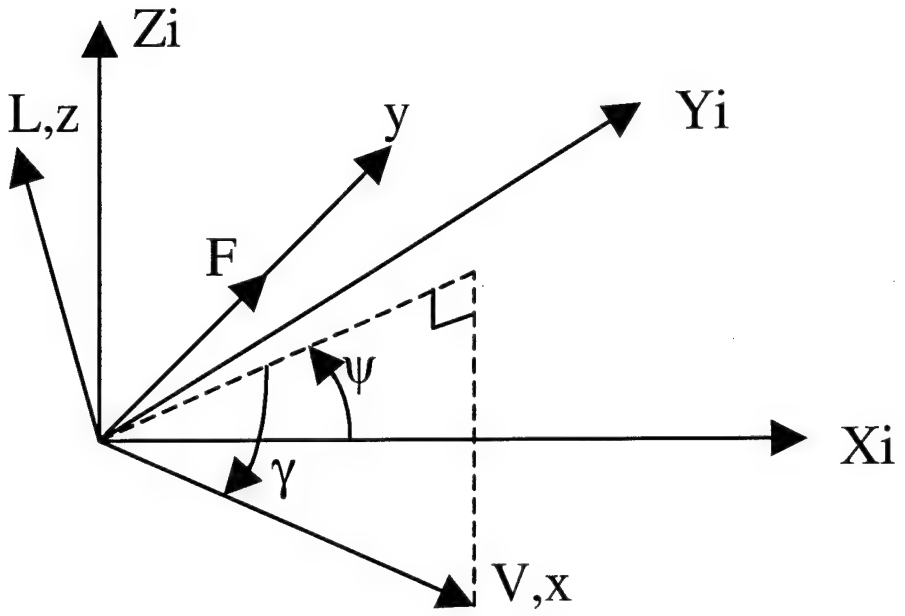

Figure 1: Wind Axes x, y, z

The aircraft's point-mass equations of motion are derived using a translating and rotating frame of reference collocated with the instantaneous position of the aircraft. The rotating frame of reference, shown in Fig. 1, is a triad of wind axes defined as follows: The x-axis is aligned with the aircraft velocity vector, the z-axis is aligned with the lift vector, and the y-axis (out of the wing) completes the right-handed coordinate system. Side force F is defined in the direction of the y-axis. The wind axes frame's attitude is specified by the ψ, γ, and ϕ Euler angles, corresponding to the aircraft "heading", "flight path angle" (in the pitch plane), and "roll angle". For the sake of clarity, the final rotation about the x-axis through the angle ϕ is not explicitly shown in Fig. 1. Also, velocity vector rolls are envisaged, for the roll maneuver is performed about the velocity vector axis.

The three angles ψ, γ, and ϕ are not unlike the Euler angles – they position the wind axes frame x, y, z relative to the inertial frame X_I , Y_I , Z_I . Note, however, that while the heading angle ψ and the flight path angle γ are state variables, the bank angle ϕ is a control variable. Also, note the polarity of the flight path angle γ, as indicated in Figure 1.

2.1. Aerodynamic Angles Definition

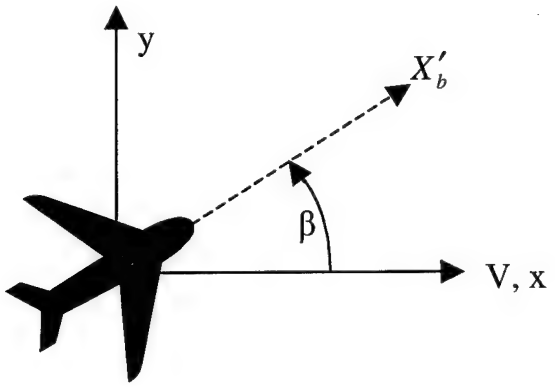

Figure 2: Sideslip Angle Definition

In this paper, wind axes, rather than body axes, are used. However, a discussion of body axes is required to define the aerodynamic angles properly. Thus, the body axes triad (X_b, Y_b, Z_b) is related to the wind axes (x, y, z) as follows: Initially, the body axes are aligned with the wind axes. First, a rotation of β degrees about the z wind axis is performed. This is followed by a rotation of α degrees about the Y_b' body axis. The broken line X_b' in Figure 2 is the projection of the X_b axis onto the (x, y) plane. We note that this definition of aerodynamic angles is not the standard definition used when body axes and rigid body dynamics are used to describe the aircraft's motion. At the same

time, the above-defined aerodynamic angles correspond to the aerodynamic angles used in wind tunnel work.

Note that, although the reference frame rotates as an actual aircraft, the aircraft model is a point mass. Since a point mass model is used, moments are not included in the analysis.

2.2. Equations of Motion

The aircraft dynamic model used in this paper exclusively employs the aircraft's "slow" states and is therefore the "right" model for model based outer-loop controller design, viz., altitude-hold, Mach-hold, and heading-hold autopilot design, and for phugoid damping controller design.

The point mass equations of motion – see, e.g., Fig. 1 and [5] – are:

$$\left.\begin{aligned} \dot{V} &= \frac{T-D}{m} + g\sin\gamma\ , \quad V(0) = V_0 \\ \dot{\gamma} &= -\frac{L\cos\phi + F\sin\phi}{mV} + \frac{g}{V}\cos\gamma\ , \quad \gamma(0) = \gamma_0 \\ \dot{\psi} &= \frac{-L\sin\phi + F\cos\phi}{mV\cos\gamma}\ , \quad \Psi(0) = 0\ , \quad 0 \le t \le t_{max} \end{aligned}\right\} \quad (1)$$

where the forces are:

$$L = \bar{q}\frac{V^2}{V_0^2}S_w a_w \alpha$$

$$T = mg\mu$$

$$D = \bar{q}\frac{V^2}{V_0^2}S_w\left(C_{D0} + Ka_w^2\alpha^2\right)$$

$$F = \bar{q}\frac{V^2}{V_0^2}S_t a_t \beta$$

and where the nominal dynamic pressure is:

$$\bar{q} = \frac{1}{2}\rho \cdot V_0^2$$

and V_0 is the initial velocity.

Nondimensional variables and parameters are introduced as follows:

$$t := \frac{g}{V_0}t$$

$$V := \frac{V}{V_0}$$

$$\bar{\omega} := \frac{V_0}{g}\bar{\omega}$$

$$\bar{q} := \frac{\bar{q}S_W}{m \cdot g}$$

$$\tilde{C}_L \equiv \frac{1}{\bar{q}}$$

$$K := K\tilde{C}_L$$

$$\tilde{\alpha} := \frac{\tilde{C}_L}{a_W}$$

$$\alpha := \frac{\alpha}{\tilde{\alpha}}$$

$$\beta := \frac{1}{\tilde{\alpha}}\left(\frac{S_t}{S_W}\right)\left(\frac{a_t}{a_W}\right)\cdot\beta$$

Similarly, the (barred) trim controls are scaled according to

$$\overline{\alpha} := \frac{\overline{\alpha}}{\tilde{\alpha}}$$

$$\overline{\beta} := \frac{1}{\tilde{\alpha}}\left(\frac{S_t}{S_W}\right)\left(\frac{a_t}{a_W}\right)\cdot\overline{\beta}$$

Remark For constant altitude and wings level flight, the trim lift coefficient $\overline{C}_L = \tilde{C}_L$. Hence, the trim lift-over-drag ratio is given by:

$$\frac{\overline{C}_L}{\overline{C}_D} = \frac{1}{C_{D0}\overline{q} + K}$$

The pertinent aircraft parameters are given in Table 1.

Table 1: Aircraft Parameter Values

Wing Lift Curve Slope	a_W	5.3	/rad
Tail Lift Curve Slope	a_T	5.3	/rad
Wing Aspect Ratio	AR	3	-
Wing Span	b	9.14	m
Zero-Lift Drag Coefficient	C_{D0}	0.015	-
Acceleration of Gravity	g	9.81	m/sec^2
Parabolic Drag Polar Constant	K	0.1118	-
Mass	m	11,336.4	kg
Dynamic Pressure	$\overline{q}$	12500	$kg/(m\cdot s^2)$
Wing Surface Area	S_W	27.87	m^2
Tail Surface Area	S_T	5.086	m^2
Initial Velocity	V_0	200	m/sec
Efficiency Factor	η	0.95	-
Atmospheric Density (@ 20,000')	ρ	5/8	kg/m^3

The nondimensional parameters and variables are given in Table 2.

Table 2: Nondimensional Parameters and Variables

	Actual	*Nondimensional*
$\tilde{C}_L$	-	0.319
$\overline{C}_L / \overline{C}_D$	-	12.1
K	0.112	0.0357
$\overline{q}$	12,500 [kg/(m·s^2)]	3.13
t	t [s]	0.0491·t
V	V [m/s]	0.05·V
α	α	16.6·α
$\tilde{\alpha}$	-	0.0602
β	β	3.03·β
$\overline{\omega}$	$\overline{\omega}$ [s^{-1}]	20.4·$\overline{\omega}$
ω_n	0.0694 [s^{-1}]	$\sqrt{2}$

Using the above parameterization in Eqs. ***(1)***, the elegant nondimensional aircraft equations of motion are derived:

Nondimensional Equations of Motion

$$\dot{V} = \sin\gamma - \overline{q}C_{D0}V^2 + \mu - KV^2\alpha^2 \ , \ V(0) = 1 \qquad \textit{(2)}$$

$$\dot{\gamma} = \frac{\cos\gamma}{V} - V(\alpha\cos\phi + \beta\sin\phi) \ , \ \gamma(0) = \gamma_0 \qquad \textit{(3)}$$

$$\dot{\psi} = \frac{V}{\cos\gamma}(-\alpha\sin\phi + \beta\cos\phi) \ , \ \psi(0) = 0 \ , \ 0 \le t \le t_{max} \ . \qquad \textit{(4)}$$

The two parameters in the equations of motion ***(2)*** - ***(4)*** are $(\overline{q}C_{D0})$ and K, where, for the flight condition considered in the research, the numerical values are $\overline{q}C_{D0} = 0.04695$ and K = 0.0357.

2.3. Chapter Summary

This chapter introduced the wind axes used to derive the aircraft's point-mass equations of motion. This is a rotating frame of reference collocated with the aircraft's

center of gravity (CG). The aerodynamic angles used in the research were defined, relating the wind axes to the inertial and the body axes. The aircraft parameters and variables were introduced, followed by the fundamental equations of motion and a series of nondimensionalizing variable and parameter definitions. These were used to derive the nondimensional equations of motion used in the rest of this thesis.

3. AIRCRAFT TRIM EQUATIONS

The equations of motion reported in the previous chapter define velocity V, flight path angle γ, and heading ψ in terms of thrust setting μ, angle of attack α, bank angle ϕ, and sideslip angle β. In this research, (V, γ, ψ) will be designated as states, controlled by the control variables $(\mu, \alpha, \phi, \beta)$. In order to use these control variables to bring about a desired state, it is necessary to know to what values the control variables should be set. However, as the task of back-solving a set of nonlinear differential equations to obtain inputs for completely arbitrary outputs is a daunting one, some simplification is in order.

The control system will be based around the idea that steady-state, or "trim", states are the desired conditions. This is useful in making the mathematics tenable because it forces the state derivatives to equal zero, changing the nonlinear differential equations into nonlinear equations.

Two trim states will be evaluated. The first, "Trim 1", is the simplest. It requires setting the derivatives of all three state variables to zero. Thus, the aircraft flies at constant speed, at constant flight path angle, and at constant heading. The second trim state, "Trim 2", is similar, but the heading is allowed to change at a constant rate. This allows the aircraft to come to a trim state in which it is maintaining a turn.

3.1. Trim 1

New values for trim states $\overline{\Psi}$, $\overline{\gamma}$, $\overline{V}$ are commanded, and the corresponding new trim control settings are $\overline{\alpha}$, $\overline{\mu}$, $\overline{\phi}$, $\overline{\beta}$.

Setting the LHS of the differential equations **(2)** - **(4)** equal to zero yields the algebraic trim equations. The latter are solved, yielding the trim control settings.

First, note that eq. **(4)** yields

$$\tan\bar{\phi} = \frac{\bar{\beta}}{\bar{\alpha}} \tag{5}$$

and, therefore, inserting eq. **(5)** into eq. **(3)** yields

$$\bar{\alpha} = \frac{1}{\bar{V}^2}\cos\bar{\gamma}\cdot\cos\bar{\phi}\,, \tag{6}$$

Next, inserting eq. **(6)** into eq. **(2)** yields

$$\bar{\mu} = \bar{q}C_{D0}\bar{V}^2 - \sin\bar{\gamma} + \frac{K}{\bar{V}^2}\cos^2\bar{\gamma}\cdot\cos^2\bar{\phi}$$

Finally, combining eq. **(5)** and **(6)**, we calculate

$$\left.\begin{aligned}
&\sin\bar{\phi} = \bar{V}^2\frac{\bar{\beta}}{\cos\bar{\gamma}}\\
&\cos\bar{\phi} = \sqrt{1-\left(\frac{\bar{V}^2\bar{\beta}}{\cos\bar{\gamma}}\right)^2}\\
&\bar{\alpha} = \sqrt{\left(\frac{\cos\bar{\gamma}}{\bar{V}^2}\right)^2 - \bar{\beta}^2}\\
&\bar{\mu} = \bar{q}C_{D0}\bar{V}^2 + \frac{K}{\bar{V}^2}\cos^2\bar{\gamma} - \sin\bar{\gamma} - K\bar{\beta}^2\bar{V}^2
\end{aligned}\right\} \tag{7}$$

In short, given that

- The new states $\bar{\Psi}$, $\bar{\gamma}$, $\bar{V}$ are specified.
- The control $\bar{\beta}$ is chosen arbitrarily

➔ The controls $\bar{\mu}$, $\bar{\alpha}$, $\bar{\phi}$, are given in Eqs. **(7)**.

Special case (a): If we set $\bar{\beta} = 0$ (no sideslip), then

$$\left.\begin{aligned} \bar{\phi} &= 0 \\ \bar{\alpha} &= \frac{\cos\bar{\gamma}}{\bar{V}^2}, \\ \text{and} \\ \bar{\mu} &= \bar{q}C_{D0}\bar{V}^2 + \frac{K}{\bar{V}^2}\cos^2\bar{\gamma} - \sin\bar{\gamma} \end{aligned}\right\} \quad (8)$$

Note: When $\bar{\psi}$ = constant, there is no aerodynamic justification for $\bar{\beta} \neq 0$. However, $\bar{\beta} \neq 0$ might be justified where LO (Low Observables) considerations are important.

Special case (b): If we allow $\bar{\phi}$ to be independently controlled, then

$$\left.\begin{aligned} \bar{\beta} &= \frac{1}{\bar{V}^2}\cos\bar{\gamma}\cdot\sin\bar{\phi} \\ \bar{\alpha} &= \frac{1}{\bar{V}^2}\cos\bar{\gamma}\cdot\cos\bar{\phi} \\ \bar{\mu} &= \bar{q}C_{D0}\bar{V}^2 + \frac{K}{\bar{V}^2}\cos^2\bar{\gamma} - \sin\bar{\gamma} - K\cos\bar{\gamma}\cdot\sin\bar{\phi}^2 \end{aligned}\right\} \quad (9)$$

Special case (c): If, in (b) above, we set $\bar{\phi} = 0$ (no bank), then

$$\bar{\beta} = 0$$

$$\bar{\alpha} = \frac{\cos\bar{\gamma}}{\bar{V}^2}$$

and

$$\bar{\mu} = \bar{q}C_{D0}\bar{V}^2 + \frac{K}{\bar{V}^2}\cos^2\bar{\gamma} - \sin\bar{\gamma}$$

This is exactly the same result as special case (a).

3.2. Trim 2

Now, to expand the set of permissible trim conditions to include constant-rate turns, command new trim values $\psi(t)$, $\overline{\gamma}$, $\overline{V}$. Again, the corresponding trim control settings are $\overline{\alpha}$, $\overline{\mu}$, $\overline{\phi}$, $\overline{\beta}$.

We command new values for the trim state: $\psi(t) = -\overline{\omega} \cdot t$, $\overline{\gamma}$, $\overline{V}$.

Note: Without loss of generality, we now consider a turn to starboard, so that the ensuing trim bank angle $\overline{\phi}$ is positive.

Recall

$$\overline{\omega} := \frac{V_0}{g} \overline{\omega}$$

$$t := \frac{g}{V_0} t$$

Inserting these nondimensionalizing definitions into the previous trim state definition produces the new trim state definitions

$$\psi = -\overline{\omega} \cdot t$$

where both t and $\overline{\omega}$ are nondimensional. The corresponding trim control settings are

$$\overline{\mu}, \overline{\alpha}, \overline{\phi}, \overline{\beta}$$

Here $\overline{\omega} > 0$, viz., without loss of generality, we consider a turn to starboard, so that the ensuing trim bank angle $\overline{\phi} > 0$.

Now, setting the LHS of the differential equations **(3)** and **(4)** equal to 0 yields

$$\left.\begin{aligned} \bar{\alpha}\sin\bar{\phi}-\bar{\beta}\cos\bar{\phi}&=\frac{\bar{\omega}}{\bar{V}}\cos\bar{\gamma}\\ \bar{\alpha}\cos\bar{\phi}+\bar{\beta}\sin\bar{\phi}&=\frac{1}{\bar{V}^2}\cos\bar{\gamma}\end{aligned}\right\} \qquad (10)$$

This is a system of two nonlinear equations in the unknowns $\bar{\alpha}$ and $\bar{\phi}$; in Eqs. **(10)**, $\bar{V}$, $\bar{\beta}$ and $\bar{\gamma}$ are parameters.

We now embark on the solution of the nonlinear system of equations **(10)**. We momentarily consider the linear system in the "unknowns" $\sin\bar{\phi}$ and $\cos\bar{\phi}$. Thus, we have

$$\begin{bmatrix}\bar{\alpha} & -\bar{\beta}\\ \bar{\beta} & \bar{\alpha}\end{bmatrix}\begin{pmatrix}\sin\phi\\ \cos\phi\end{pmatrix}=\frac{\cos\bar{\gamma}}{\bar{V}^2}\begin{pmatrix}\bar{V}\bar{\omega}\\ 1\end{pmatrix}$$

The solution of this linear system in $\sin\bar{\phi}$ and $\cos\bar{\phi}$ is

$$\sin\bar{\phi}=\frac{1}{\bar{\alpha}^2+\bar{\beta}^2}\frac{\cos\bar{\gamma}}{\bar{V}^2}\left(\bar{\alpha}\,\bar{\omega}\bar{V}+\bar{\beta}\right)$$

$$\cos\bar{\phi}=\frac{1}{\bar{\alpha}^2+\bar{\beta}^2}\frac{\cos\bar{\gamma}}{\bar{V}^2}\left(\bar{\alpha}-\bar{\beta}\bar{\omega}\bar{V}\right)$$

Now,

$$\sin^2\bar{\phi}+\cos^2\bar{\phi}=1$$

→

$$\frac{1}{\left(\bar{\alpha}^2+\bar{\beta}^2\right)^2}\frac{\cos^2\bar{\gamma}}{\bar{V}^4}\left(\bar{\alpha}^2\bar{\omega}^2\bar{V}^2+\bar{\beta}^2+\bar{\alpha}^2+\bar{\beta}^2\bar{\omega}^2\bar{V}^2\right)=1$$

→

$$\bar{\alpha}^2+\bar{\beta}^2=\frac{\cos^2\bar{\gamma}}{\bar{V}^4}\left(1+\bar{\omega}^2\bar{V}^2\right)$$

→

$$\left.\begin{aligned}
\bar{\alpha} &= \sqrt{\frac{\cos^2\bar{\gamma}}{\bar{V}^4}\left(1+\bar{\omega}^2\bar{V}^2\right)-\bar{\beta}^2} \\
\sin\bar{\phi} &= \frac{\bar{V}^2}{\cos\bar{\gamma}}\ \frac{1}{1+\bar{\omega}^2\bar{V}^2}\left(\bar{\omega}\bar{V}\sqrt{\frac{\cos^2\bar{\gamma}}{\bar{V}^4}\left(1+\bar{\omega}^2\bar{V}^2\right)-\bar{\beta}^2}+\bar{\beta}\right) \\
\cos\bar{\phi} &= \frac{\bar{V}^2}{\cos\bar{\gamma}}\ \frac{1}{1+\bar{\omega}^2\bar{V}^2}\left(\sqrt{\frac{\cos^2\bar{\gamma}}{\bar{V}^4}\left(1+\bar{\omega}^2\bar{V}^2\right)-\bar{\beta}^2}-\bar{\omega}\bar{V}\bar{\beta}\right)
\end{aligned}\right\} \quad (11)$$

Finally,

$$\bar{\mu} = \bar{q}C_{D0}\bar{V}^2 - \sin\bar{\gamma} + \frac{K}{\bar{V}^2}\cos^2\bar{\gamma}\left(1+\bar{\omega}^2\bar{V}^2\right) - K\bar{\beta}^2\bar{V}^2$$

Special case: $\bar{\beta} = 0$. Then

$$\left.\begin{aligned}
\bar{\alpha} &= \frac{\cos\bar{\gamma}}{\bar{V}^2}\sqrt{1+\bar{\omega}^2\bar{V}^2} \\
\sin\bar{\phi} &= \frac{\bar{\omega}\bar{V}}{\sqrt{1+\bar{\omega}^2\bar{V}^2}} \\
\cos\bar{\phi} &= \frac{1}{\sqrt{1+\bar{\omega}^2\bar{V}^2}} \\
\bar{\mu} &= \bar{q}C_{D0}\bar{V}^2 - \sin\bar{\gamma} + \frac{K}{\bar{V}^2}\cos^2\bar{\gamma}\left(1+\bar{\omega}^2\bar{V}^2\right)
\end{aligned}\right\} \quad (12)$$

In the special case $\bar{\omega} = 0$, $\bar{\beta} \neq 0$, the TRIM1 results in Eqs. **(7)** are recovered. Indeed, TRIM1 (Eqs. **(7)**) is a special case of TRIM2 (Eqs. **(10)**).

3.3. Trim Equation Summary:

Given the new trim conditions $\bar{V}, \bar{\gamma}, -\bar{\omega}$, the corresponding trim control settings are:

$$
\left.
\begin{aligned}
\overline{\beta} &= K_{\overline{\beta},\overline{\omega}} \cdot (-\overline{\omega}) \\
\overline{\alpha} &= \sqrt{\frac{\cos^2\overline{\gamma}}{\overline{V}^4}\left(1+\overline{\omega}^2\overline{V}^2\right) - K_{\overline{\beta},\overline{\omega}}^2\overline{\omega}^2} \\
\overline{\mu} &= \overline{q}\overline{V}^2 C_{D0} - \sin\overline{\gamma} + \frac{K}{\overline{V}^2}\left(1+\overline{\omega}^2\overline{V}^2\right)\cos^2\overline{\gamma} - K\overline{V}^2 K_{\overline{\beta},\overline{\omega}}^2\overline{\omega}^2 \\
\sin\overline{\phi} &= \frac{\overline{V}^2}{1+\overline{\omega}^2\overline{V}^2}\frac{1}{\cos\overline{\gamma}}\left[\overline{\omega}\overline{V}\sqrt{\frac{1+\overline{\omega}^2\overline{V}^2}{\overline{V}^4}\cos^2\overline{\gamma} - K_{\overline{\beta},\overline{\omega}}^2\overline{\omega}^2} - K_{\overline{\beta},\overline{\omega}}\overline{\omega}\right] \\
\cos\overline{\phi} &= \frac{\overline{V}^2}{1+\overline{\omega}^2\overline{V}^2}\frac{1}{\cos\overline{\gamma}}\left[\sqrt{\frac{1+\overline{\omega}^2\overline{V}^2}{\overline{V}^4}\cos^2\overline{\gamma} - K_{\overline{\beta},\overline{\omega}}^2\overline{\omega}^2} + K_{\overline{\beta},\overline{\omega}}\overline{\omega}^2\overline{V}\right]
\end{aligned}
\right\} \quad (13)
$$

It is remarkable that the aerodynamic controls $\overline{\alpha}$ and $\overline{\phi}$ are not dependent on the problem parameters $\left(\overline{q}C_{D_0}\right)$ and K. The throttle setting, $\overline{\mu}$, is however, dependent on the problem parameters $\left(\overline{q}C_{D_0}\right)$ and K.

A reasonable choice for $K_{\overline{\beta},\overline{\omega}}$ is

$$K_{\overline{\beta},\overline{\omega}} = 0.05$$

Indeed, the following holds:

$$3.03\overline{\beta} = K_{\overline{\beta},\overline{\omega}} \cdot 20.4 \cdot \overline{\omega}$$

where $\overline{\beta}$ and $\overline{\omega}$ are the physical (original) variables.

For $\overline{\omega} = 15°/\sec$, use $\overline{\beta} = 5°$

$$\rightarrow \quad 3.03 \cdot 5 = K_{\overline{\beta},\overline{\omega}} \cdot 20.4 \cdot 15$$

$$\rightarrow \quad K_{\overline{\beta},\overline{\omega}} = \frac{3.03}{20.4 \cdot 3} \approx 0.05$$

Remarks

- For coordinated "bank-to-turn" turns (BTT), there is no sideslip angle; choose

$$K_{\bar{\beta},\bar{\omega}} = 0$$

- Conversely, for skid-to-turn (STT) control there is no bank; set

$$\bar{\phi} = 0$$

which leads to

$$\left.\begin{aligned} \bar{\alpha} &= \frac{1}{\bar{V}^2}\cos\bar{\gamma} \\ \bar{\beta} &= -\frac{\bar{\omega}}{\bar{V}}\cos\bar{\gamma} \\ \bar{\mu} &= C_{D0}\bar{q}\bar{V}^2 - \sin\bar{\gamma} + \frac{K}{\bar{V}^2}\cos^2\bar{\gamma} \end{aligned}\right\} \quad \textit{(14)}$$

- If $\bar{\phi}$ is independently controlled, e.g., in order to point the air vehicle's weapons for target tracking and fire control, the trim equations are

$$\begin{bmatrix} \cos\bar{\phi} & \sin\bar{\phi} \\ -\sin\bar{\phi} & \cos\bar{\phi} \end{bmatrix}\begin{pmatrix} \bar{\alpha} \\ \bar{\beta} \end{pmatrix} = \frac{1}{\bar{V}^2}\cos\bar{\gamma}\begin{pmatrix} 1 \\ -\bar{\omega}\bar{V} \end{pmatrix}$$

whereupon the solution is obtained

$$\left.\begin{aligned} \bar{\alpha} &= \frac{1}{\bar{V}^2}\left(\cos\bar{\phi} + \bar{\omega}\bar{V}\sin\bar{\phi}\right)\cos\bar{\gamma} \\ \bar{\beta} &= \frac{1}{\bar{V}^2}\left(\sin\bar{\phi} - \bar{\omega}\bar{V}\cos\bar{\phi}\right)\cos\bar{\gamma} \\ \bar{\mu} &= C_{D0}\bar{q}\bar{V}^2 - \sin\bar{\gamma} + \frac{K}{\bar{V}^2}\left(\bar{\omega}\bar{V}\sin\bar{\phi} + \cos\bar{\phi}\right)^2\cos^2\bar{\gamma} \end{aligned}\right\} \quad \textit{(15)}$$

3.4. Chapter Summary:

Given the equations of motion, the required control inputs were solved for a given desired steady-state, or "trim", set of states. Two trim configurations were investigated: "Trim 1", a simple straight-line flight path ($\overline{\psi}$, $\overline{\gamma}$, $\overline{V}$), and "Trim 2", a trim condition that allowed steady turns ($\psi = \overline{\omega}t$, $\overline{\gamma}$, $\overline{V}$). The fact that there are four control variables and only three states means that the system is over-determined; ϕ and β are redundant. Cases where each was used were examined. Table 3 shows the equation numbers for the various trim control laws presented herein.

Table 3: Trim Control Laws Summary

	$\overline{\beta}$ Controlled Independently	$\overline{\beta}=0$	$\overline{\beta}=K_{\overline{\beta},\overline{\omega}}(-\overline{\omega})$	$\overline{\phi}=0$	$\overline{\phi}$ Controlled Independently
Trim1 $\overline{V}, \overline{\gamma}, \overline{\psi}$	Eqs. 7	Eqs. 8	N/A	Eqs. 8	Eqs. 9
Trim2 $\overline{V}, \overline{\gamma}, -\overline{\omega}$	Eqs. 11	Eqs. 12	Eqs. 13	Eqs. 14	Eqs. 15

4. LINEARIZATION ABOUT THE NEW TRIM $\overline{V}, \overline{\gamma}, -\overline{\omega}$

Modern control theory, with its vast assortment of mathematical tools, is predominantly concerned with linear models. In order to take advantage of this, the nonlinear aircraft model must be linearized. Linearization takes place about a specified operating point. Two such operating points are introduced: one straight and level, the other, a wings-level climb. Flight conditions entail a constant velocity. This choice of trim points for linearization allows decoupling of the lateral and longitudinal channels.

The differential equations in the perturbation states v, γ, ψ and in the controls' perturbations are:

$$\dot{v} = \cos\overline{\gamma}\cdot\gamma - 2\overline{q}C_{D0}\overline{V}\cdot v + \mu - 2K\overline{V}\overline{\alpha}^2\cdot v - 2K\overline{V}^2\overline{\alpha}\cdot\alpha$$

$$\dot{\gamma} = -\frac{\sin\overline{\gamma}}{\overline{V}}\cdot\gamma - \frac{\cos\overline{\gamma}}{\overline{V}^2}\cdot v - \left(\overline{\alpha}\cos\overline{\phi} - \overline{\beta}\sin\overline{\phi}\right)\cdot v - \overline{V}\left(\cos\overline{\phi}\cdot\alpha - \overline{\alpha}\sin\overline{\phi}\cdot\phi + \sin\overline{\phi}\cdot\beta + \overline{\beta}\cos\overline{\phi}\cdot\phi\right)$$

$$\dot{\psi} = \frac{1}{\cos\overline{\gamma}}\left(-\overline{\alpha}\sin\overline{\phi} + \overline{\beta}\cos\overline{\phi}\right)\cdot v + \frac{\overline{V}\sin\overline{\gamma}}{\cos^2\overline{\gamma}}\left(-\overline{\alpha}\sin\overline{\phi} + \overline{\beta}\cos\overline{\phi}\right)\cdot\gamma$$
$$+ \frac{\overline{V}}{\cos\overline{\gamma}}\left(-\sin\overline{\phi}\cdot\alpha - \overline{\alpha}\cos\overline{\phi}\cdot\phi + \cos\overline{\phi}\cdot\beta - \overline{\beta}\sin\overline{\phi}\cdot\phi\right)$$

Use trim equation $\boxed{\overline{\alpha}\cos\overline{\phi} + \overline{\beta}\sin\overline{\phi} = \frac{\cos\overline{\gamma}}{\overline{V}^2}}$

➔

$$\dot{\gamma} = -\frac{\sin\overline{\gamma}}{\overline{V}}\cdot\gamma - 2\frac{\cos\overline{\gamma}}{\overline{V}^2}\cdot v - \overline{V}\cos\overline{\phi}\cdot\alpha - \overline{V}\sin\overline{\phi}\cdot\beta + \overline{V}\left(\overline{\alpha}\sin\overline{\phi} - \overline{\beta}\cos\overline{\phi}\right)\cdot\phi$$

Now, trim relations also yield $\boxed{\overline{\alpha}\sin\overline{\phi} - \overline{\beta}\cos\overline{\phi} = \frac{\overline{\omega}\cos\overline{\gamma}}{\overline{V}}}$

➔

$$\dot{\gamma} = -2\frac{\cos\overline{\gamma}}{\overline{V}^2}\cdot v - \frac{\sin\overline{\gamma}}{\overline{V}}\cdot\gamma - \overline{V}\cos\overline{\phi}\cdot\alpha + \overline{\omega}\cos\overline{\gamma}\cdot\phi - \overline{V}\sin\overline{\phi}\cdot\beta$$

$$\dot{\psi} = -\frac{\bar{\omega}}{\bar{V}} \cdot v - \bar{\omega} \tan\bar{\gamma} \cdot \gamma - \frac{\bar{V}}{\cos\bar{\gamma}} \sin\bar{\phi} \cdot \alpha - \frac{1}{\bar{V}} \cdot \phi + \frac{\bar{V}}{\cos\bar{\gamma}} \cos\bar{\phi} \cdot \beta$$

Hence, the linear perturbations equations are

$$\frac{d}{dt}\begin{bmatrix} v \\ \gamma \\ \psi \end{bmatrix} = A\begin{bmatrix} v \\ \gamma \\ \psi \end{bmatrix} + B\begin{bmatrix} \mu \\ \alpha \\ \phi \\ \beta \end{bmatrix}$$

where the dynamics matrix is:

$$A = \begin{bmatrix} -2\bar{V}\left(\bar{q}C_{D0} + K\bar{\alpha}^2\right) & \cos\bar{\gamma} & 0 \\ -2\dfrac{\cos\bar{\gamma}}{\bar{V}^2} & -\dfrac{\sin\bar{\gamma}}{\bar{V}} & 0 \\ -\dfrac{\bar{\omega}}{\bar{V}} & -\bar{\omega}\tan\bar{\gamma} & 0 \end{bmatrix}$$

and the control matrix is:

$$B = \begin{bmatrix} 1 & -2K\bar{V}^2\bar{\alpha} & 0 & 0 \\ 0 & -\bar{V}\cos\bar{\phi} & \bar{\omega}\cos\bar{\gamma} & -\bar{V}\sin\bar{\phi} \\ 0 & -\bar{V}\dfrac{\sin\bar{\phi}}{\cos\bar{\gamma}} & -\dfrac{1}{\bar{V}} & \bar{V}\dfrac{\cos\bar{\phi}}{\cos\bar{\gamma}} \end{bmatrix}$$

Using the expression for the trim AOA (angle of attack) $\bar{\alpha}$, we calculate the A and B matrices' parameters

$$\bar{q}C_{D0} + K\bar{\alpha}^2 = \bar{q}C_{D0} + K\left(1 + \bar{\omega}^2\bar{V}^2\right)\frac{\cos^2\bar{\gamma}}{\bar{V}^4} - K\bar{\beta}^2$$

and

$$K\bar{V}^2\bar{\alpha} = K\sqrt{\cos^2\bar{\gamma} \cdot \left(1 + \bar{\omega}^2\bar{V}^2\right) - \bar{\beta}^2\bar{V}^4}$$

Similarly, inserting the expression for $\bar{\phi}$, we calculate the additional B matrix parameters

$$\overline{V}\sin\overline{\phi} = \frac{\overline{V}^3}{1+\overline{\omega}^2\overline{V}^2}\frac{1}{\cos\overline{\gamma}}\left(\overline{\omega}\overline{V}\sqrt{\frac{1+\overline{\omega}^2\overline{V}^2}{\overline{V}^4}\cos^2\overline{\gamma}-\overline{\beta}^2}+\overline{\beta}\right)$$

$$\overline{V}\cos\overline{\phi} = \frac{\overline{V}^3}{1+\overline{\omega}^2\overline{V}^2}\frac{1}{\cos\overline{\gamma}}\left(\sqrt{\frac{1+\overline{\omega}^2\overline{V}^2}{\overline{V}^4}\cos^2\overline{\gamma}-\overline{\beta}^2}-\overline{\omega}\overline{V}\overline{\beta}\right)$$

4.1. Linearization About Wings Level Climbing Flight, Trim Speed = Initial Speed

Now, for the special case

$$\overline{V}=1,\ \overline{\phi}=0,\ \overline{\beta}=0,\ \overline{\omega}=0$$

we calculate the parameters

$$\overline{q}C_{D0}+K\overline{\alpha}^2=\overline{q}C_{D0}+K\cos^2\overline{\gamma}$$

$$K\overline{V}^2\overline{\alpha}=K\cos\overline{\gamma}$$

Hence, the dynamics matrix

$$A=\left[\begin{array}{cc:c} -2\left(\overline{q}C_{D0}+K\cos^2\overline{\gamma}\right) & \cos\overline{\gamma} & 0 \\ -2\cos\overline{\gamma} & -\sin\overline{\gamma} & 0 \\ \hdashline 0 & 0 & 0 \end{array}\right]$$

$$=\left[\begin{array}{cc:c} -2\dfrac{C_{D_{TRIM}}}{\tilde{C}_L} & \cos\overline{\gamma} & 0 \\ -2\cos\overline{\gamma} & -\sin\overline{\gamma} & 0 \\ \hdashline 0 & 0 & 0 \end{array}\right]$$

and the control matrix

$$B=\left[\begin{array}{cc:cc} 1 & -2K\cos\overline{\gamma} & 0 & 0 \\ 0 & -1 & 0 & 0 \\ \hdashline 0 & 0 & -1 & \dfrac{1}{\cos\overline{\gamma}} \end{array}\right]$$

Note that the block diagonal structure of the A and B matrices renders the longitudinal channel $\begin{pmatrix} V \\ \gamma \end{pmatrix}$ decoupled from the lateral directional channel ψ.

4.2. Linearization About Trimmed Wings Level, Constant Altitude Flight, Trim Speed = Initial Speed

Now, for the important special case

$$\overline{V}=1,\ \overline{\phi}=0,\ \overline{\gamma}=0,\ \overline{\beta}=0,\ \overline{\alpha}=1,\ \overline{\omega}=0$$

we obtain the dynamics matrix

$$A=\left[\begin{array}{cc:c} -2(\overline{q}C_{D0}+K) & 1 & 0 \\ -2 & 0 & 0 \\ \hdashline 0 & 0 & 0 \end{array}\right]$$

and the control matrix

$$B=\left[\begin{array}{cc:cc} 1 & -2K & 0 & 0 \\ 0 & -1 & 0 & 0 \\ \hdashline 0 & 0 & -1 & 1 \end{array}\right]$$

Moreover, it is readily verifiable that

$$\overline{q}C_{D0}+K=\frac{\overline{C}_D}{\overline{C}_L}$$

where $\overline{C}_D$ and $\overline{C}_L$ are the lift and drag coefficients for wings level, constant altitude, trimmed flight.

Hence, the dynamics matrix is

$$A=\left[\begin{array}{cc:c} -2/(\overline{C}_L/\overline{C}_D) & 1 & 0 \\ -2 & 0 & 0 \\ \hdashline 0 & 0 & 0 \end{array}\right]$$

Thus, the phugoid dynamics are exclusively determined by the solution of the characteristic equation

$$\lambda^2 + 2 \cdot \frac{1}{\left(\frac{\overline{C}_L}{\overline{C}_D}\right)} \lambda + 2 = 0$$

i.e.,

$$\lambda = -\frac{1}{\left(\frac{\overline{C}_L}{\overline{C}_D}\right)} \pm j \sqrt{2 - \frac{1}{\left(\frac{\overline{C}_L}{\overline{C}_D}\right)^2}}$$

Discussion:

The nondimensional natural frequency is

$$\omega_n = \sqrt{2},$$

the dimensional natural frequency is

$$\omega_n = \frac{g}{V_0} \sqrt{2},$$

and the damping ratio is

$$\xi = \frac{1}{\sqrt{2}} \frac{1}{\left(\frac{\overline{C}_L}{\overline{C}_D}\right)}$$

We see that the higher the lift over drag ratio, the lower the damping of the phugoid is. Moreover, the phugoid is oscillatory. The phugoid ceases to be oscillatory for very low lift to drag ratios

$$\frac{\overline{C}_L}{\overline{C}_D} < \frac{1}{\sqrt{2}}$$

Note: In our case, $\overline{C}_L = 0.319$, $\overline{C}_D = 0.0264$, and $\frac{\overline{C}_L}{\overline{C}_D} = 12.1$

4.3. Chapter Summary

In order to design the (model-based) small signal controller, the nonlinear aircraft model was linearized. Linearization takes place about a specified operating (trim) point. Two such operating points were introduced: one straight, level, constant velocity, the other, a level climb with constant velocity. This choice of linearization allowed decoupling of the lateral and longitudinal channels.

5. LINEAR CONTROL DESIGN

The aircraft model was linearized in the previous chapter. Thus, a linear small-signal controller can be designed. The small-signal linear controller is driven by error signals. Since the nonlinear plant will be operated about a new set point, a nonlinear feed-forward controller is used in parallel with the linear feedback portion. The nonlinear feed-forward module, the "trim solver", is based on the aircraft trim equations derived in Chapter 3. Proportional controllers, using the linearized plant dynamics, are designed separately for both lateral and longitudinal channel control, and integral action is included in the lateral channel. Three separate equivalent gain options are calculated for the longitudinal channel's small-signal controller, referred to as options (1a), (1b), and (2).

5.1. Theory

Consider the nonlinear plant

$$\dot{x} = f(x,u), \quad x(0) = x_0, \; x, x_0 \in \Re^n, \; u \in \Re^m, \; 0 \le t$$

$$y = x$$

and the reference signal

$$r = \bar{x}$$

where $\bar{x}$ is a rest point (or equilibrium point, or trim point) of the dynamical system. In other words, $\exists\, \bar{u} \in \Re^m$ s.t. $f(\bar{x},\bar{u}) = 0$.

Consider the set of trim points of interest $X \subset \Re^n$.

Hypothesis:

$\forall\, \bar{x} \in X \; \exists\, \bar{u} \in \Re^m$ s.t. $f(\bar{x},\bar{u}) = 0$.

Moreover, under some mild assumptions on the function f(x,u), the implicit function theorem yields:

$\exists$ smooth function $g : \Re^n \rightarrow \Re^m$ s.t. $\bar{u} = g(\bar{x})$

In other words,

$$f(\bar{x}, g(\bar{x})) = 0 \quad \forall\ \bar{x} \in X$$

i.e.,

$$f(\bar{x}, g(\bar{x})) = 0 \qquad \textit{(end of hypothesis)}$$

Given the reference signal $r = \bar{x}$ ($\equiv$ constant), consider the control law

$$u = g(r) - v$$

where v is the output of the linear controller. The dynamics then are

$$\dot{x} = f(x, g(\bar{x}) - v) \qquad x(0) = x_0 \qquad 0 \le t$$

$$y = x$$

We'll linearize the function f about the trim point $(\bar{x}, g(\bar{x}))$. Thus,

$$f(x, g(\bar{x}) - v) = f(\bar{x}, g(\bar{x})) + A(x - \bar{x}) - Bv + \text{H.O.T.}$$

$$= 0 + A(x - \bar{x}) - Bv + d$$

where

$$A \equiv \left.\frac{\partial f}{\partial x}\right|_{(\bar{x}, g(\bar{x}))}, \qquad B \equiv \left.\frac{\partial f}{\partial u}\right|_{(\bar{x}, g(\bar{x}))}, \qquad d \equiv \text{H.O.T. (higher order terms)}$$

Hence

$$-\dot{e} = -Ae - Bv - d$$

where

$$e \equiv r - y = \bar{x} - x$$

Therefore, the perturbation dynamics are

$$\dot{e} = Ae + Bv + d$$

Tracking of a constant command signal r is guaranteed, provided that the control signal v is generated by a stabilizing state feedback control law. We'll use a PI control law. We need integral action because we need to reject the linearization-induced disturbance d [9]. Moreover, although we do not need integral action for tracking the constant set point command when the linearized dynamics with d = 0 are used, integral action might also help with tracking a dynamic reference signal.

Hence, we augment the perturbation dynamics as follows:

$$\dot{e} = Ae + Bv + d$$

$$\dot{z} = e$$

where z is the "charge" on the integrator.

Use the linear control law

$$v = K_P e + K_I z$$

In matrix form, closed-loop dynamics are

$$\frac{d}{dt}\begin{bmatrix} e \\ z \end{bmatrix} = \begin{bmatrix} A & 0 \\ I & 0 \end{bmatrix}\begin{bmatrix} e \\ z \end{bmatrix} + \begin{bmatrix} B \\ 0 \end{bmatrix} v + \begin{bmatrix} I \\ 0 \end{bmatrix} d$$

and the linear controller output is

$$v = \begin{bmatrix} K_P & K_I \end{bmatrix}\begin{pmatrix} e \\ z \end{pmatrix}$$

By substitution,

$$\frac{d}{dt}\begin{pmatrix} e \\ z \end{pmatrix} = \begin{bmatrix} A + BK_P & BK_I \\ I & 0 \end{bmatrix}\begin{pmatrix} e \\ z \end{pmatrix} + \begin{bmatrix} I \\ 0 \end{bmatrix} d, \qquad \begin{matrix} e(0) = e_0 \\ z(0) = 0 \end{matrix}$$

Remark: We want $e \to 0$ ($\equiv$ tracking). This implies $BK_I z + d = 0$. Since d is arbitrary, need (BK_I) invertible ➔ need B and K_I invertible.

Now,

$$\det\left(\begin{bmatrix} A + BK_P & BK_I \\ I & 0 \end{bmatrix}\right) = \det(BK_I)$$

Hence, we conclude that the dynamics matrix $\begin{bmatrix} A + BK_P & BK_I \\ I & 0 \end{bmatrix}$ does not have zero eigenvalues.

Moreover, we require $\begin{bmatrix} A + BK_P & BK_I \\ I & 0 \end{bmatrix}$ to be a stability matrix, i.e. a matrix whose eigenvalues all have strictly negative real parts. This is not a problem because the poles of $\begin{bmatrix} A & 0 \\ I & 0 \end{bmatrix}$ are assignable. Indeed, the pair $\left(\begin{bmatrix} A & 0 \\ I & 0 \end{bmatrix}, \begin{bmatrix} B \\ 0 \end{bmatrix}\right)$ is controllable. Thus:

$$\text{Rank}\left(\left[\begin{array}{c:c} B & AB \\ 0 & B \end{array}\right]\right) = 2n$$

because B is an nxm full-rank (= n) matrix.

Furthermore: $\begin{bmatrix} A + BK_P & BK_I \\ I & 0 \end{bmatrix}$ is a stability matrix

➔ $A + BK_P$ a stability matrix. Again, the poles of the pair (A, B) are assignable because (A, B) is a controllable pair (in view of the fact that the nxn matrix B is nonsingular.)

Hence, we first design the proportional controller. This "governs" the tracking error dynamics. The second step entails the setting of the integral gains.

Note: Integral action is not strictly needed when

a) There are no disturbances, viz., the linearized dynamics are used, and

b) The reference signal $r = \bar{x} \equiv$ constant.

5.2. Phugoid Damping Controller

The phugoid damping control system's block diagram is shown in Figure 3.

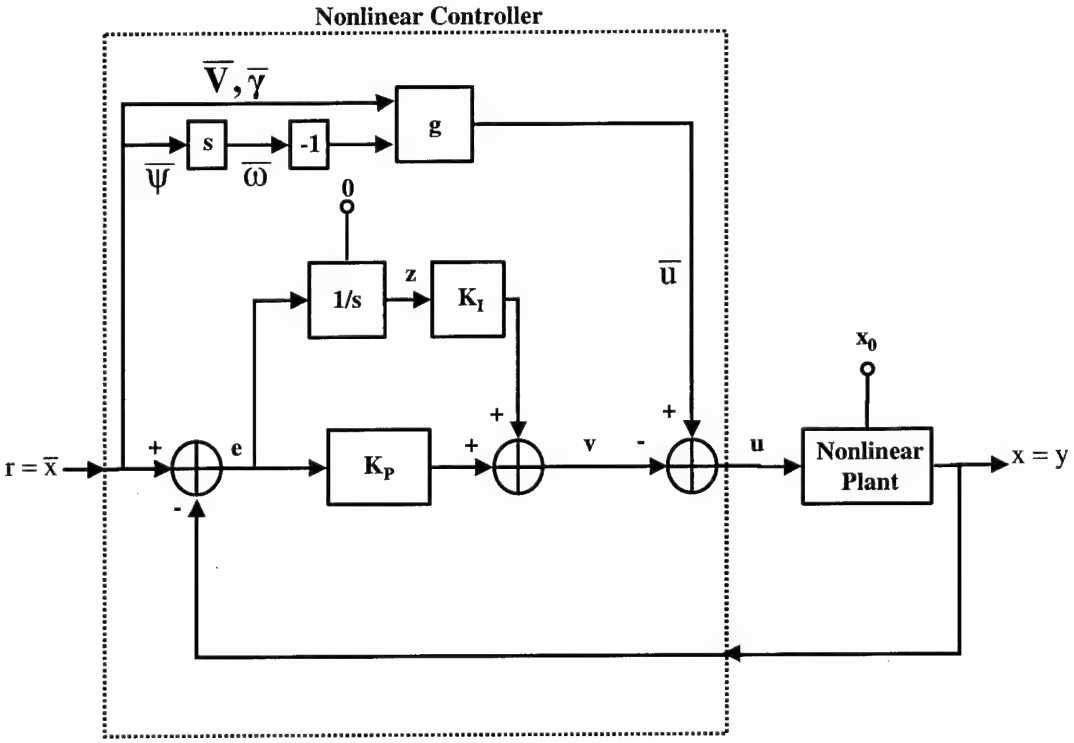

Figure 3: Phugoid Damping Control System

Here

$$y = x$$

$$e = r - y$$

$$\dot{z} = e\,, \quad z(0) = 0$$

$$u = g(r) - K_P e - K_I z$$

where, we recall,

$$r = \begin{pmatrix} \bar{v} \\ \bar{\gamma} \\ \bar{\psi} \end{pmatrix}, \quad x = \begin{pmatrix} v \\ \gamma \\ \psi \end{pmatrix}, \quad u = \begin{pmatrix} \mu \\ \alpha \\ \phi \\ \beta \end{pmatrix}$$

Zooming in on the ψ-channel – see Figure 4:

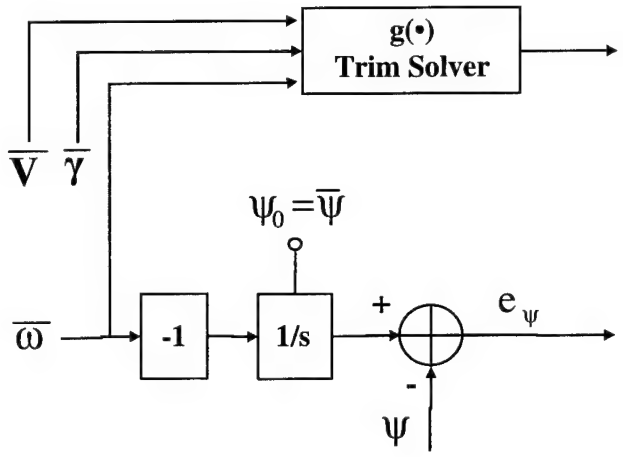

Figure 4: ψ-Channel Block Diagram

The function g(•) implements the nonlinear trim signal calculation developed in Chapter 3. The nonlinear trim function g(•) is explicitly specified as follows:

$$\begin{pmatrix} \bar{\mu} \\ \bar{\alpha} \\ \bar{\phi} \end{pmatrix} = g\left(\bar{v}, \bar{\gamma}, \bar{\omega}; \bar{\beta}\right)$$

where (see Eqs. **(11)**)

$$\bar{\mu} = \bar{q} C_{D0} \bar{V}^2 - \sin\bar{\gamma} + \frac{K}{\bar{V}^2} \cos^2\bar{\gamma}\left(1 + \bar{\omega}^2\bar{V}^2\right) - K\bar{\beta}^2\bar{V}^2$$

$$\bar{\alpha} = \sqrt{\frac{\cos^2\bar{\gamma}}{\bar{V}^4}\left(1 + \bar{\omega}^2\bar{V}^2\right) - \bar{\beta}^2}$$

$$\sin\bar{\phi} = \frac{\bar{V}^2}{\cos\bar{\gamma}} \frac{1}{1+\bar{\omega}^2\bar{V}^2}\left(\bar{\omega}\bar{V}\sqrt{\frac{\cos^2\bar{\gamma}}{\bar{V}^4}\left(1+\bar{\omega}^2\bar{V}^2\right)-\bar{\beta}^2}+\bar{\beta}\right)$$

$$\cos\bar{\phi} = \frac{\bar{V}^2}{\cos\bar{\gamma}} \frac{1}{1+\bar{\omega}^2\bar{V}^2}\left(\sqrt{\frac{\cos^2\bar{\gamma}}{\bar{V}^4}\left(1+\bar{\omega}^2\bar{V}^2\right)-\bar{\beta}^2}-\bar{\omega}\bar{V}\bar{\beta}\right)$$

5.3. Proportional Control

The controller's design is based on the linearized special case of trimmed, wings level, constant altitude flight, with trim speed = initial speed. Control of the lateral and longitudinal channels is addressed.

5.3.1. Lateral / Directional Channel

The desired flight control system (FCS) lateral channel's aircraft control parameters are specified in Table 4.

Table 4: Desired Parameters of Lateral FCS Channel

	Dimensional	***Nondimensional***
τ	10 [sec]	0.49
ξ_P	$\sqrt{2}/2$	$\sqrt{2}/2$
ω_{n_P}	$\sqrt{2}\frac{g}{V_0}$	$\sqrt{2}$

Note: The lateral/directional control channels' nondimensional time constant

$$\tau := \tau \cdot \frac{g}{V_0}$$

In the lateral / directional channel, the reference signal is $\bar{\Psi}$, and thus the error signal is

$$e_\psi \equiv \bar{\Psi} - \psi \quad [\text{rad}]$$

Now, the linearized lateral directional equation of motion is

$$\dot{e}_{\psi} = -\phi + \beta$$

The controls are

$$\phi = K_{\phi,\psi} \cdot e_{\psi}$$

$$\beta = K_{\beta,\psi} \cdot e_{\psi}$$

➔

$$\dot{e}_{\psi} = -K_{\phi,\psi} e_{\psi} + K_{\beta,\psi} e_{\psi}$$

$$= -\left(K_{\phi,\psi} - K_{\beta,\psi}\right) e_{\psi}$$

➔

$$e_{\psi}(t) = e^{-\left(K_{\phi,\psi} - K_{\beta,\psi}\right)t} e_{\psi}(0)$$

We want

$$e_{\psi}(t) = e^{-\frac{t}{\tau}} e_{\psi}(0)$$

Hence, set

$$K_{\phi,\psi} - K_{\beta,\psi} = \frac{1}{\tau}$$

Note that τ is the specified nondimensional directional time constant.

Choosing a dimensional $\tau = 10$ sec ➔ nondimensional $\tau = 0.5$.

➔ $$K_{\phi,\psi} - K_{\beta,\psi} = 2 \qquad \textit{(16)}$$

If a BTT control strategy is employed, then $K_{\beta,\psi} = 0\,\phi$

➔ $$K_{\phi,\psi} = 2 \qquad \textit{(17)}$$

If, instead, an STT control strategy is employed, then $K_{\phi,\psi} = 0$

$$\rightarrow \quad K_{\beta,\psi} = -2 \tag{18}$$

In conclusion:

1. The design specification is the directional channel's time constant τ.
2. We operate on e_ψ
3. The control variables are ϕ and/or β.
4. The actual control signals are:

$$\left.\begin{aligned}
\phi &= -K_{\phi,\psi} e_\psi + A \sin\left[\frac{\overline{V}^2}{\cos\bar{\gamma}} \frac{1}{1+\overline{\omega}^2\overline{V}^2}\left(\overline{\omega}\overline{V}\sqrt{\frac{\cos^2\bar{\gamma}}{\overline{V}^4}\left(1+\overline{\omega}^2\overline{V}^2\right)+K_{\bar{\beta},\overline{\omega}}^2\overline{\omega}^2}-K_{\bar{\beta},\overline{\omega}}\overline{\omega}\right)\right] \\
&= -2e_\psi + A \sin\left[\frac{\overline{V}^2}{\cos\bar{\gamma}} \frac{1}{1+\overline{\omega}^2\overline{V}^2}\left(\overline{\omega}\overline{V}\sqrt{\frac{\cos^2\bar{\gamma}}{\overline{V}^4}\left(1+\overline{\omega}^2\overline{V}^2\right)+K_{\bar{\beta},\overline{\omega}}^2\overline{\omega}^2}-K_{\bar{\beta},\overline{\omega}}\overline{\omega}\right)\right] \\
\beta &= -K_{\beta,\psi} e_\psi - K_{\bar{\beta},\overline{\omega}}\overline{\omega}
\end{aligned}\right\} \tag{19}$$

5. In pure BTT control, $K_{\beta,\psi} = K_{\bar{\beta},\overline{\omega}} = 0$, viz., $\beta = 0$.
6. In pure STT control, $\phi = 0$.

5.3.2. Longitudinal Channel

The reference signals are $\overline{V}$ and $\bar{\gamma}$, and thus the error signals are

$$e_V \equiv \overline{V} - V$$

$$e_\gamma \equiv \bar{\gamma} - \gamma \quad [\text{rad}]$$

which are fed back to the linear controller. Thus, the linear controller operates on feedback signals e_v and e_γ. The control variables for the aircraft longitudinal channel are α and μ. We need to specify the four controller gains $K_{\alpha V}$, $K_{\alpha\gamma}$, $K_{\mu V}$, $K_{\mu\gamma}$. We will use

ω_{n_P} (longitudinal channel's natural frequency) and ξ_P (longitudinal channel's damping ratio) as the longitudinal channel's design specs.

The design equations are derived as follows:

The closed-loop system's dynamics matrix is

$$A_{CL_P} = \begin{bmatrix} -2\frac{\overline{C}_D}{\overline{C}_L} + K_{\mu V} - 2K \cdot K_{\alpha V} & 1 + K_{\mu\gamma} - 2K \cdot K_{\alpha\gamma} \\ -2 - K_{\alpha V} & -K_{\alpha\gamma} \end{bmatrix}$$

The characteristic equation for a 2x2 matrix is

$$\begin{aligned} 0 &= \lambda^2 + 2\xi_P\omega_{n_P} + \omega_{n_P}^2 \\ &= \lambda^2 - \text{trace}(A_{CL_P}) + \det(A_{CL_P}) \end{aligned}$$

Hence, the design equations are

$$\text{Trace}(A_{CL_P}) = -2\xi_P\omega_{n_P}$$

$$\text{Det}(A_{CL_P}) = \omega_{n_P}^2$$

Thus, the design equations yield two equations in four unknowns (the gains $K_{\alpha V}$, $K_{\alpha\gamma}$, $K_{\mu V}$, $K_{\mu\gamma}$):

$$K_{\alpha\gamma} + 2K \cdot K_{\alpha V} - K_{\mu V} = 2\left(\xi_P\omega_{n_P} - \frac{\overline{C}_D}{\overline{C}_L}\right)$$

$$K_{\alpha\gamma}\left(2K \cdot K_{\alpha V} - K_{\mu V} + 2\frac{\overline{C}_D}{\overline{C}_L}\right) + (2 + K_{\alpha V})(1 + K_{\mu\gamma} - 2K \cdot K_{\alpha\gamma}) = \omega_{n_P}^2$$

The first equation yields

$$2K \cdot K_{\alpha V} - K_{\mu V} + 2\frac{\overline{C}_D}{\overline{C}_L} = 2\xi_P\omega_{n_P} - K_{\alpha\gamma}$$

Inserting this expression in the second equation yields

$$K_{\alpha\gamma}\left(2\xi_P\omega_{n_P}-K_{\alpha\gamma}\right)+\left(2+K_{\alpha V}\right)\left(1+K_{\mu\gamma}-2K\cdot K_{\alpha\gamma}\right)=\omega_{n_P}^2$$

Hence, we have obtained the two design equations

$$K_{\alpha\gamma}+2KK_{\alpha V}-K_{\mu V}=2\left(\xi_P\omega_{n_P}-\frac{\overline{C}_D}{\overline{C}_L}\right) \qquad (19)$$

$$K_{\alpha\gamma}\left(2\xi_P\omega_{n_P}-K_{\alpha\gamma}\right)+\left(2+K_{\alpha V}\right)\left(1+K_{\mu\gamma}-2KK_{\alpha\gamma}\right)=\omega_{n_P}^2 \qquad (20)$$

In summary, we have two equations in the four unknowns $K_{\alpha V}$, $K_{\alpha\gamma}$, $K_{\mu V}$, $K_{\mu\gamma}$. In the design equations, only the problem parameter K features – and, of course, the design specs ξ_P and ω_{n_P}.

Finally, the complete control law is

$$\left.\begin{aligned}
\mu &= \overline{q}\overline{V}^2C_{D0}-\sin\overline{\gamma}+\frac{K}{\overline{V}^2}\left(1+\overline{\omega}^2\overline{V}^2\right)\cos^2\overline{\gamma}-K\overline{V}^2K_{\overline{\beta},\overline{\omega}}^2\overline{\omega}^2-K_{\mu V}\cdot e_V-K_{\mu\gamma}\cdot e_\gamma\\
\alpha &= \sqrt{\frac{\cos^2\overline{\gamma}}{\overline{V}^4}\left(1+\overline{\omega}^2\overline{V}^2\right)-K_{\overline{\beta},\overline{\omega}}^2\overline{\omega}^2}-K_{\alpha V}\cdot e_V-K_{\alpha\gamma}\cdot e_\gamma\\
\phi &= A\sin\left\{\frac{\overline{V}^2}{1+\overline{\omega}^2\overline{V}^2}\frac{1}{\cos\overline{\gamma}}\left[\overline{\omega}\overline{V}\sqrt{\frac{1+\overline{\omega}^2\overline{V}^2}{\overline{V}^4}\cos^2\overline{\gamma}-K_{\overline{\beta},\overline{\omega}}^2\overline{\omega}^2}-K_{\overline{\beta},\overline{\omega}}\overline{\omega}\right]\right\}-K_{\phi,\psi}\cdot e_\psi\\
\beta &= K_{\overline{\beta},\overline{\omega}}\cdot\left(-\overline{\omega}\right)-K_{\beta,\psi}e_\psi
\end{aligned}\right\} \qquad (21)$$

Obviously, when $K_{\alpha V}=K_{\alpha\gamma}=K_{\mu V}=K_{\mu\gamma}=0$, we are back to the open loop case. Hence, the design equations yield

$$\xi_P\cdot\omega_{n_P}=\frac{\overline{C}_D}{\overline{C}_L}$$

$$\omega_{n_P}=\sqrt{2}$$

→

$\omega_{n_P} = \sqrt{2} = \omega_n$, and $\xi_P = \frac{1}{\sqrt{2}} \frac{\overline{C}_D}{\overline{C}_L} = \xi$, as expected.

1. Choose $K_{\alpha V} = 0$, $K_{\mu\gamma} = 0$

This set of gain restrictions is somewhat arbitrary. It is chosen because it is intuitively obvious. Within the controller, velocity error has no effect on AOA, and flight path angle error has no effect on thrust setting. This implies that AOA is affected only by an error in flight path angle e_γ, while thrust setting is controlled solely using velocity error e_V. This is similar to the logic that a pilot might use to maneuver an aircraft in certain situations, using pitch to control the direction of the aircraft and the throttle to control the speed. Thus, the design equations are:

$$K_{\alpha\gamma} - K_{\mu V} = 2\left(\xi_P \omega_{n_P} - \frac{\overline{C}_D}{\overline{C}_L}\right)$$

$$2\xi_P \omega_{n_P} K_{\alpha\gamma} - K_{\alpha\gamma}^2 + 2 - 4KK_{\alpha\gamma} = \omega_{n_P}^2$$

Thus, we have two equations in the two unknowns $K_{\alpha\gamma}$ and $K_{\mu V}$. The second design equation is a quadratic equation in $K_{\alpha\gamma}$:

$$K_{\alpha\gamma}^2 + 2\left(2K - \xi_P \omega_{n_P}\right)K_{\alpha\gamma} + \omega_{n_P}^2 - 2 = 0$$

→

$$K_{\alpha\gamma} = \xi_P \omega_{n_P} - 2K \pm \sqrt{\left(\xi_P{}^2 - 1\right)\omega_{n_P}^2 + 2 + 4K^2 - 4K\xi_P \omega_{n_P}}$$

$$K_{\mu V} = 2\frac{\overline{C}_D}{\overline{C}_L} - 2K - \xi_P \omega_{n_P} \pm \sqrt{\left(\xi_P^2 - 1\right)\omega_{n_P}^2 + 2 + 4K^2 - 4K\xi_P \omega_{n_P}}$$

If we specify

$$\xi_P = \frac{\sqrt{2}}{2}$$

then the two solutions are

$$\left.\begin{aligned} \text{a)}\qquad K_{\alpha\gamma} &= \frac{\sqrt{2}}{2}\omega_{n_P} - 2K + \sqrt{\left(\frac{\sqrt{2}}{2}\omega_{n_P} - 2K\right)^2 + 2 - \omega_{n_P}^2} \\ K_{\mu V} &= 2\frac{\overline{C}_D}{\overline{C}_L} - \frac{\sqrt{2}}{2}\omega_{n_P} - 2K + \sqrt{\left(\frac{\sqrt{2}}{2}\omega_{n_P} - 2K\right)^2 + 2 - \omega_{n_P}^2} \end{aligned}\right\} \quad (22)$$

and

$$\left.\begin{aligned} \text{b)}\qquad K_{\alpha\gamma} &= \frac{\sqrt{2}}{2}\omega_{n_P} - 2K - \sqrt{\left(\frac{\sqrt{2}}{2}\omega_{n_P} - 2K\right)^2 + 2 - \omega_{n_P}^2} \\ K_{\mu V} &= 2\frac{\overline{C}_D}{\overline{C}_L} - \frac{\sqrt{2}}{2}\omega_{n_P} - 2K - \sqrt{\left(\frac{\sqrt{2}}{2}\omega_{n_P} - 2K\right)^2 + 2 - \omega_{n_P}^2} \end{aligned}\right\} \quad (23)$$

We want to increase the bandwidth of the closed-loop flight control system in order to enhance tracking performance. Hence, we will specify

$$\omega_{n_P} \geq \omega_n = \sqrt{2}$$

Remark 1: If we should choose $\omega_{n_P} = \omega_n = \sqrt{2}$, then in case (a)

$$K_{\alpha\gamma} = 2(1 - 2K) = 1.8572 \approx 2$$

$$K_{\mu V} = 2\left(\frac{\overline{C}_D}{\overline{C}_L} - 2K\right) = 0.0226 \approx 0$$

and in case (b)

$$K_{\alpha\gamma} = 0$$

$$K_{\mu V} = 2\left(\frac{\overline{C}_D}{\overline{C}_L} - 1\right) = -1.8572 \approx -2$$

This choice of ω_n and ξ effectively changes the damping of the closed-loop system while retaining the natural frequency found in the open-loop system. Since settling time is related to natural frequency, system response can be improved by increasing the natural frequency. Therefore, we will arbitrarily increase the desired natural frequency to $\omega_{n_P} = \sqrt{3}$. Note that ω_{n_P} could be increased further, at the expense of increasing the gains of the controller matrix.

Note also that, in each case, three of the four gains are set to approximately zero. These are particularly low-gain controllers. This is not surprising, given the limited design requirements given.

Remark 2: A physically realizable controller matrix is required to be composed of all real parts. A negative discriminant would produce complex gains. We need a nonnegative discriminant, viz.,

$$\left(\frac{\sqrt{2}}{2}\omega_{n_P} - 2K\right)^2 \geq \omega_{n_P}^2 - 2$$

→

$$0 < \omega_{n_P} < 2\left(\sqrt{1+4K^2} - \sqrt{2}K\right)$$

Hence, choose, e.g.,

$$\omega_{n_P} = \sqrt{3}$$

Then

a) $$K_{\alpha\gamma} = \frac{1}{\sqrt{2}}\left(\sqrt{1-4\sqrt{6}K+8K^2} + \sqrt{3} - 2\sqrt{2}K\right)$$

$$K_{\mu V} = 2\frac{\bar{C}_D}{\bar{C}_L} + \frac{1}{\sqrt{2}}\left(\sqrt{1-4\sqrt{6}K+8K^2} - \sqrt{3} - 2\sqrt{2}K\right)$$

Thus, $K_{\alpha\gamma} > 0$ and $K_{\mu V} < 0$, as required.

b) $$K_{\alpha\gamma} = \frac{1}{\sqrt{2}}\left(-\sqrt{1-4\sqrt{6}K+8K^2}+\sqrt{3}-2\sqrt{2}K\right)$$

$$K_{\mu V} = 2\frac{\overline{C}_D}{\overline{C}_L} - \frac{1}{\sqrt{2}}\left(\sqrt{1-4\sqrt{6}K+8K^2}+\sqrt{3}-2\sqrt{2}K\right)$$

Again, $K_{\alpha\gamma} > 0$ and $K_{\mu V} < 0$, as required. Now the gain $K_{\alpha\gamma}$ is lower than before, and the gain $K_{\mu V}$ is higher.

2. Choose $K_{\alpha\gamma} = 0$, $K_{\mu V} = 0$

Now, within the controller, velocity error has no effect on thrust setting, and flight path angle error has no effect on AOA. This implies that AOA is affected only by an error in velocity error e_V, while thrust setting is controlled solely using flight path angle e_γ. This is the opposite of the previous option, and may also be used naturally by pilots flying in certain situations. Then the gains are:

$$\left.\begin{aligned} K_{\alpha V} &= \frac{1}{K}\left(\xi_P\omega_{n_P} - \frac{\overline{C}_D}{\overline{C}_L}\right) \\ K_{\mu\gamma} &= \frac{\omega_{n_P}^2 - 2 + \frac{1}{K}\left(\frac{\overline{C}_D}{\overline{C}_L} - \xi_P\omega_{n_P}\right)}{2 + \frac{1}{K}\left(\xi_P\omega_{n_P} - \frac{\overline{C}_D}{\overline{C}_L}\right)} \end{aligned}\right\} \textit{(24)}$$

Again, specify

$$\xi_P = \frac{\sqrt{2}}{2}$$

Thus

$$K_{\alpha V} = \frac{1}{K}\left(\frac{1}{\sqrt{2}}\omega_{n_P} - \frac{\overline{C}_D}{\overline{C}_L}\right)$$

$$K_{\mu\gamma} = \frac{\omega_{n_P}^2 - 2 + \frac{1}{K}\left(\frac{\overline{C}_D}{\overline{C}_L} - \frac{1}{\sqrt{2}}\omega_{n_P}\right)}{2 + \frac{1}{K}\left(\frac{1}{\sqrt{2}}\omega_{n_P} - \frac{\overline{C}_D}{\overline{C}_L}\right)}$$

If, in addition, we specified $\omega_{n_P} = \sqrt{2}$, to maintain the open-loop natural frequency in the closed-loop system while increasing damping ratio to the specified $\xi_P = \frac{\sqrt{2}}{2}$, then

$$K_{\alpha V} = \frac{1}{K}\left(1 - \frac{\overline{C}_D}{\overline{C}_L}\right)$$

$$K_{\mu\gamma} = \frac{\frac{\overline{C}_D}{\overline{C}_L} - 1}{2K + 1 - \frac{\overline{C}_D}{\overline{C}_L}}$$

Choosing, as before,

$$\omega_{n_P} = \sqrt{3}$$

➔

$$K_{\alpha V} = \frac{1}{K}\left(\sqrt{\frac{3}{2}} - \frac{\overline{C}_D}{\overline{C}_L}\right) > 0$$

$$K_{\mu\gamma} = \frac{K + \frac{\overline{C}_D}{\overline{C}_L} - \sqrt{\frac{3}{2}}}{2K + \sqrt{\frac{3}{2}} - \frac{\overline{C}_D}{\overline{C}_L}} < 0$$

Concerning the polarity of the gains: We see that when an increase in airspeed is required ($e_V > 0$), the control law brings about a reduction in the angle of attack, as expected. However, when an increase in flight path angle (toward a steeper dive) is required, the control law brings about an increase in thrust setting, i.e., the polarity of $K_{\mu\gamma}$

does not make physical sense, although the linearized closed-loop flight control system is stable; we would prefer $K_{\mu\gamma} > 0$.

Demanding $K_{\mu\gamma} > 0$ requires

$$\omega_{n_P}^2 - 2\omega_{n_P}\frac{1}{2\sqrt{2}K} + \frac{1}{K}\frac{\bar{C}_D}{\bar{C}_L} - 2 \geq 0$$

$\rightarrow$

$$0 < \omega_{n_P} < \frac{1}{2\sqrt{2}}\frac{1}{K}\left(1 - \sqrt{1 + 8K\left(2K - \frac{\bar{C}_D}{\bar{C}_L}\right)}\right)$$

or

$$\omega_{n_P} > \frac{1}{2\sqrt{2}}\frac{1}{K}\left(1 + \sqrt{1 + 8K\left(2K - \frac{\bar{C}_D}{\bar{C}_L}\right)}\right)$$

Numerically, this is equivalent to

$$0 < \omega_{n_P} < 0.01596$$
$$\approx 0.0112\sqrt{2}$$

which entails a very low bandwidth.

Alternatively,

$$\omega_{n_P} > 19.794$$
$$\approx 14\sqrt{2}$$

yielding a very high bandwidth.

Thus, given the constraints of setting gains $K_{\alpha\gamma} = K_{\mu V} = 0$, the intuitively expected gain sign configuration can be achieved, but only if ω_n is set to a very high or very low level. Setting it to such a low level as $0.0112\sqrt{2}$ is tantamount to removing the controller completely; phugoid oscillations would continue for a long time. On the other

hand, setting $\omega_n = 14\sqrt{2}$ could produce desirable results. Settling time would be decreased greatly. However, the gains required for such performance would be much higher than those calculated previously. These higher gains force the control actuators to work harder, possibly to the undesirable point of saturation. Even worse, the system response could be increased to a point where system phase margins decrease to levels where actuator lag affects system stability.

It is apparent that there is nothing "wrong" with the analysis; all specifications were met, and the system is stable. These are the gains required to bring about the stated ξ and ω_n , given that two variables (or degrees of freedom) were expended in choosing $K_{\alpha\gamma} = K_{\mu V} = 0$. On the other hand, this "curiosity" in the gain polarity is reflected in the system's performance. For example, given a excess velocity error, the controller will command an increase in AOA. The gain involved in this step is much higher than the others calculated, so the AOA increase is relatively high. The aircraft will, naturally, begin to climb. The curious gain polarity then will cause the thrust setting to increase. This thrust increase further perturbs the dynamics, exacerbating the error. However, the AOA increase is sufficiently high to force a velocity decrease in spite of the thrust increase. The gains work against each other, balanced in such a way as to produce the desired ξ and ω_n. This is obviously inefficient in terms of actuator usage, but it is unavoidable unless the design specifications are changed.

5.4. Integral Action Control

Let

$$e \equiv \begin{pmatrix} v_e \\ \gamma_e \\ \psi_e \end{pmatrix} \in \Re^3, \quad z \equiv \begin{pmatrix} z_V \\ z_\gamma \\ z_\psi \end{pmatrix} \in \Re^3, \quad d \equiv \begin{pmatrix} d_v \\ d_\gamma \\ d_\psi \end{pmatrix} \in \Re^3$$

where e is the error signal, z is the integrator "charge", and d is the disturbance signal.

We analyze and simulate the linear system

$$\dot{e} = Ae + Bv + d, \quad e(0) = e_0$$

$$\dot{z} = e, \quad z(0) = 0$$

where

$$A = \left[\begin{array}{cc:c} -2/(\bar{C}_L/\bar{C}_D) & 1 & 0 \\ -2 & 0 & 0 \\ \hdashline 0 & 0 & 0 \end{array}\right], \quad B = \left[\begin{array}{cc:cc} 1 & -2K & 0 & 0 \\ 0 & -1 & 0 & 0 \\ \hdashline 0 & 0 & -1 & 1 \end{array}\right]$$

First consider the BTT scenario, where $\beta \equiv 0$ and thus $v \equiv \begin{pmatrix} \mu \\ \alpha \\ \beta \end{pmatrix}$, and B is a 3x3

matrix. The control signal is formed according to

$$v = K_P e + K_I v$$

where the gains are

$$K_P = \left[\begin{array}{cc:c} K_{\mu,V} & K_{\mu,\gamma} & 0 \\ K_{\alpha,V} & K_{\alpha,\gamma} & 0 \\ \hdashline 0 & 0 & K_{\phi,\psi} \end{array}\right], \quad K_I = \left[\begin{array}{cc:c} K_{\mu,z_V} & K_{\mu,z_\gamma} & 0 \\ K_{\alpha,z_V} & K_{\alpha,z_\gamma} & 0 \\ \hdashline 0 & 0 & K_{\phi,z_\psi} \end{array}\right]$$

Hence, the closed-loop control system is described by

$$\frac{d}{dt}\begin{pmatrix} e \\ z \end{pmatrix} = \begin{pmatrix} A + BK_P & BK_I \\ I_3 & 0_3 \end{pmatrix}\begin{pmatrix} e \\ z \end{pmatrix} + \begin{pmatrix} I_3 \\ 0_3 \end{pmatrix} d, \quad \begin{array}{l} e(0) = e_0 \\ z(0) = 0 \end{array}$$

The system is composed of two independent channels: lateral and longitudinal. The two channels can be decoupled in the same manner as was done in the proportional controller. The lateral / directional channel dynamics are

$$\dot{\psi}_e = -K_{\phi,\psi}\psi_e - K_{\phi,z_\psi} z_\psi + d_\psi \ , \ \psi_{e_0}(0) = r_\psi$$

$$\dot{z}_\psi = \psi_e \ , \qquad z_\psi(0) = 0$$

i.e.,

$$\frac{d}{dt}\begin{pmatrix}\psi_e \\ z_\psi\end{pmatrix} = \begin{pmatrix}-K_{\phi,\psi} & -K_{\phi,z_\psi} \\ 1 & 0\end{pmatrix}\begin{pmatrix}\psi_e \\ z_\psi\end{pmatrix} + \begin{pmatrix}1 \\ 0\end{pmatrix} d_\psi$$

$$\psi_e(0) = \psi_{e_0}$$
$$z_\psi(0) = 0$$

5.4.1. Lateral / Directional Channel

Recall the form of the closed-loop system description

$$\dot{e} = Ae + Bv$$

where A is the closed-loop linear dynamics matrix = $\begin{bmatrix} A + BK_P & BK_I \\ I & 0 \end{bmatrix}$. For this channel,

$$A = 0 \ , \ B = [-1, 1] \ , \ v = \begin{pmatrix}\phi \\ \beta\end{pmatrix}$$

$$K_P = \begin{bmatrix} K_{\phi,\psi} \\ K_{\beta,\psi} \end{bmatrix}$$

$$K_I = \begin{bmatrix} K_{\phi,z} \\ K_{\beta,z} \end{bmatrix}$$

Thus, the closed-loop linear dynamics matrix is

$$\begin{bmatrix} A+BK_P & BK_I \\ I & 0 \end{bmatrix} = \begin{bmatrix} -K_{\phi,\psi}+K_{\beta,\psi} & -K_{\phi,z}+K_{\beta,z} \\ 1 & 0 \end{bmatrix}$$

and the characteristic equation is

$$\lambda^2 + \left(K_{\phi,\psi} - K_{\beta,\psi}\right)\lambda + K_{\phi,z} - K_{\beta,z} = 0$$

We want

$$\omega_{n_L}^2 = K_{\phi,z} - K_{\beta,z}$$

$$2\xi_L\omega_{n_L} = K_{\phi,\psi} - K_{\beta,\psi}$$

Choosing, as before,

$$K_{\phi,\psi} - K_{\beta,\psi} = \frac{1}{\tau}$$

and

$$\xi_L = \frac{\sqrt{2}}{2}$$

→

$$\omega_{n_L} = \frac{1}{\sqrt{2}\cdot\tau}$$

Choosing the same time constant as was selected in the previous proportional case would allow the proportional and the integral parts of the controller to track similar dynamic reference signals. Therefore, choosing $\tau = ½$, as before, yields

$$\omega_{n_L} = \sqrt{2}$$

Hence, the integral action gains satisfy the equation

$$K_{\phi,z} - K_{\beta,z} = 2 \qquad (25)$$

If a BTT control strategy is employed, implying $K_{\beta,\psi} = K_{\beta,z} = 0$, this defines $K_{\phi,z}$:

$$\left.\begin{aligned} K_{\beta,\psi} &= K_{\beta,z} = 0 \\ K_{\phi,\psi} &= K_{\phi,z} = 2 \end{aligned}\right\} \quad (26)$$

If a STT control strategy is employed, implying $K_{\phi,\psi} = K_{\phi,z} = 0$, this defines $K_{\beta,z}$:

$$\left.\begin{aligned} K_{\phi,\psi} &= K_{\phi,z} = 0 \\ K_{\beta,\psi} &= K_{\beta,z} = -2 \end{aligned}\right\} \quad (27)$$

If a hybrid BTT/STT control strategy is used, we could somewhat arbitrarily choose, e.g.,

$$K_{\phi,\psi} = K_{\phi,z} = 1.5$$

$$K_{\beta,\psi} = K_{\beta,z} = -0.5$$

to weight bank angle twice as heavily as sideslip angle in the controller.

5.3.2. Summary

When integral action is used in the lateral / directional channel, the complete control law is augmented as follows:

$$\phi = A\sin\left\{\frac{\overline{V}^2}{1+\overline{\omega}^2\overline{V}^2}\frac{1}{\cos\overline{\gamma}}\left[\overline{\omega}\overline{V}\sqrt{\frac{1+\overline{\omega}^2\overline{V}^2}{\overline{V}^4}\cos^2\overline{\gamma} - K_{\overline{\beta},\overline{\omega}}^2\overline{\omega}^2} - K_{\overline{\beta},\overline{\omega}}\overline{\omega}\right]\right\}$$
$$- K_{\phi,\psi}\cdot e_\psi - K_{\phi,z_\psi}\cdot z_\psi$$

$$\beta = -K_{\overline{\beta},\overline{\omega}}\cdot\overline{\omega} - K_{\beta,\psi}e_\psi - K_{\beta,z_\psi}\cdot z_\psi$$

5.5. Chapter Summary

Since the aircraft model was linearized in the previous chapter, a linear controller could be implemented in this chapter. The theory of the control system was introduced, with the controller driven by error signals. Since the plant was nonlinear and had to be operated about a nonzero set point, a nonlinear feed-forward design was implemented in

parallel with the linear feedback portion. This feed-forward portion, the "trim solver", was based on the aircraft trim equations derived in Chapter 3. Proportional controllers were designed separately for both lateral and longitudinal channel control, and integral action is added to the lateral channel. Three separate equivalent gain options were calculated for the longitudinal channel, referred to as options (1a), (1b), and (2). A summary of the gains used in the linear compensator is given in Table 5. The nonlinear portion of the control law was summarized previously in Table 3.

Table 5: Linear Control Gains Summary

	Lateral			Longitudinal		
	Generic	BTT	STT	$K_{\alpha\gamma}=K_{\mu V}=0$ (Option 1a)	$K_{\alpha\gamma}=K_{\mu V}=0$ (Option 1b)	$K_{\alpha V}=K_{\mu\gamma}=0$ (Option 2)
Proportional	Eq. 16	Eq. 17	Eq. 18	Eqs. 23	Eqs. 24	Eqs. 25
Integral	Eq. 26	Eqs. 27	Eqs. 28	N/A	N/A	N/A

6. DYNAMICS DEPENDENCE ON OPERATING POINT

The phugoid dynamics aircraft model under consideration is strongly nonlinear. Since high amplitude maneuvers and, conversely, large excursions in the state variables are contemplated, it is most instructive to investigate the linearized dynamics' dependence on the state variables.

6.1. Drag Polar

At trim, the aircraft's "drag polar", or plot of drag vs. velocity, is equal to the thrust required to maintain that trim state. This thrust, calculated previously, was found to be $\bar{\mu} = C_{D0}\bar{q}\bar{V}^2 - \sin\bar{\gamma} + \frac{K}{\bar{V}^2}\left(\bar{\omega}\bar{V}\sin\bar{\phi} + \cos\bar{\phi}\right)^2\cos^2\bar{\gamma}$. At the trim conditions, $\bar{\gamma} = \bar{\omega} = \bar{\phi} = 0$, thrust $\bar{\mu}$ varies with velocity as shown in Figure 5.

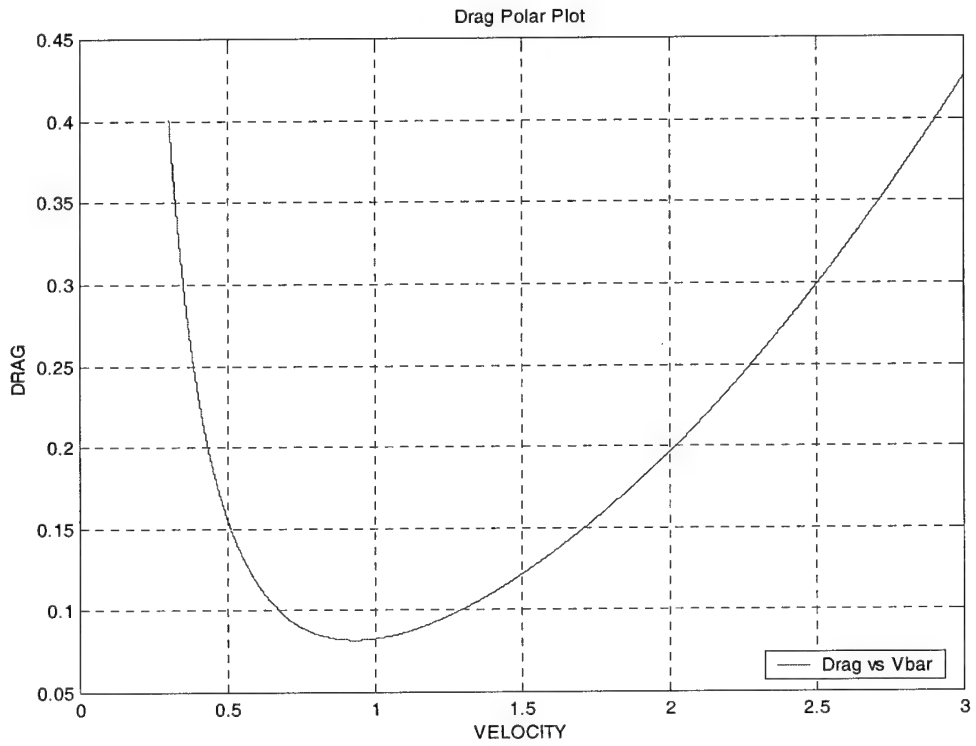

Figure 5: Drag Polar

The minimum drag value 0.0819 occurs at $\overline{V} = 0.9337$. Above this speed, the vehicle experiences increasing profile drag. Below this speed, the aircraft must increase its angle of attack α in order to maintain level flight path angle γ. The required α increases more rapidly at very low speeds, causing increasing induced drag. Thus, there are two values of velocity for a given drag (or thrust level): one "behind the power curve", i.e. at a lower velocity, and another one "ahead of the power curve". The effects of this phenomenon can be seen in Chapter 7, Figure 22, where $\overline{V}$ is reduced to 0.9. Despite the velocity change, the required trim thrust setting $\overline{\mu}$ remains virtually the same because we move to an operating point "behind the power curve."

6.2. Pitch Dynamics Velocity Dependence

We investigate the $\overline{V}$ dependence of the linearized pitch dynamics for $\overline{\omega} = \overline{\gamma} = 0$:

6.2.1. Open-loop plant:

$$A(\overline{V}) = \begin{bmatrix} -2\overline{V}\left(\overline{q}C_{D0} + \dfrac{K}{\overline{V}^4}\right) & 1 \\ -\dfrac{2}{\overline{V}^2} & 0 \end{bmatrix}$$

$$B(\overline{V}) = \begin{bmatrix} 1 & -2K \\ 0 & -\overline{V} \end{bmatrix}$$

Here, the characteristic equation is

$$\lambda^2 + 2\lambda\overline{V}\left(\overline{q}C_{D_0} + \frac{K}{\overline{V}^4}\right) + \frac{2}{\overline{V}^2} = 0$$

Hence, natural frequency ω_n and damping ratio ξ can be written as functions of trim velocity $\overline{V}$:

$$\omega_n(\overline{V}) = \frac{\sqrt{2}}{\overline{V}}$$

$$\xi(\overline{V}) = \frac{\sqrt{2}}{2}\left(\overline{q}C_{D_0}\overline{V}^2 + \frac{K}{\overline{V}^2}\right)$$

The damping ratio is minimal at $\overline{V} = \sqrt[4]{\frac{K}{\overline{q}C_{D_0}}} = 0.9337$ and the minimal damping ratio is

$\xi = \sqrt{2K\overline{q}C_{D_0}} = 0.0579$.

This damping ratio, found near the trim velocity, is very low, and is the reason for the need of the damping controller.

Figure 6: Open-Loop Natural Frequency of Phugoid vs. Velocity

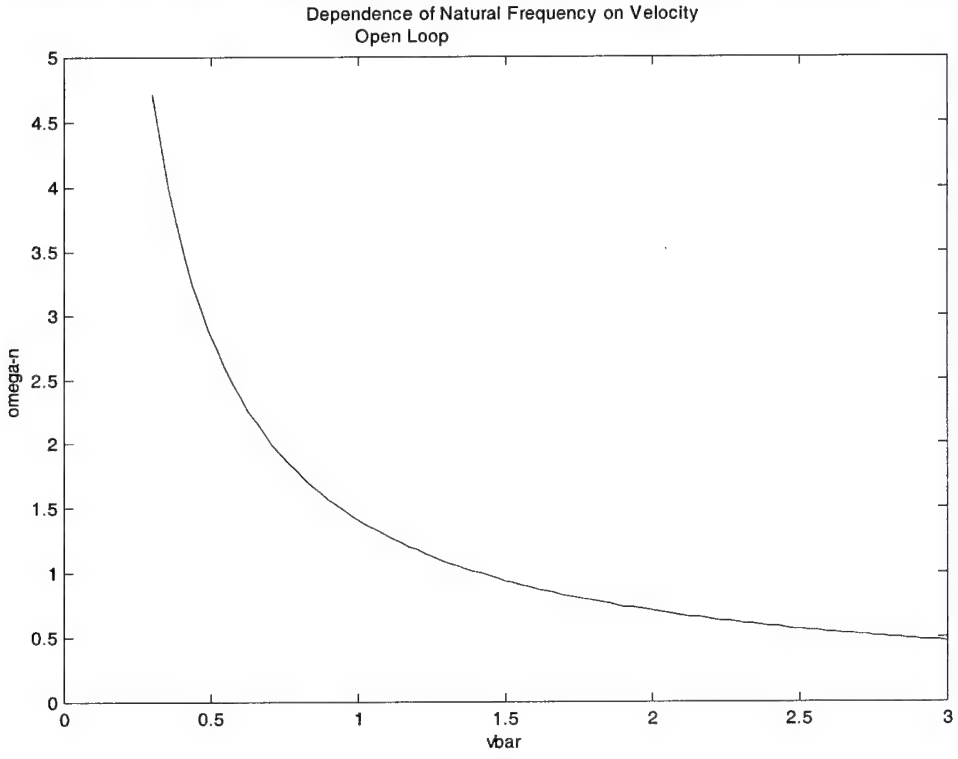

Figure 7: Open-Loop Damping Ratio of Phugoid vs. Velocity

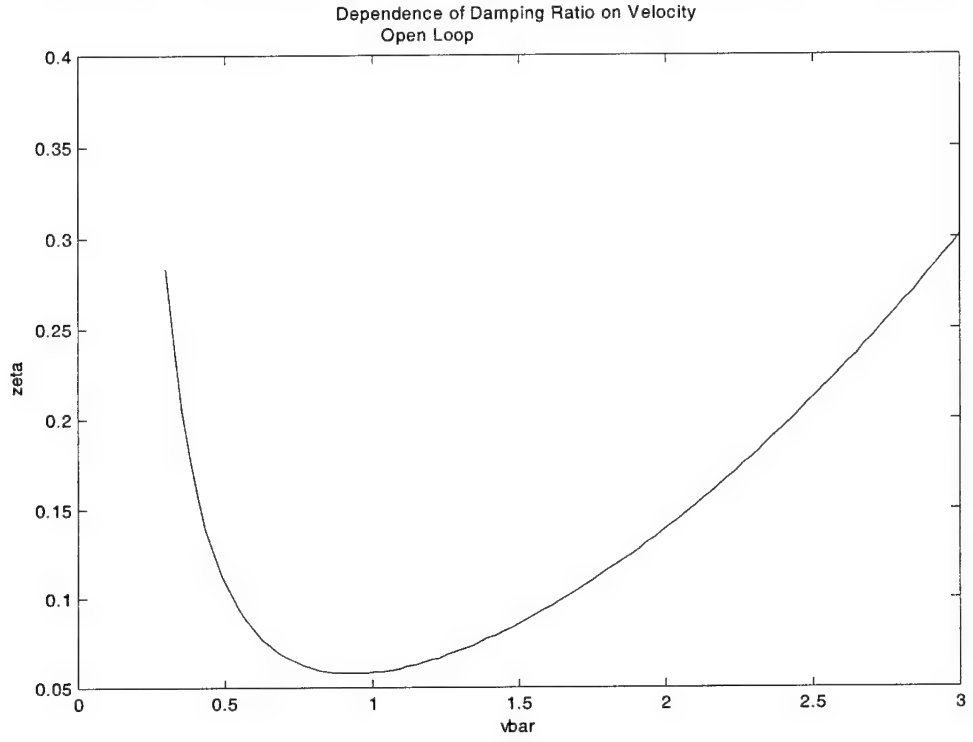

The maximal angle of attack for an actual F-16 is approximately 25° and hence, at 20,000', we calculate the stall speed $\overline{V}_{min} = 0.346$. Also, the approximate value of maximum velocity $\overline{V}_{max} = 3$. Plots of the open-loop natural frequency and damping ratio for the above speed range are shown in Figure 6 and Figure 7.

The open-loop plant is under-damped for all values of velocity of interest. Since the region of interest is squarely centered in the region with lowest damping, the autopilot must furnish additional damping.

6.2.2. Closed-loop Control System

The proportional controller is specified by the gains matrix

$$K_P = \begin{bmatrix} K_{\mu V} & K_{\mu\gamma} \\ K_{\alpha V} & K_{\alpha\gamma} \end{bmatrix}$$

and the closed-loop dynamics are

$$A_{CL} = A + BK_P = \begin{bmatrix} K_{\mu V} - 2\left(\overline{V}\overline{q}C_{D0} + \frac{K}{\overline{V}^3} + K \cdot K_{\alpha V}\right) & 1 + K_{\mu\gamma} - 2K \cdot K_{\alpha\gamma} \\ -\frac{2}{\overline{V}^2} - \overline{V}K_{\alpha V} & -\overline{V}K_{\alpha\gamma} \end{bmatrix}$$

The characteristic equation is

$$\lambda^2 + 2\lambda\left(\overline{q}C_{D_0}\overline{V} + \frac{K}{\overline{V}^4} + K \cdot K_{\alpha V} + \frac{1}{2}\overline{V}K_{\alpha\gamma} - \frac{1}{2}K_{\mu V}\right)$$
$$+ 2\overline{q}C_{D_0}\overline{V}^2K_{\alpha\gamma} + \frac{2}{\overline{V}^2}\left(1 + K_{\mu\gamma} - K \cdot K_{\alpha\gamma}\right) + \overline{V}K_{\alpha V}\left(1 + K_{\mu\gamma} - 2K \cdot K_{\alpha\gamma}\right) - K_{\mu V} \cdot K_{\alpha\gamma} = 0$$

Recall the two solutions of gains option 1, where $K_{\alpha V} = 0$, $K_{\mu\gamma} = 0$, implying that the controller employs thrust to control velocity, and AOA to control flight path angle. In this case,

$$\omega_n = \frac{\sqrt{2}}{\overline{V}}\sqrt{\left(1 - K \cdot K_{\alpha\gamma}\right) + \overline{q}C_{D_0}\overline{V}^3K_{\alpha\gamma} - \frac{1}{2}\overline{V}^2K_{\mu V} \cdot K_{\alpha\gamma}} = \sqrt{3}$$

$$\xi = \frac{\sqrt{2}}{2} \cdot \frac{\overline{q}C_{D_0}\overline{V}^2 + \frac{K}{\overline{V}^3} + \frac{1}{2}\overline{V}^2K_{\alpha\gamma} - \frac{1}{2}\overline{V}K_{\mu V}}{\sqrt{\left(1 - K \cdot K_{\alpha\gamma}\right) + \overline{q}C_{D_0}\overline{V}^3K_{\alpha\gamma} - \frac{1}{2}\overline{V}^2K_{\mu V} \cdot K_{\alpha\gamma}}} = \frac{\sqrt{2}}{2}$$

for $\overline{V} = 1$ (trim state). Natural frequency and damping ratio for gains option 2, in which thrust controls flight path angle and AOA controls velocity, are found similarly. Plots of the closed-loop natural frequency and damping ratio vs. velocity are shown in Figures (8) through (13), where the proportional gains, calculated previously, are repeated below:

$$K_P = \begin{bmatrix} K_{\mu V} & K_{\mu\gamma} \\ K_{\alpha V} & K_{\alpha\gamma} \end{bmatrix} = \begin{bmatrix} -0.5561 & 0 \\ 0 & 1.728 \end{bmatrix} \qquad \text{(Option 1a)}$$

$$K_P = \begin{bmatrix} K_{\mu V} & K_{\mu\gamma} \\ K_{\alpha V} & K_{\alpha\gamma} \end{bmatrix} = \begin{bmatrix} -1.7055 & 0 \\ 0 & 0.5787 \end{bmatrix} \qquad \text{(Option 1b)}$$

$$K_P = \begin{bmatrix} K_{\mu V} & K_{\mu\gamma} \\ K_{\alpha V} & K_{\alpha\gamma} \end{bmatrix} = \begin{bmatrix} 0 & -0.9118 \\ 31.9955 & 0 \end{bmatrix} \qquad \text{(Option 2)}$$

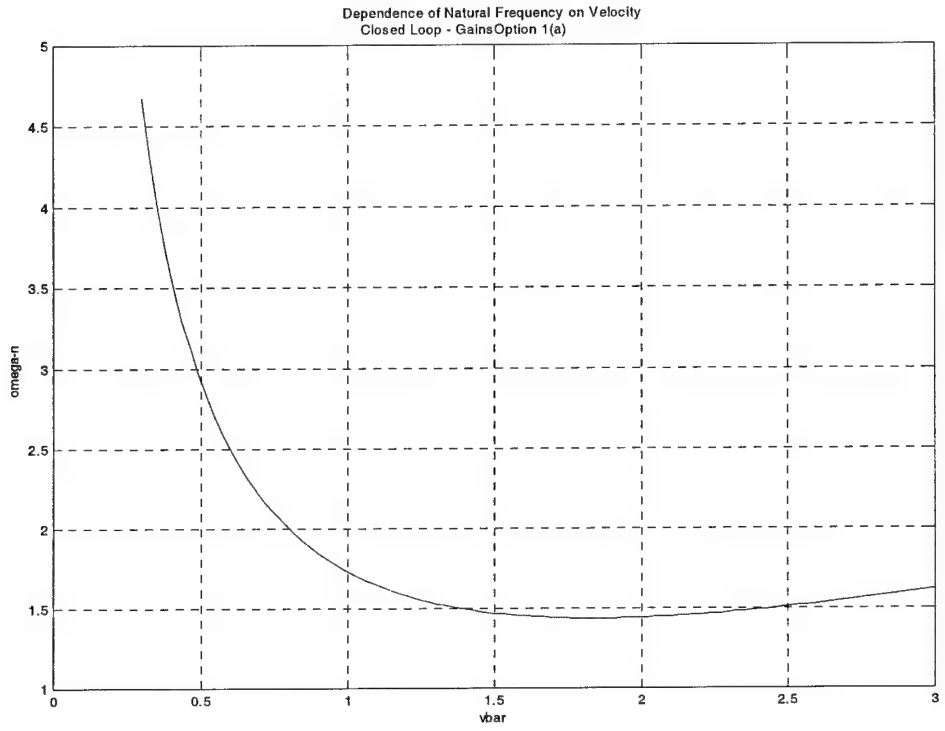

Figure 8: Closed-Loop Natural Frequency vs. Velocity (Option 1a)

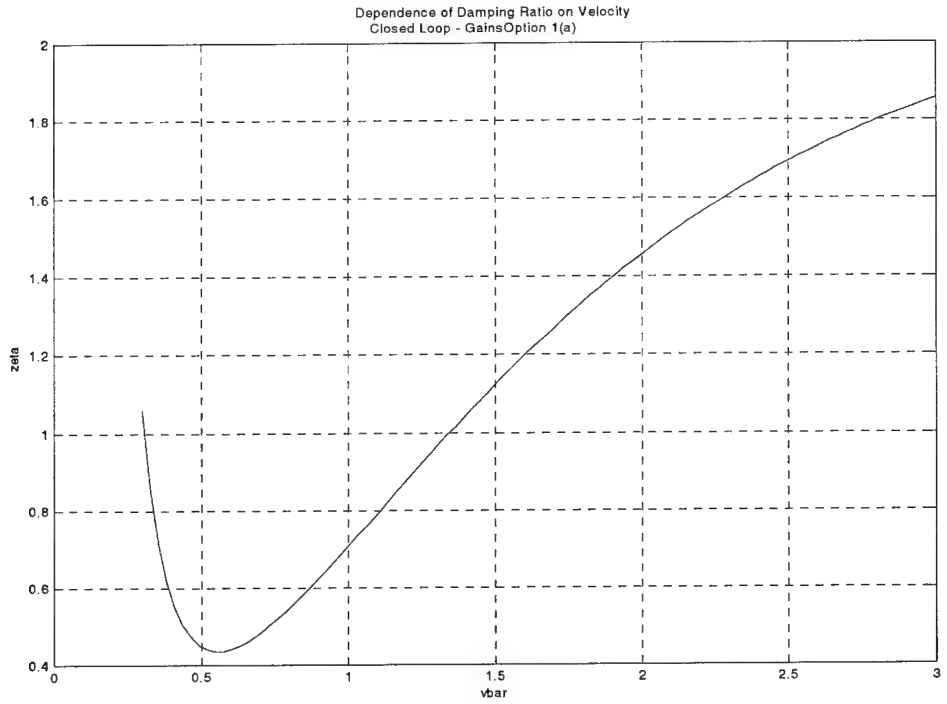

Figure 9: Closed-Loop Damping Ratio vs. Velocity (Option 1a)

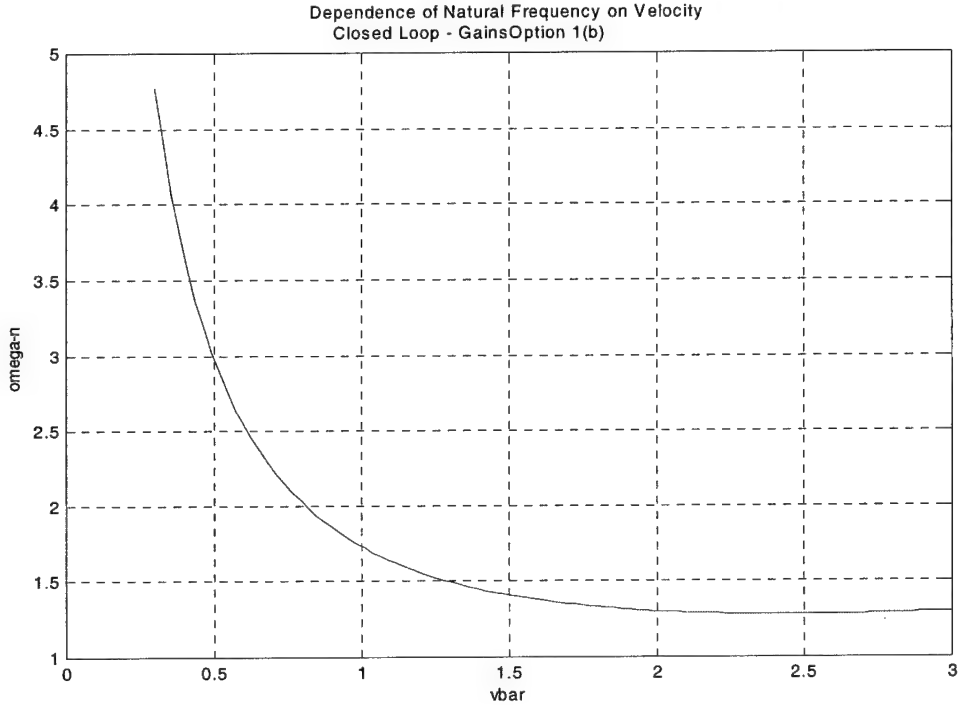

Figure 10: Closed-Loop Natural Frequency vs. Velocity (Option 1b)

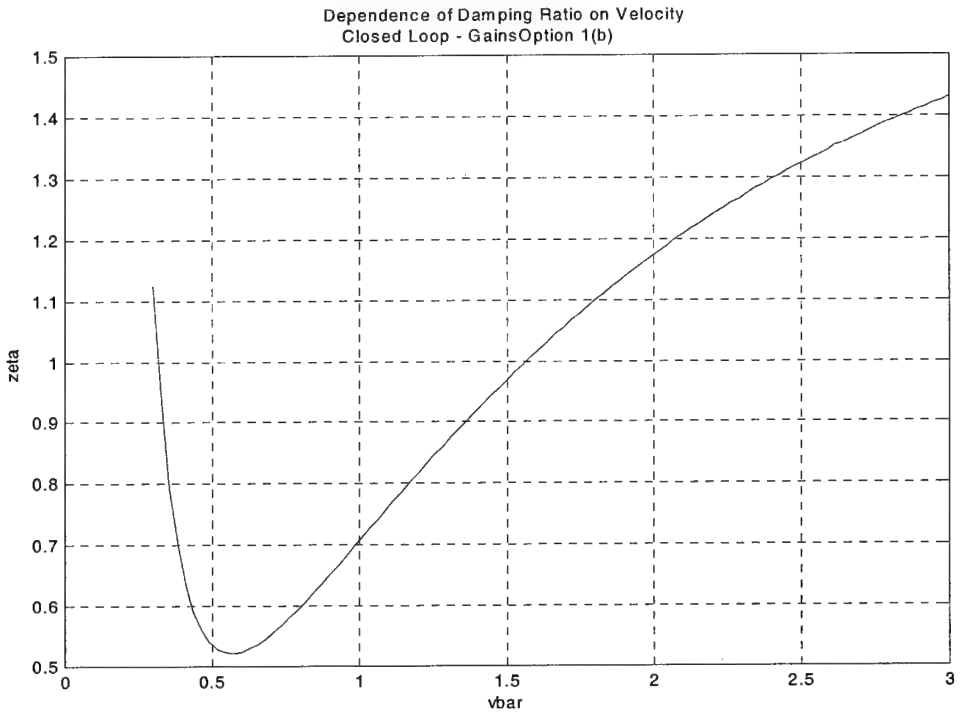

Figure 11: Closed-Loop Damping Ratio vs. Velocity (Option 1b)

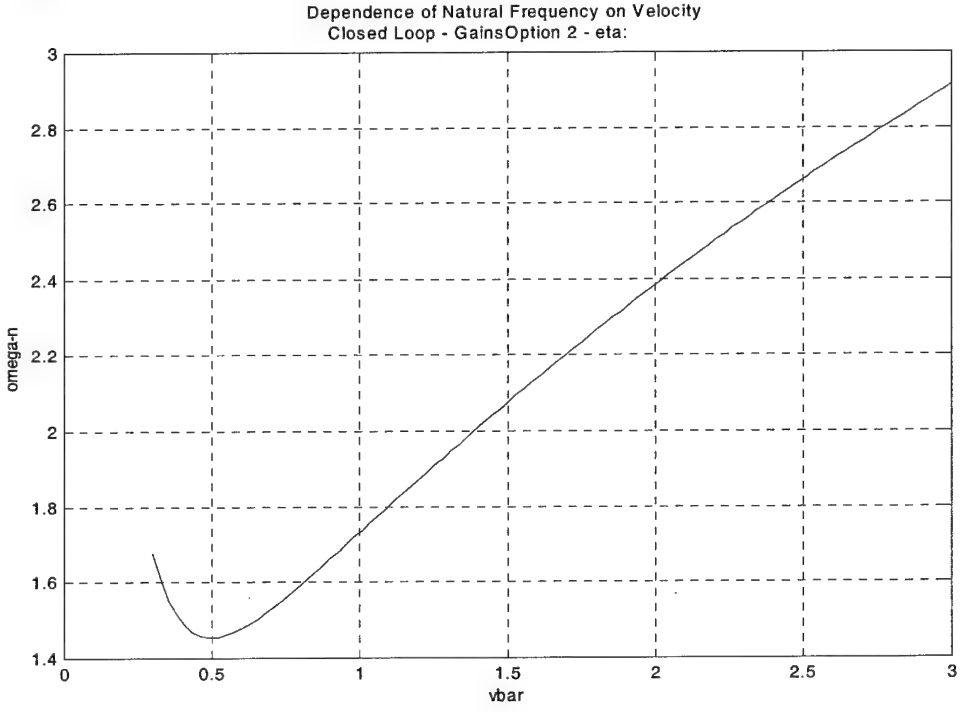

Figure 12: Closed-Loop Natural Frequency vs. Velocity (Option 2)

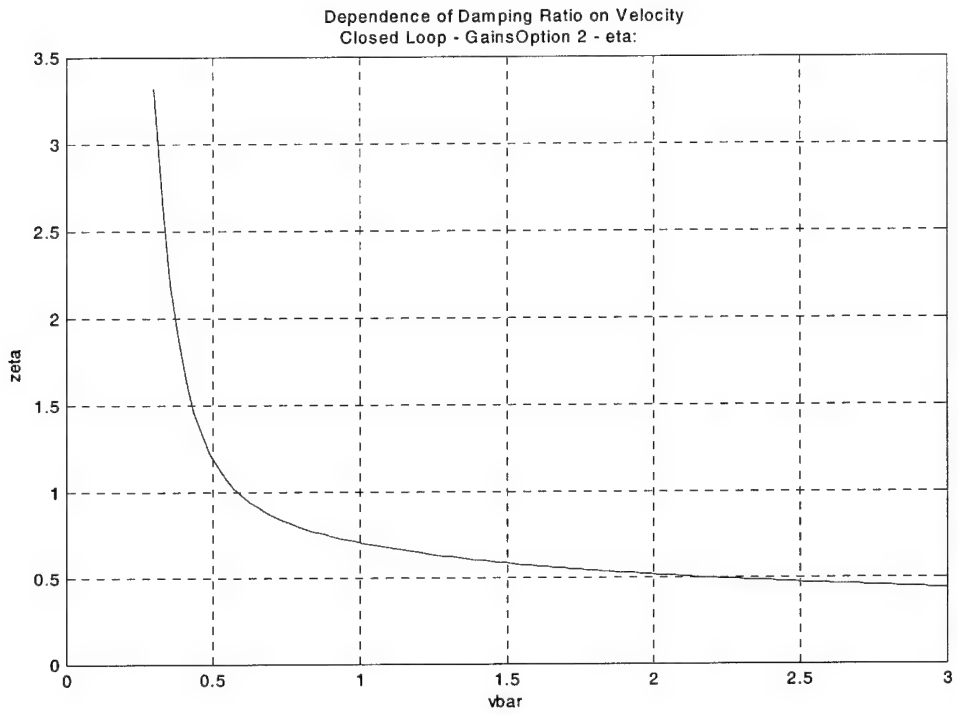

Figure 13: Closed-Loop Damping Ratio vs. Velocity (Option 2)

Using gain options 1a and 1b, the natural frequency of the closed-loop system is fairly constant for high speeds, but it changes rapidly in the low-speed region. The damping ratio is greatly increased over the open-loop case. While the damping ratio at $\overline{V} = 1$ is set at $\sqrt{2}/2$, higher speeds cause much higher damping, and lower speeds yield low damping. The lower damping would be expected to cause larger overshoot in V and γ. This analysis partially explains our simulation results in Chapter 7, where it becomes apparent that the operational envelope of the Mach hold autopilot is more restricted in the low speed range compared to high-speed set points.

The plots for gain option 2 look markedly different. Above the trim velocity, natural frequency increases steadily with velocity, while damping decreases slightly.

Regardless of gain choice, natural frequency and damping ratio increase rapidly for very low velocity, i.e. $V < 0.5$.

Overall, each gain selection appears to have improved the damping ratio across the range of velocities of interest. However, there are both areas in which the damping is too low, and areas in which the damping is higher than desired. Of particular concern are the regions of low damping, which could cause large overshoot by transient signals.

6.3. Pitch Dynamics Flight Path Angle Dependence

We investigate the $\bar{\gamma}$ dependence of the linearized pitch dynamics for $\bar{\omega} = 0, \bar{V} = 1$:

6.3.1. Open-loop plant:

$$A(\bar{\gamma}) = \begin{bmatrix} -2\left(\bar{q}C_{D0} + K\cos^2\bar{\gamma}\right) & \cos\bar{\gamma} \\ -2\cos\bar{\gamma} & -\sin\bar{\gamma} \end{bmatrix}$$

$$B(\bar{\gamma}) = \begin{bmatrix} 1 & -2K\cos\bar{\gamma} \\ 0 & -1 \end{bmatrix}$$

Here, the characteristic equation is

$$\lambda^2 + 2\lambda\left(\bar{q}C_{D_0} + K\cos^2\bar{\gamma} + \frac{1}{2}\sin\bar{\gamma}\right) + 2\left[\cos^2\bar{\gamma} + \left(\bar{q}C_{D_0} + K\cos^2\bar{\gamma}\right)\sin\bar{\gamma}\right] = 0$$

→

$$\omega_n(\bar{\gamma}) = \sqrt{2}\sqrt{\cos^2\bar{\gamma} + \left(\bar{q}C_{D_0} + K\cos^2\bar{\gamma}\right)\sin\bar{\gamma}}$$

$$\xi(\bar{\gamma}) = \frac{\sqrt{2}}{2}\frac{\bar{q}C_{D_0} + K\cos^2\bar{\gamma} + \frac{1}{2}\sin\bar{\gamma}}{\sqrt{\cos^2\bar{\gamma} + \left(\bar{q}C_{D_0} + K\cos^2\bar{\gamma}\right)\sin\bar{\gamma}}}$$

The damping ratio ξ is zero at $\bar{\gamma} = \text{a}\sin\left(\frac{1-\sqrt{1+16K(\bar{q}C_{D_0}+K)}}{4K}\right) = -0.1642 \approx -9.4°$.

For $\bar{\gamma} < -0.1642$, the damping ratio ξ is negative; i.e., the open-loop system is unstable in any significant climb. Additionally, since

$$\cos^2\bar{\gamma} + \left(\bar{q}C_{D_0} + K\cos^2\bar{\gamma}\right)\sin\bar{\gamma} \geq 0$$

$$\rightarrow \quad K\sin^3\bar{\gamma} + \sin^2\bar{\gamma} - \left(\bar{q}C_{D_0} + K\right)\sin\bar{\gamma} - 1 \leq 0,$$

ω_n does not exist for climb angles steeper than $\bar{\gamma} = -1.3511 = -77.4°$; in other words, for $\bar{\gamma} < -77.4°$, the dynamics are not oscillatory. Plots of the open-loop natural frequency and damping ratio for the range of –77.4° to 90° flight path angles are shown in Figure 14 and Figure 15.

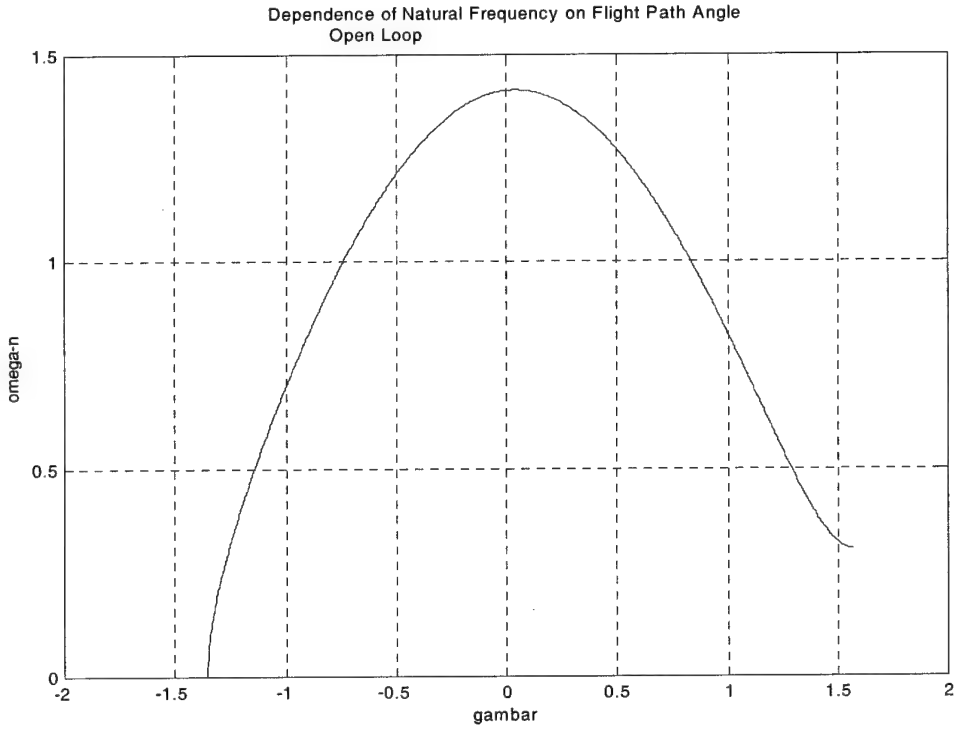

Figure 14: Open-Loop Natural Frequency vs. Flight Path Angle

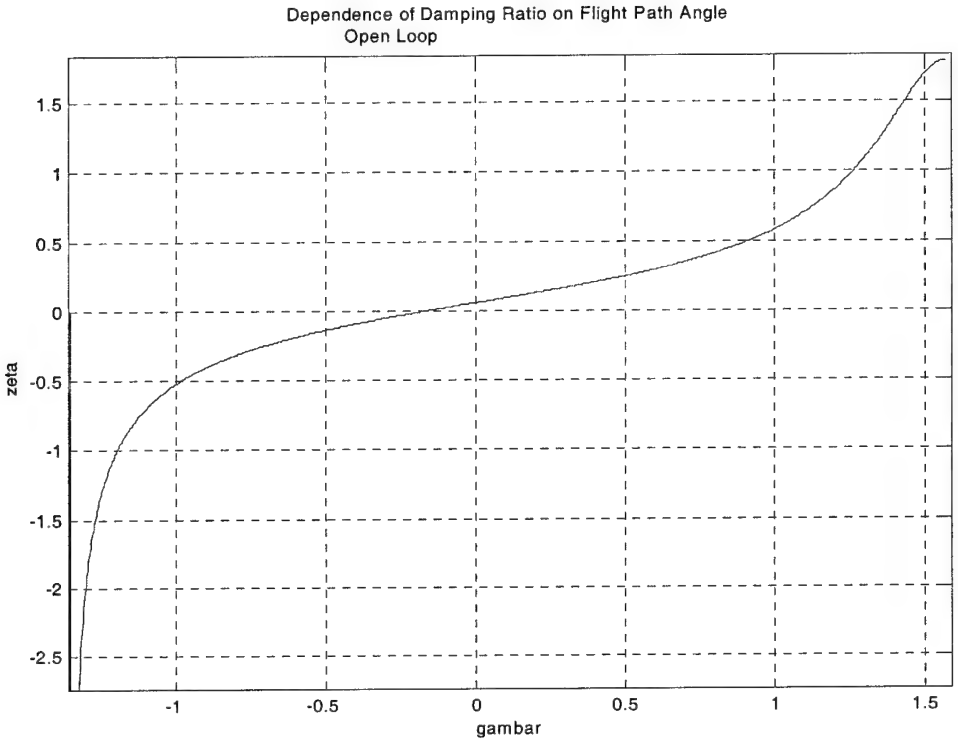

Figure 15: Open-Loop Damping Ratio vs. Flight Path Angle

6.3.2. Closed-loop Control System

The proportional controller is specified by

$$K_P = \begin{bmatrix} K_{\mu V} & K_{\mu\gamma} \\ K_{\alpha V} & K_{\alpha\gamma} \end{bmatrix}$$

and the closed-loop dynamics are

$$A_{CL} = A + BK_P = \begin{bmatrix} K_{\mu V} - 2\left(\bar{q}C_{D0} + K\cos^2\bar{\gamma} - K\cos\bar{\gamma}\cdot K_{\alpha V}\right) & \cos\bar{\gamma} + K_{\mu\gamma} - 2K\cos\bar{\gamma}\cdot K_{\alpha\gamma} \\ -2\cos\bar{\gamma} - K_{\alpha V} & -\sin\bar{\gamma} - K_{\alpha\gamma} \end{bmatrix}$$

The characteristic equation is

$$\lambda^2 + 2\lambda\left(\bar{q}C_{D_0} + K\cos^2\bar{\gamma} + K\cos\bar{\gamma}\cdot K_{\alpha V} + \frac{1}{2}K_{\alpha\gamma} - \frac{1}{2}K_{\mu V} + \frac{1}{2}\sin\bar{\gamma}\right)$$
$$+ \left(2\bar{q}C_{D_0} - K_{\mu V}\right)\left(K_{\alpha\gamma} + \sin\bar{\gamma}\right) + 2\left(\cos^2\bar{\gamma} + K_{\mu\gamma}\cos\bar{\gamma} - K\cdot K_{\alpha\gamma}\cos^2\bar{\gamma} + K\cos^2\bar{\gamma}\sin\bar{\gamma}\right)$$
$$+ K_{\alpha V}\left(\cos\bar{\gamma} + K_{\mu\gamma} + 2K\cos\bar{\gamma}\sin\bar{\gamma}\right) = 0$$

In general,

$$\omega_n = \sqrt{\left(2\bar{q}C_{D_0} - K_{\mu V}\right)\left(K_{\alpha\gamma} + \sin\bar{\gamma}\right) + 2\left(\cos^2\bar{\gamma} + K_{\mu\gamma}\cos\bar{\gamma} - K\cdot K_{\alpha\gamma}\cos^2\bar{\gamma} + K\cos^2\bar{\gamma}\sin\bar{\gamma}\right) + K_{\alpha V}\left(\cos\bar{\gamma} + K_{\mu\gamma} + 2K\cos\bar{\gamma}\sin\bar{\gamma}\right)}$$

$$\xi = \frac{\bar{q}C_{D_0} + K\cos^2\bar{\gamma} + K\cos\bar{\gamma}\cdot K_{\alpha V} + \frac{1}{2}K_{\alpha\gamma} - \frac{1}{2}K_{\mu V} + \frac{1}{2}\sin\bar{\gamma}}{\omega_n}$$

In case 1, where $K_{\alpha V} = 0$, $K_{\mu\gamma} = 0$,

$$\omega_n = \sqrt{2}\sqrt{\left(\bar{q}C_{D_0} - \frac{1}{2}K_{\mu V}\right)\left(K_{\alpha\gamma} + \sin\bar{\gamma}\right) + \cos^2\bar{\gamma} - K\cdot K_{\alpha\gamma}\cos^2\bar{\gamma} + K\cos^2\bar{\gamma}\sin\bar{\gamma}}$$

$$\xi = \frac{\sqrt{2}}{2}\cdot\frac{\bar{q}C_{D_0} + K\cos^2\bar{\gamma} + \frac{1}{2}K_{\alpha\gamma} - \frac{1}{2}K_{\mu V} + \frac{1}{2}\sin\bar{\gamma}}{\sqrt{\left(\bar{q}C_{D_0} - \frac{1}{2}K_{\mu V}\right)\left(K_{\alpha\gamma} + \sin\bar{\gamma}\right) + \cos^2\bar{\gamma} - K\cdot K_{\alpha\gamma}\cos^2\bar{\gamma} + K\cos^2\bar{\gamma}\sin\bar{\gamma}}}$$

In case 2, where $K_{\alpha\gamma} = 0$, $K_{\mu V} = 0$,

$$\omega_n = \sqrt{2}\sqrt{\bar{q}C_{D_0}\sin\bar{\gamma} + \cos^2\bar{\gamma} + K_{\mu\gamma}\cos\bar{\gamma} + K\cos^2\bar{\gamma}\sin\bar{\gamma} + K_{\alpha V}\left(\cos\bar{\gamma} + K_{\mu\gamma} + 2K\cos\bar{\gamma}\sin\bar{\gamma}\right)}$$

$$\xi = \frac{\sqrt{2}}{2}\cdot\frac{\bar{q}C_{D_0} + K\cos^2\bar{\gamma} + K\cos\bar{\gamma}\cdot K_{\alpha V} + \frac{1}{2}\sin\bar{\gamma}}{\sqrt{\bar{q}C_{D_0}\sin\bar{\gamma} + \cos^2\bar{\gamma} + K_{\mu\gamma}\cos\bar{\gamma} + K\cos^2\bar{\gamma}\sin\bar{\gamma}}}$$

In either case, setting $\bar{\gamma} = 0$ returns the expected

$$\omega_n = \sqrt{3}$$

$$\xi = \frac{\sqrt{2}}{2}$$

Plots of the closed-loop natural frequency and damping ratio vs. flight path angle are shown in Figures 16 through 20, where the proportional gains are

$$K_P = \begin{bmatrix} K_{\mu V} & K_{\mu\gamma} \\ K_{\alpha V} & K_{\alpha\gamma} \end{bmatrix} = \begin{bmatrix} -0.5561 & 0 \\ 0 & 1.728 \end{bmatrix} \quad \text{(Option 1a)}$$

$$K_P = \begin{bmatrix} K_{\mu V} & K_{\mu\gamma} \\ K_{\alpha V} & K_{\alpha\gamma} \end{bmatrix} = \begin{bmatrix} -1.7055 & 0 \\ 0 & 0.5787 \end{bmatrix} \quad \text{(Option 1b)}$$

$$K_P = \begin{bmatrix} K_{\mu V} & K_{\mu\gamma} \\ K_{\alpha V} & K_{\alpha\gamma} \end{bmatrix} = \begin{bmatrix} 0 & -0.9118 \\ 31.9955 & 0 \end{bmatrix} \quad \text{(Option 2)}$$

Recall that gains found by options (1a) and (1b) were calculated by assuming the controller changes thrust to control velocity, and AOA to control flight path angle, while the gains found by option (2) were calculated by assuming controller changes AOA to control velocity, and thrust to control flight path angle.

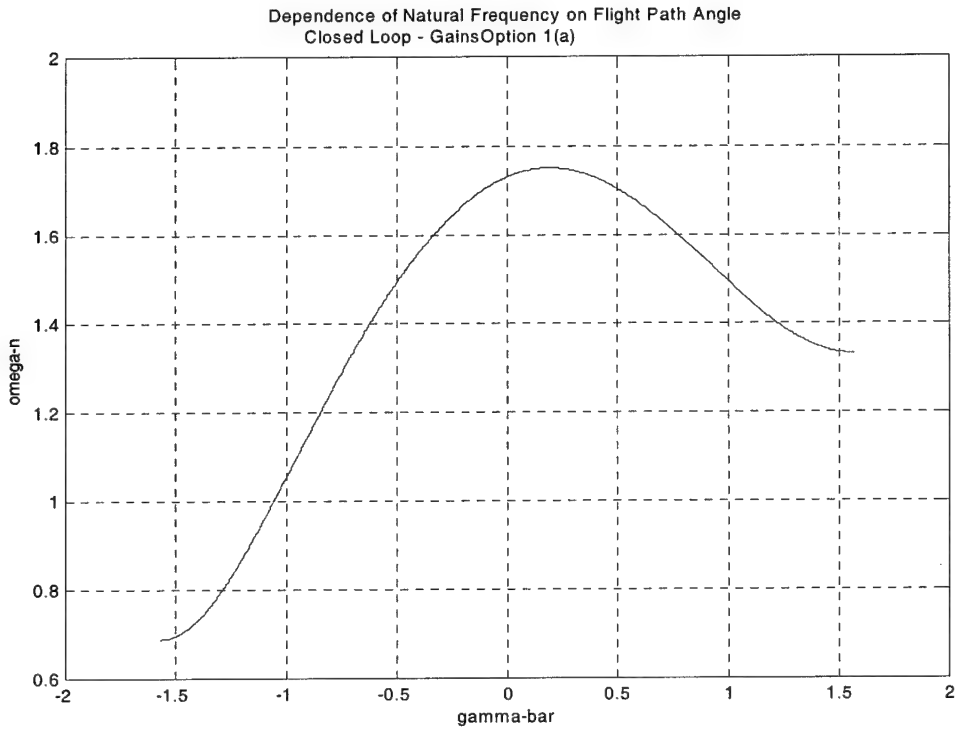

Figure 16: Closed-Loop Natural Frequency vs. Flight Path Angle (1a)

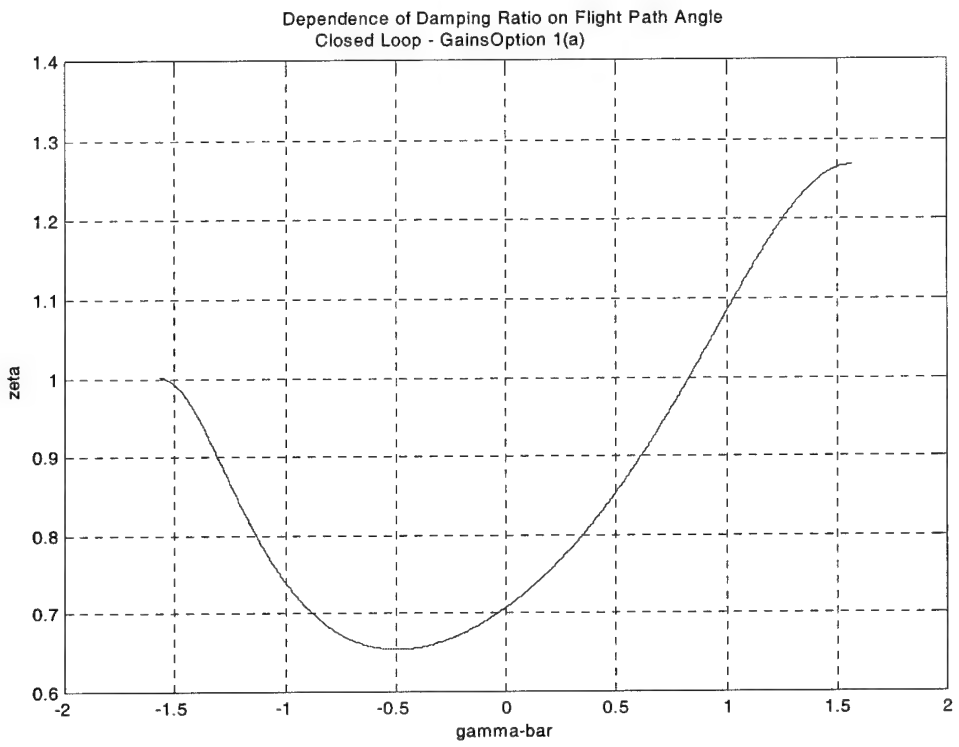

Figure 17: Closed-Loop Damping Ratio vs. Flight Path Angle (1a)

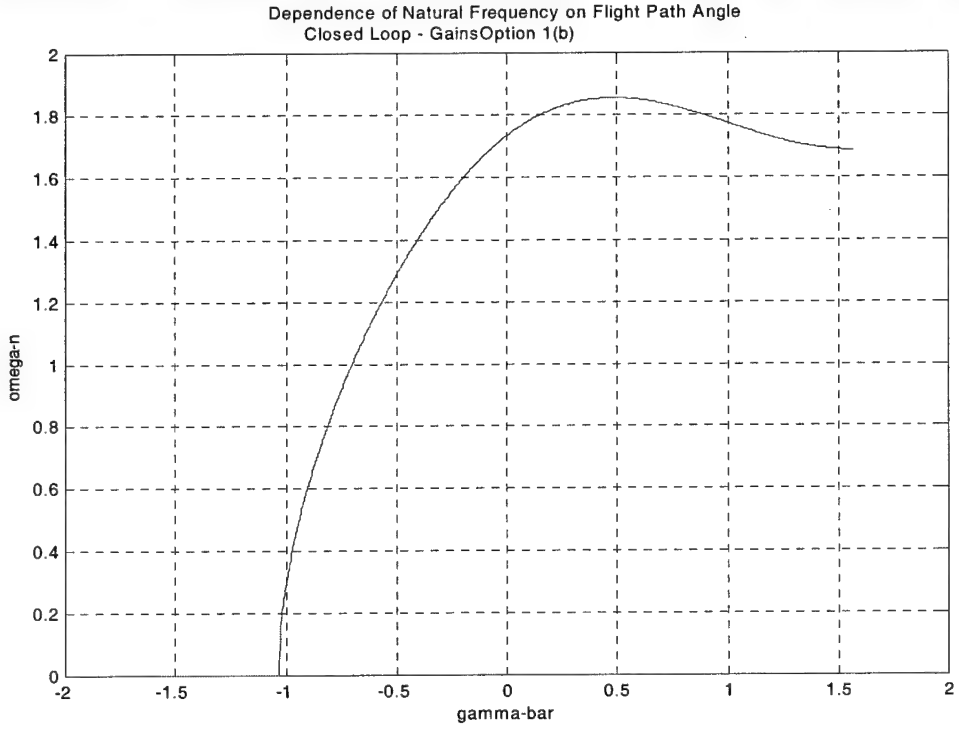

Figure 18: Closed-Loop Natural Frequency vs. Flight Path Angle (1b)

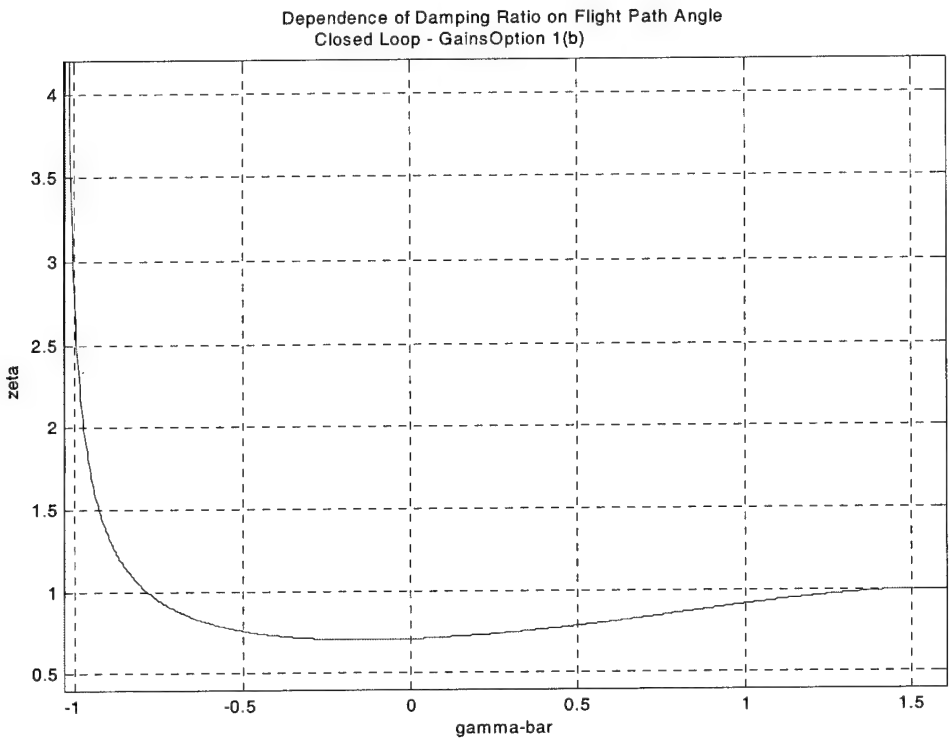

Figure 19: Closed-Loop Damping Ratio vs. Flight Path Angle (1b)

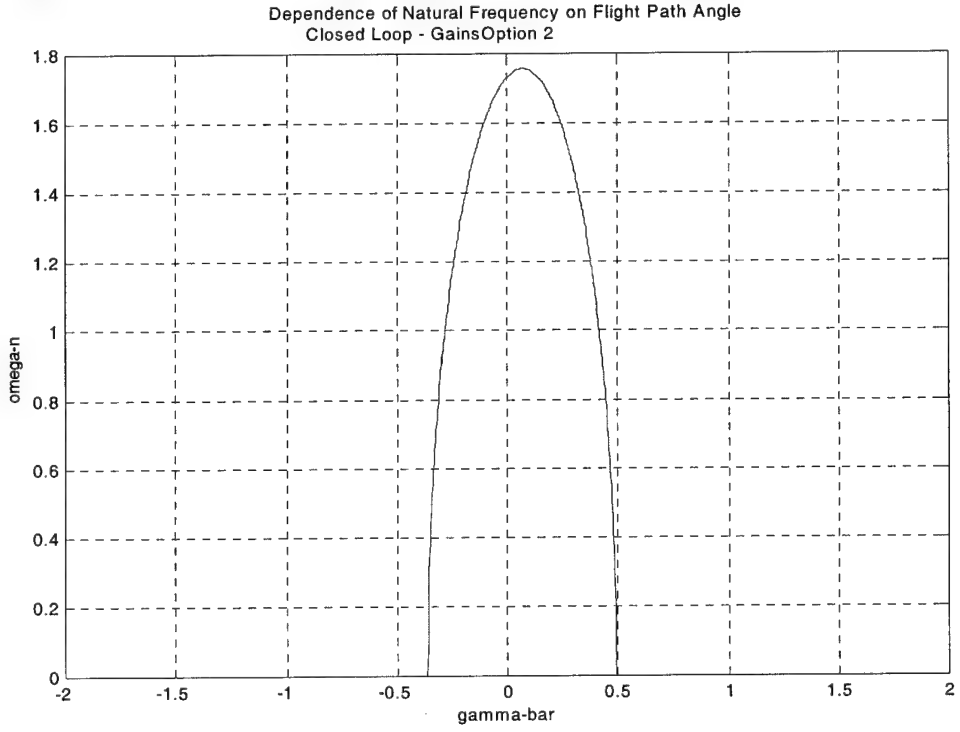

Figure 20: Closed-Loop Natural Frequency vs. Flight Path Angle (2)

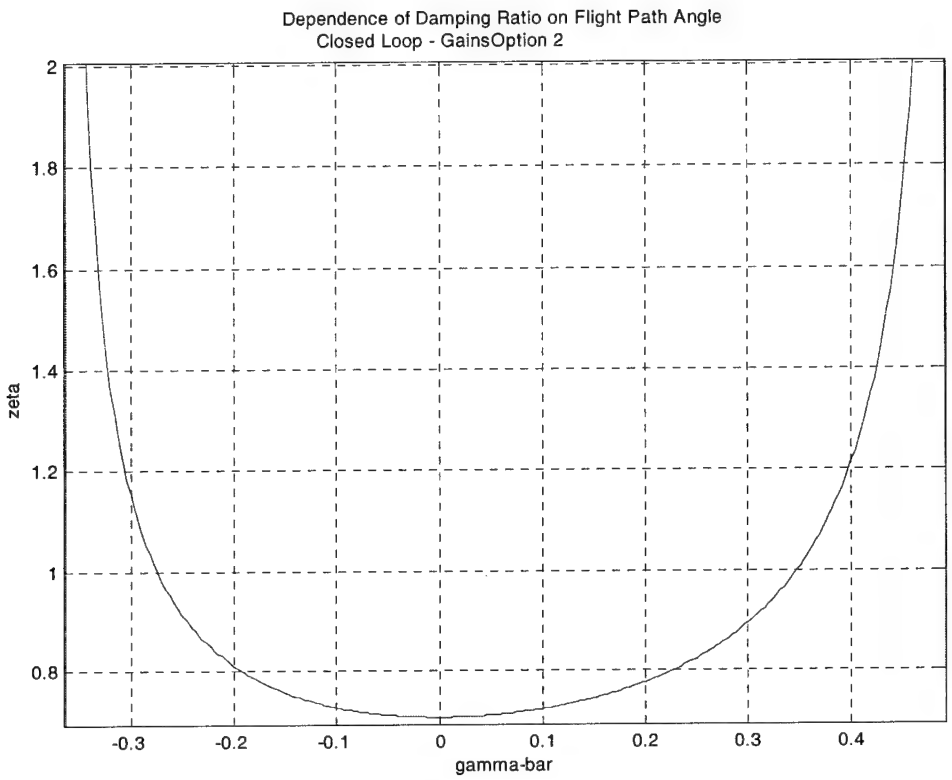

Figure 21: Closed-Loop Damping Ratio vs. Flight Path Angle (2)

Figure 16 and Figure 17 show the natural frequency and damping ratio versus flight path angle for the system with compensator gains set as in option (1a). The peak ω_n, approximately the desired $\sqrt{3}$, is found near $\bar{\gamma} = 0$. The natural frequency drops off above and below this peak, with a minimum of 0.7 in a vertical climb. Similarly, the damping ratio is near its minimum at $\bar{\gamma} = 0$, increasing above and below this point to a maximum 1.27 in a vertical dive.

Figure 18 and Figure 19 show the natural frequency and damping ratio versus flight path angle for the system with compensator gains set as in option (1b). While the peak ω_n again is found in a slight dive, at approximately $\gamma = -1$ the natural frequency

goes to zero, while the damping ratio goes to infinity. Climbs steeper than this exhibit unstable dynamics.

Figures 20 and 21 show the natural frequency and damping ratio versus flight path angle for the system with compensator gains set as in option (2). The peak ω_n, approximately the desired $\sqrt{3}$, again is found near $\bar{\gamma} = 0$. The frequency drops off sharply above and below this peak, reaching zero at approximately –0.35 and 0.50. Similarly, the damping ratio is near its minimum at $\bar{\gamma} = 0$, increasing above and below this point toward infinity at –0.35 and 0.50. Outside this range, the system is unstable.

In summary:

- Gains option 1a yields stable dynamics for all velocities and flight path angles of interest. This is the best set of gains.
- Gains option 1b yields stable dynamics except for a small range of steep vertical climb angles.
- Gains option 2 yields stable dynamics only for a narrow region around a horizontal flight path.

6.4. Dynamic Reference Signals

We can deal with piecewise constant reference signals r, provided that the periods of constancy ≥ settling time t_s of closed-loop flight control system. Hence, when employing a zero-order hold (ZOH) device to sample the dynamic reference signals r_V, r_γ, and r_ω, we should use a sampling rate for r_V, r_γ, of at least

$$f_{s_P} = \frac{1}{t_{s_P}} \qquad (28)$$

and, for r_ω, use a sapling rate of at least

$$f_{s_L} = \frac{1}{t_{s_\psi}} \qquad (29)$$

where t_{s_P} is the settling time of the pitch channel variables (the v and γ states) and t_{s_ψ} is the settling time in the lateral/directional channel (the heading ψ). Moreover, $t_{s_P} = \max\left(t_{s_V}, t_{s_\gamma}\right)$, where t_{s_V} and t_{s_γ} are the settling times for the V and γ states, respectively.

Thus, the following conditions must hold:

- $f_s = \frac{1}{t_s}$ *(30)*

precludes the "windup" of the trim calculation-based control system. Windup is a stability problem with PI controllers applied to actuators that can saturate. If the proportional channel saturates the actuators, the integrating channel may build up huge, saturating error output levels. As the proportional controller causes the error to decrease, the integrating channel continues to "charge". The integrator output does not begin to decrease until the error changes its sign. Thus, the actuators can remain saturated even if the output is at the desired level.[7]

Next, in order to achieve good tracking performance, enforce:

- $f_s \geq 2f_B$ *(31)*

This is Shannon's sampling rate requirement, where f_B is the bandwidth of the pertinent reference signal. Thus, condition **(31)** imposes a bandwidth constraint on the reference

signal. Specifically, we require $f_{s_P} \geq 2f_{B_{\overline{V}}}$, $f_{s_P} \geq 2f_{B_{\overline{\gamma}}}$, and $f_{s_L} \geq 2f_{B_{\overline{\omega}}}$, where $f_{B_{\overline{V}}}$, $f_{B_{\overline{\gamma}}}$, and $f_{B_{\overline{\omega}}}$ are the bandwidths of the $\overline{V}$, $\overline{\gamma}$, and $\overline{\omega}$ reference signals, respectively.

Finally, we require:

- A small overshoot is required, so that the response of the dynamical system, e.g., $\psi(t)$, indeed tracks the piecewise constant reference signal at the output of the ZOH device. This mandates "good" damping ratios, e.g.,

$$\xi_P = \frac{1}{\sqrt{2}}, \quad \xi_L = \frac{1}{\sqrt{2}} \qquad (32)$$

Obviously, condition **(22)** ➔ output of ZOH device is close to the dynamic reference signal, e.g., $\psi(t)$. Hence, if the three conditions **(30)**-**(32)** are satisfied, good tracking of a dynamic reference signal is achieved.

Remark: Note that both t_s and the degree of overshoot are determined by the linear control module, viz., the gains, K_P and K_I of the controller. Several parameters used in calculating the gains, i.e., ω_n, were chosen arbitrarily. If the dynamic reference signals to be tracked are of sufficiently high frequency and / or amplitude, they could begin to act as constraints on the choices of these parameters.

6.5. Chapter Summary

The phugoid dynamics aircraft model under consideration is strongly nonlinear. Since high amplitude maneuvers and, consequently, large excursions in the state variables are contemplated, it is most instructive to investigate the linearized dynamics' dependence on the state variables. Thus, recall that the small-signal linear controller module is based on the linearized plant dynamics model. It was found that the linearized system's dynamics are strongly dependent on these state variables. The drag polar plot

showed that the aircraft flies "behind the power curve", i.e., in a region where it must increase trim thrust to decrease trim velocity, in a significant portion of its operational envelope. Even when operated in closed-loop, the effective values of ω_n and ξ vary greatly with velocity. The relationship between these design parameters and flight path angle are even more extreme; control options (1b) and (2) are unstable for some flight path angles. Given the failure of these two gain solutions, only gains option (1a) will tested with dynamic reference signals and roll disturbances in the following chapter. Finally, an analysis of requirements for accurate tracking of dynamic references was performed.

7. SIMULATION RESULTS

The Phugoid Damping flight control system is simulated using the Matlab Simulink software. Subroutines for the trim solving equations, the aircraft dynamics equations, and a function to translate the dynamics into the (x,y,z) coordinate system are each placed in one of Simulink's "S-Function" blocks, while the rest of the simulation follows the structure given previously in Figure 3. The controller is first exercised with set point commands, the specifics of which are described in each figure. The objective is to establish the operational envelope of the controller. In addition, the controller is also exercised with dynamic reference signals, thus demonstrating phugoid damping control. For all simulations, the initial reference signal $\left(\overline{V}, \overline{\gamma}, \overline{\omega}\right) = (1, 0, 0)$, while the set point or dynamic commands are intended to force the initial states toward some desired states. A Matlab "M-File" prepares the desired gains option (1a, 1b, or 2), invokes the "ODE45" Simulink differential equations solver / simulator, plots the results, and adds the simulation parameters text descriptions to the diagram.

The simulation results are summarized in the figures below. A series of maneuvers types are simulated with the intent of examining the system performance at the limits of the controller's operational envelope. High amplitude excursions in velocity, flight path angle, and yaw angle are commanded, followed by simultaneously commanded, viz., multivariable, set point changes for all three states.

After exercising each of the three gain configurations in this manner, the roll disturbance rejection capability is examined using the option (1a) gains, which were found to yield the widest operational envelope. Finally, the system's ability to track a dynamic reference input is determined, thus demonstrating phugoid damping control.

7.1 Gain Option 1(a)

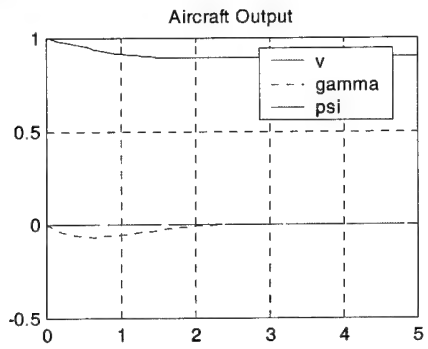

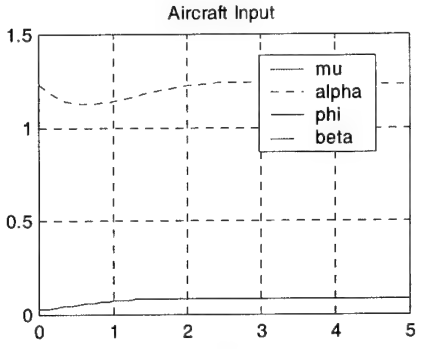

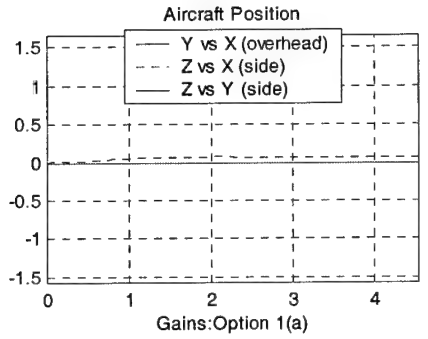

		-INITIAL-	-DESIRED-
STATE:	V:	1.00	0.90 (350 kts)
	gamma:	0.00	0.00 (0 deg)
	omega:	0.00	0.00 (0 deg/sec)
	psi0:		0.00 (0 deg)
CONTROL:	mu:	0.08	0.08 (8%)
	alpha:	1.00	1.23 (4 deg)
	phi:	0.00	0.00 (0 deg)
	beta:	0.00	0.00 (0 deg)

Figure 22: Decrease Speed to 0.9

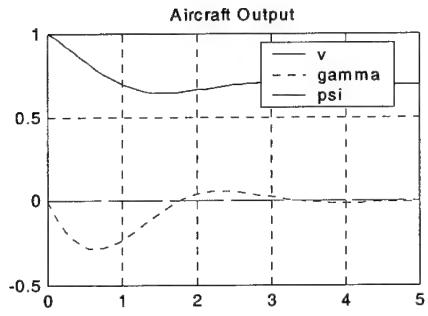

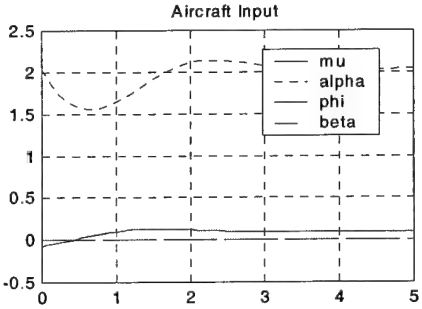

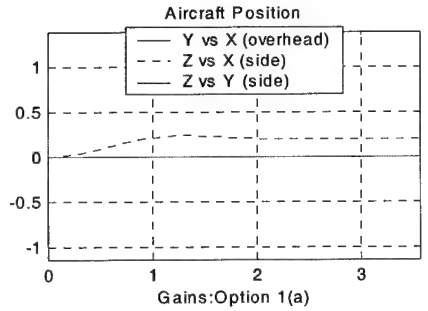

		-INITIAL-	-DESIRED-
STATE:	V:	1.00	0.70 (272 kts)
	gamma:	0.00	0.00 (0 deg)
	omega:	0.00	0.00 (0 deg/sec)
	psi0:		0.00 (0 deg)
CONTROL:	mu:	0.08	0.10 (10%)
	alpha:	1.00	2.04 (7 deg)
	phi:	0.00	0.00 (0 deg)
	beta:	0.00	0.00 (0 deg)

Figure 23: Decrease Speed to 0.7

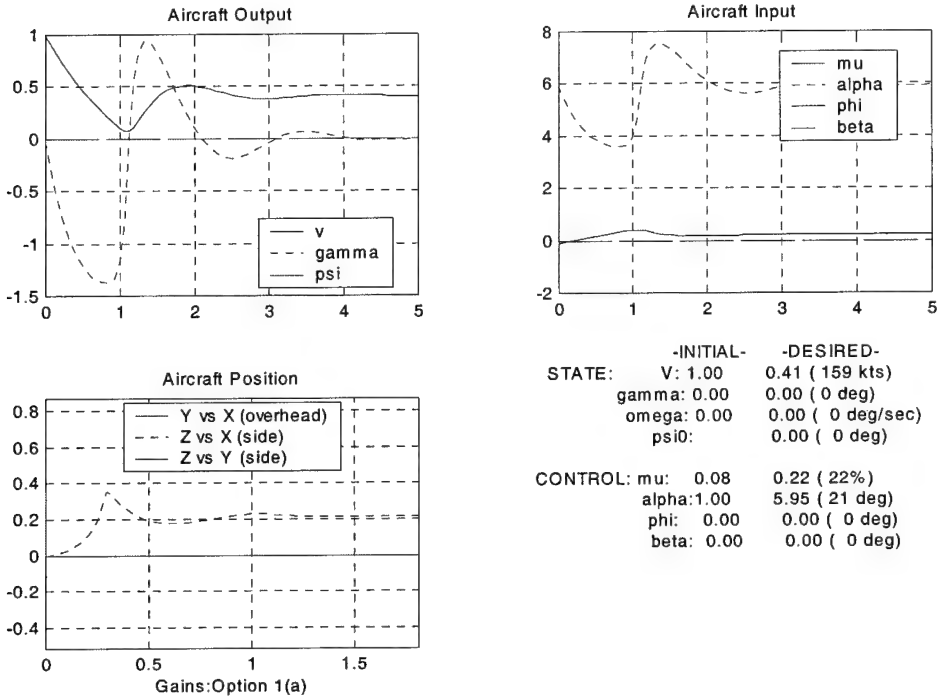

Figure 24: Decrease Speed to 0.41

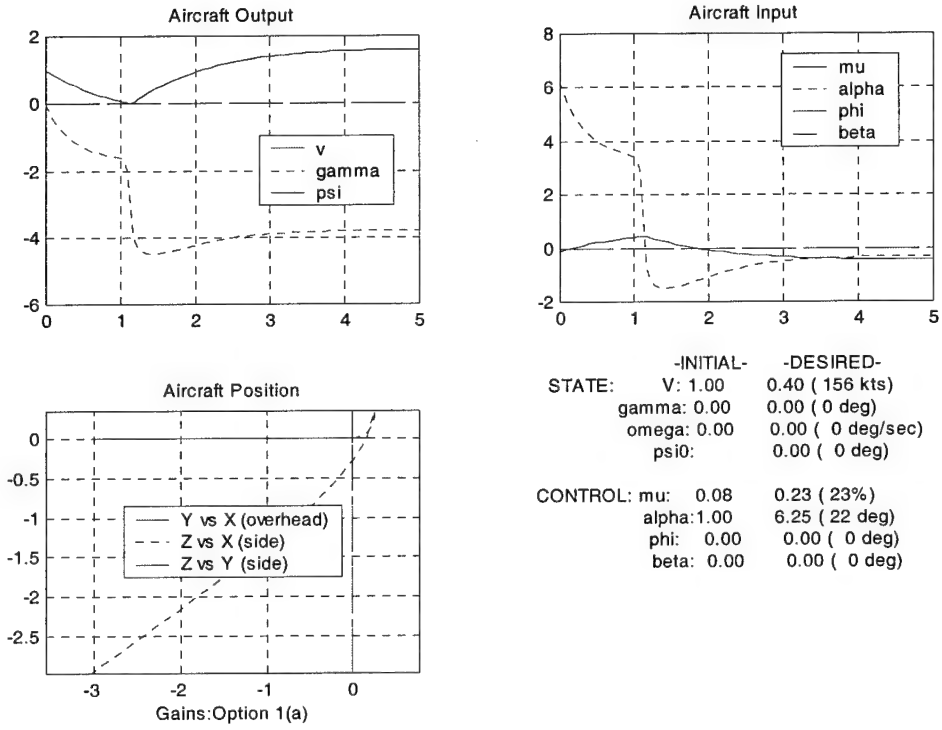

Figure 25: Decrease Speed to 0.40

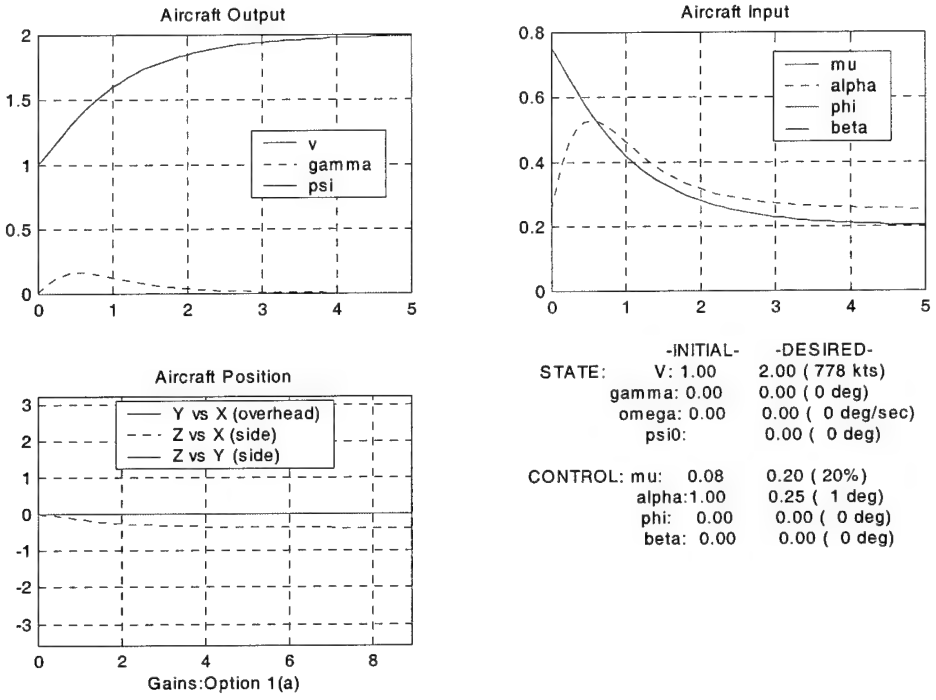

Figure 26: Increase Speed to 2

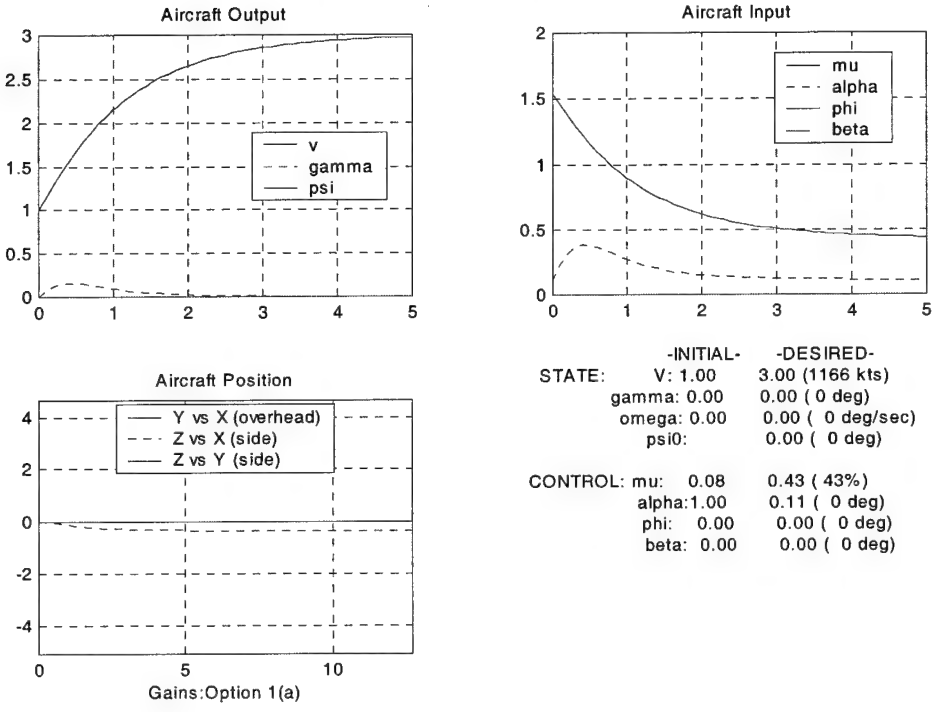

Figure 27: Increase Speed to 3

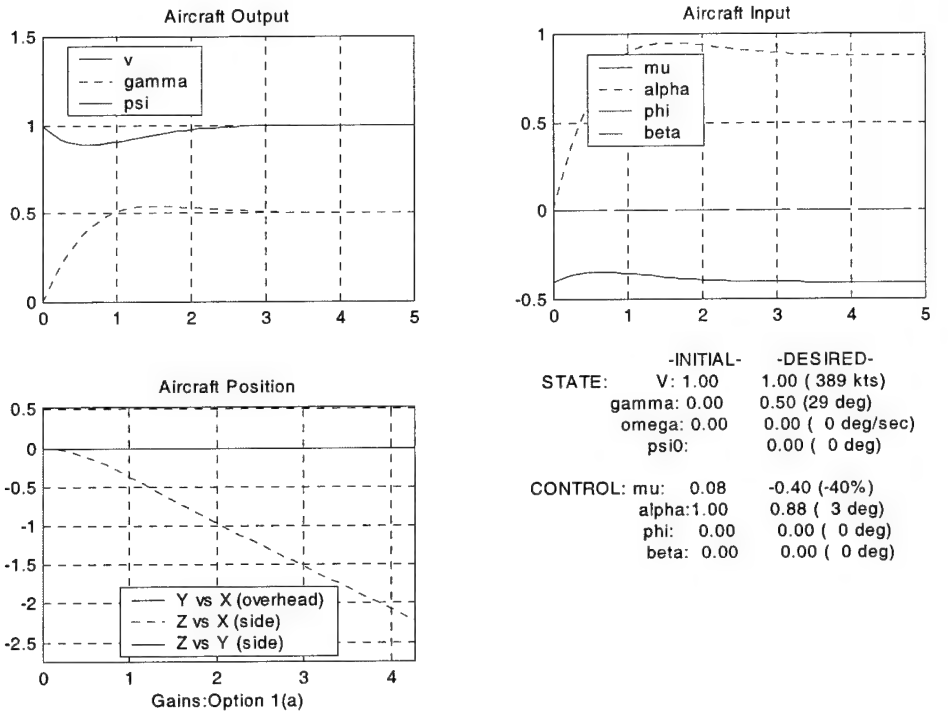

Figure 28: Dive

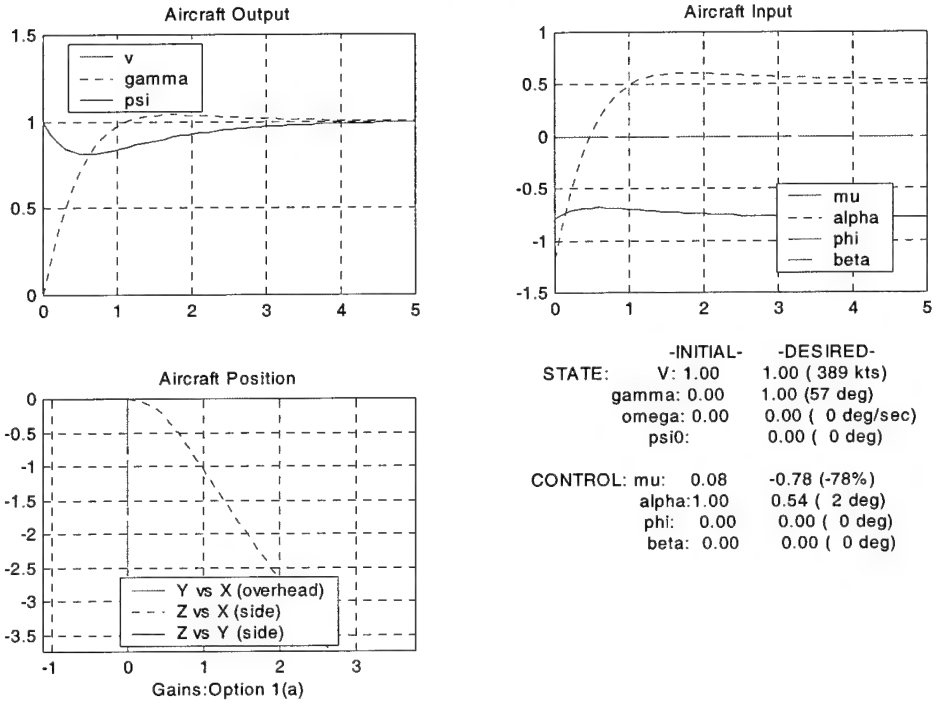

Figure 29: Steep Dive

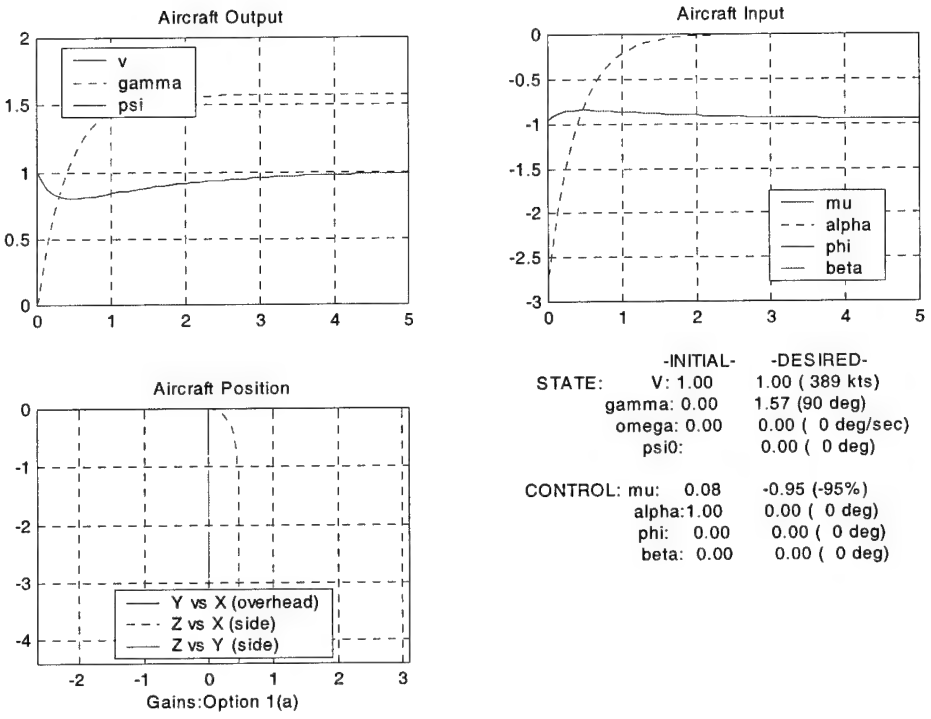

Figure 30: Vertical Dive

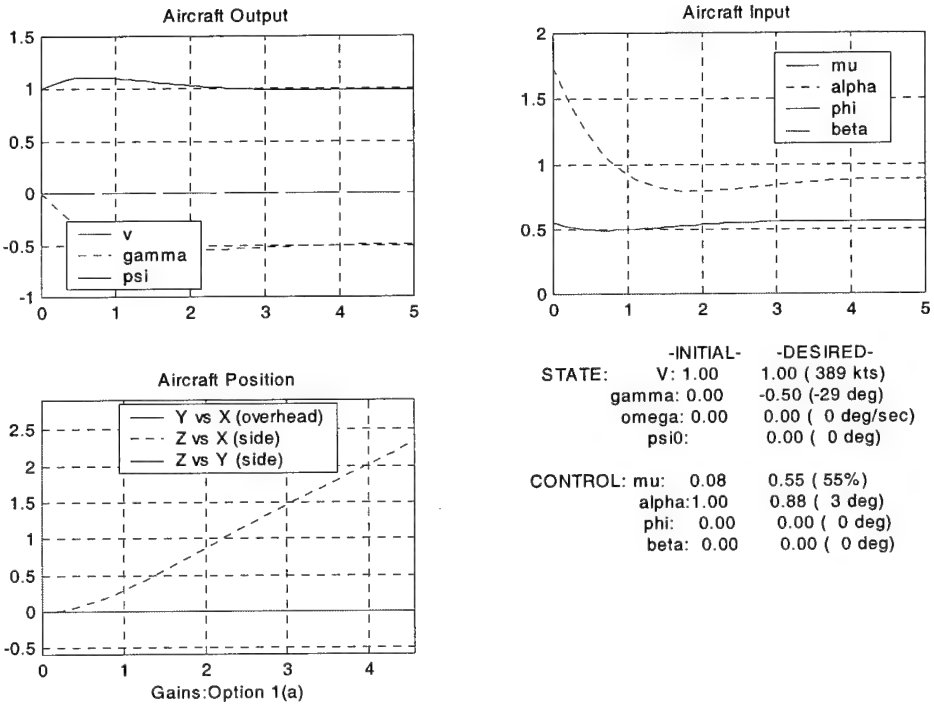

Figure 31: Climb

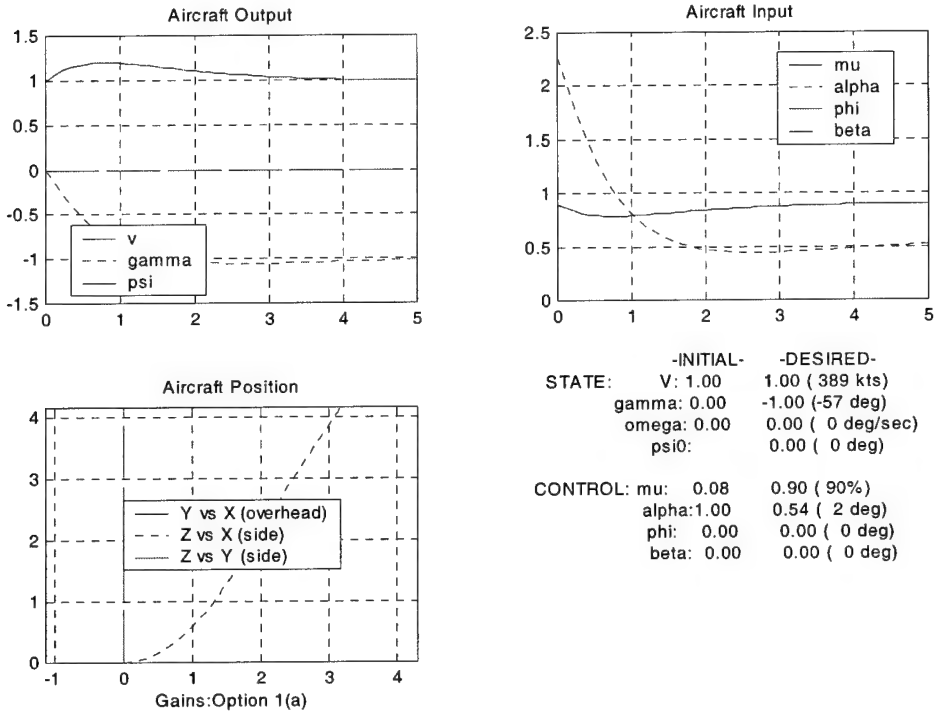

Figure 32: Steep Climb

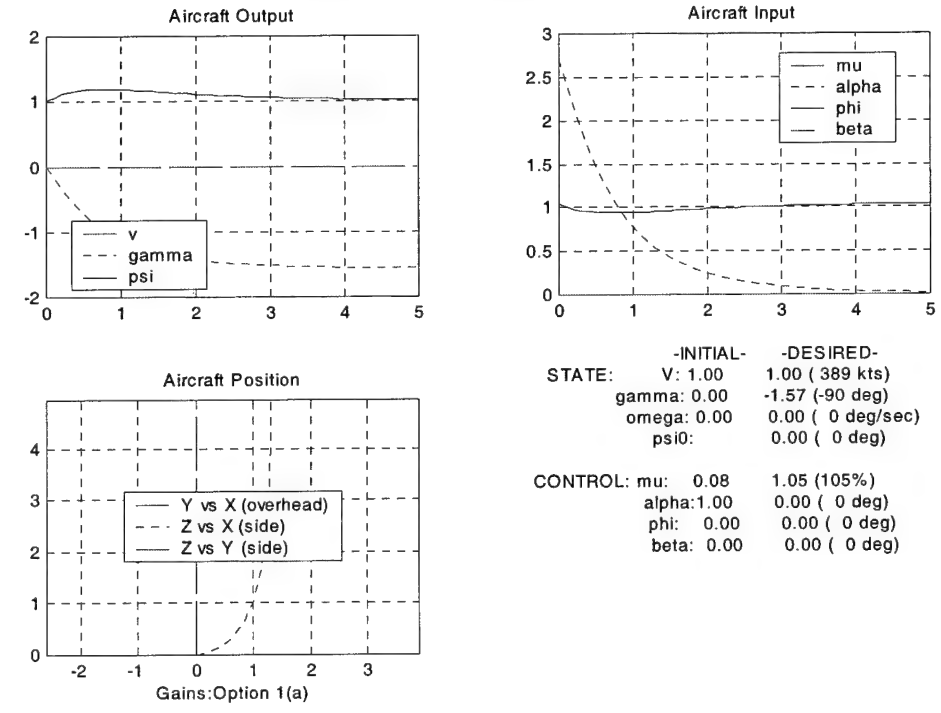

Figure 33: Vertical Climb

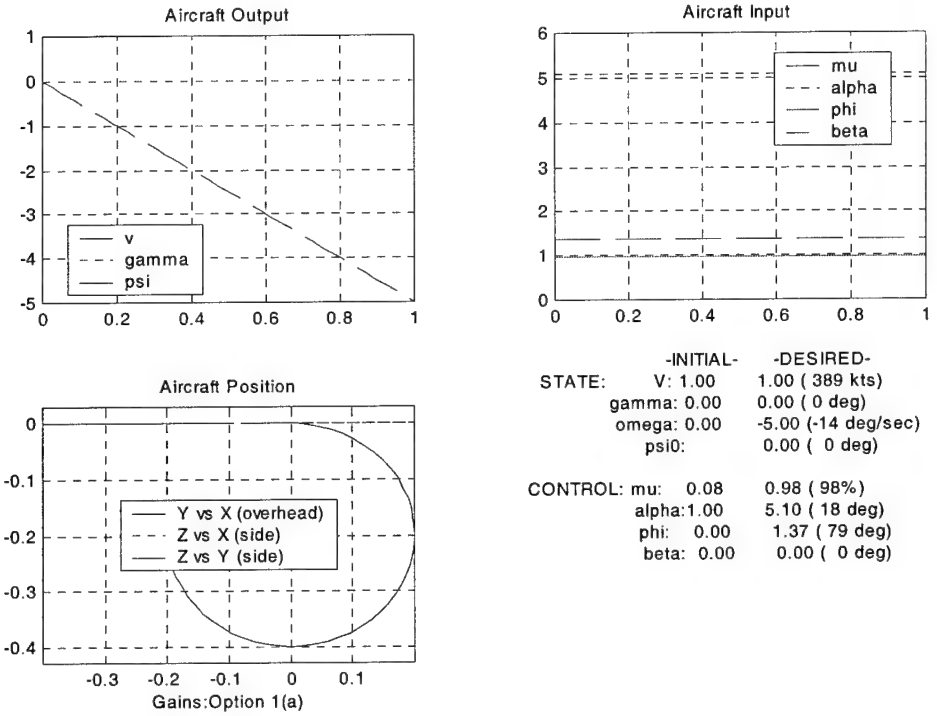

Figure 34: Right Turn

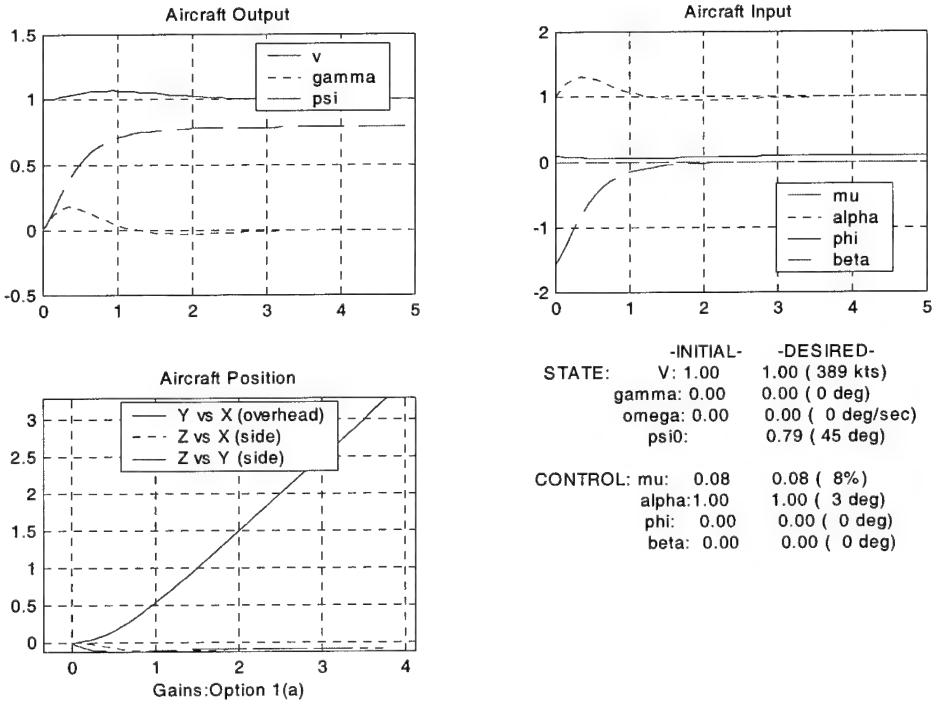

Figure 35: 45 Degree Heading Change

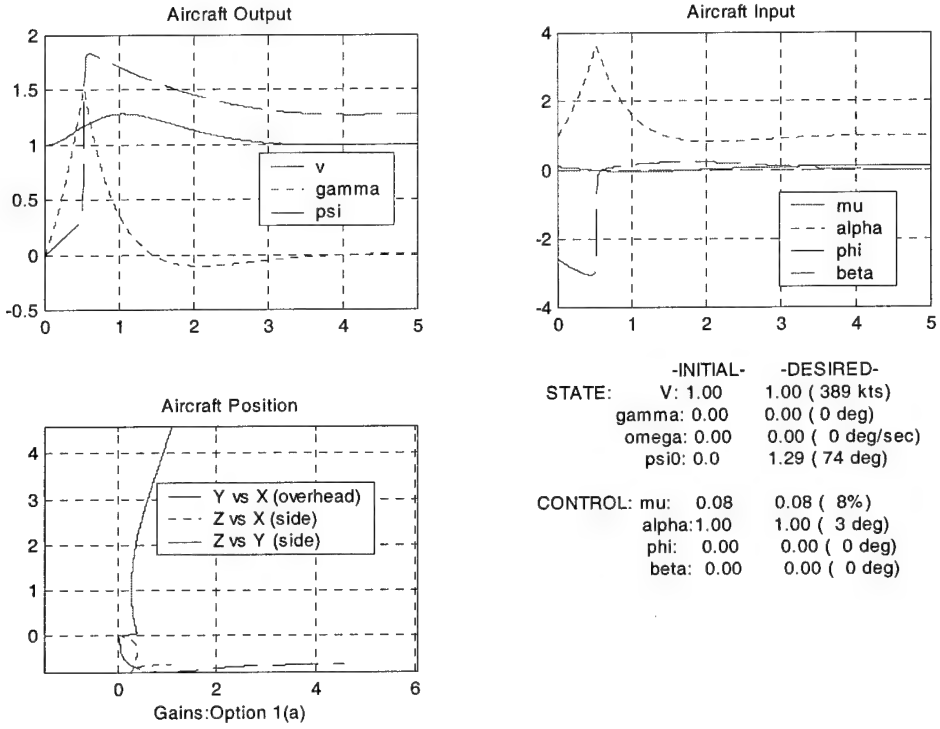

Figure 36: 74 Degree Heading Change

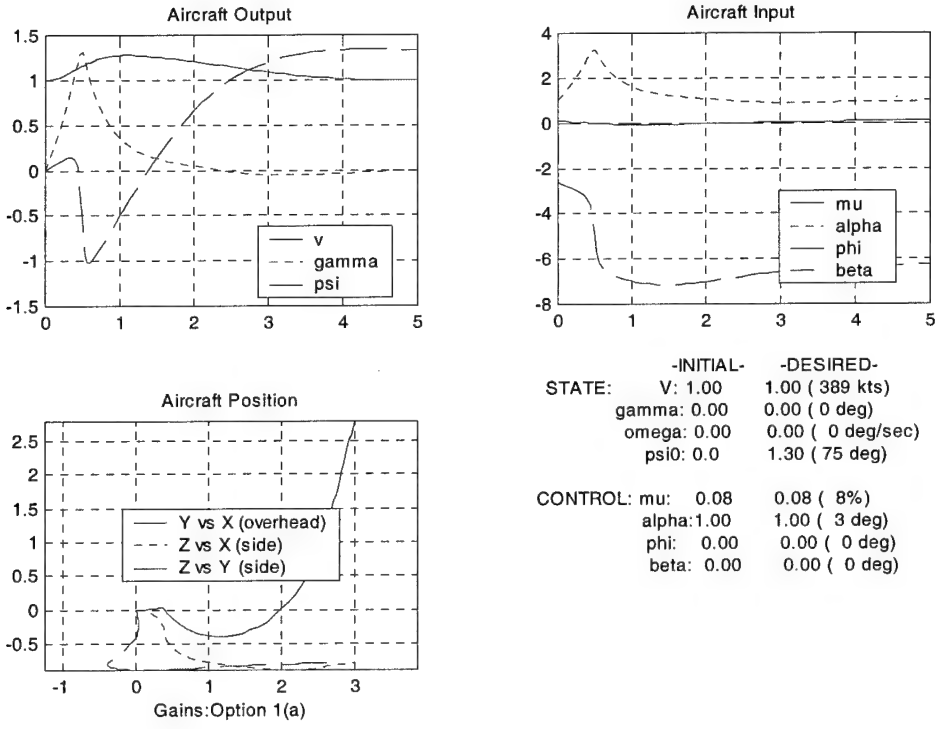

Figure 37: 75 Degree Heading Change

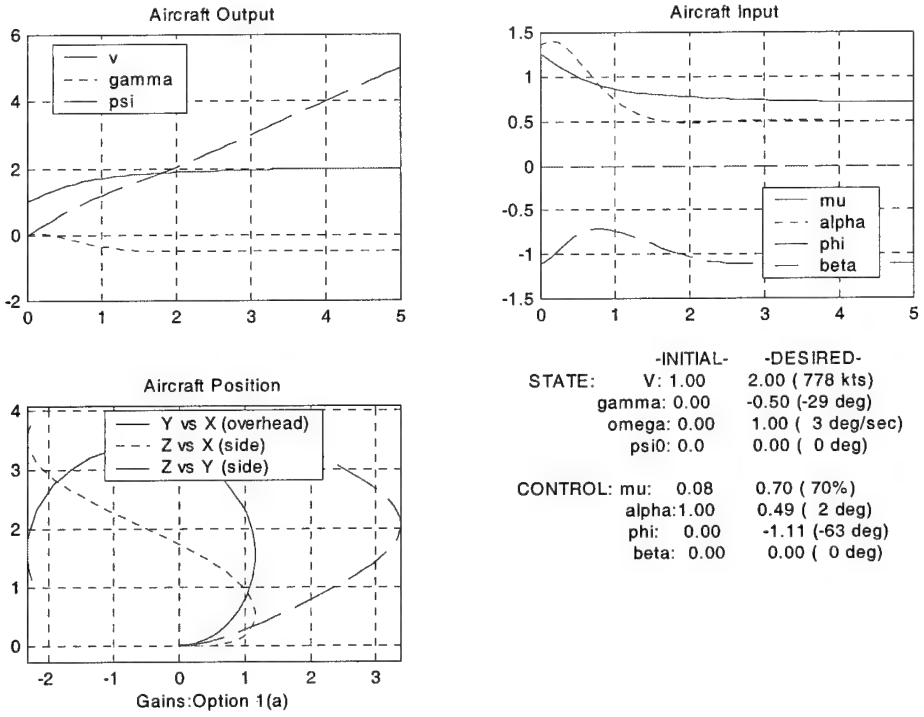

Figure 38: Accelerate, Climb, Turn

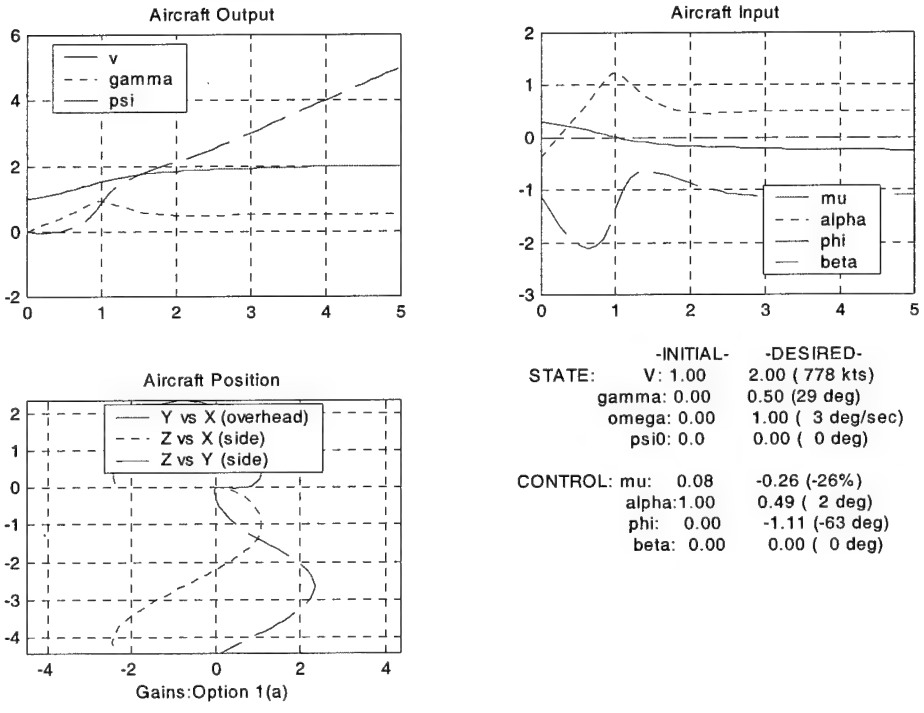

Figure 39: Accelerate, Dive, Turn

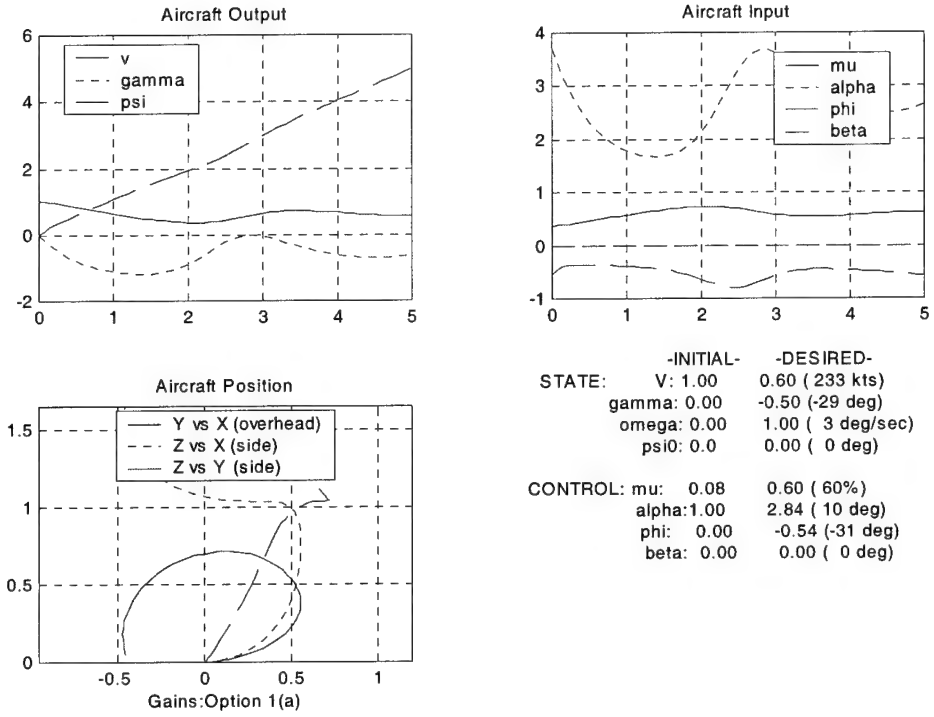

Figure 40: Decelerate, Climb, Turn

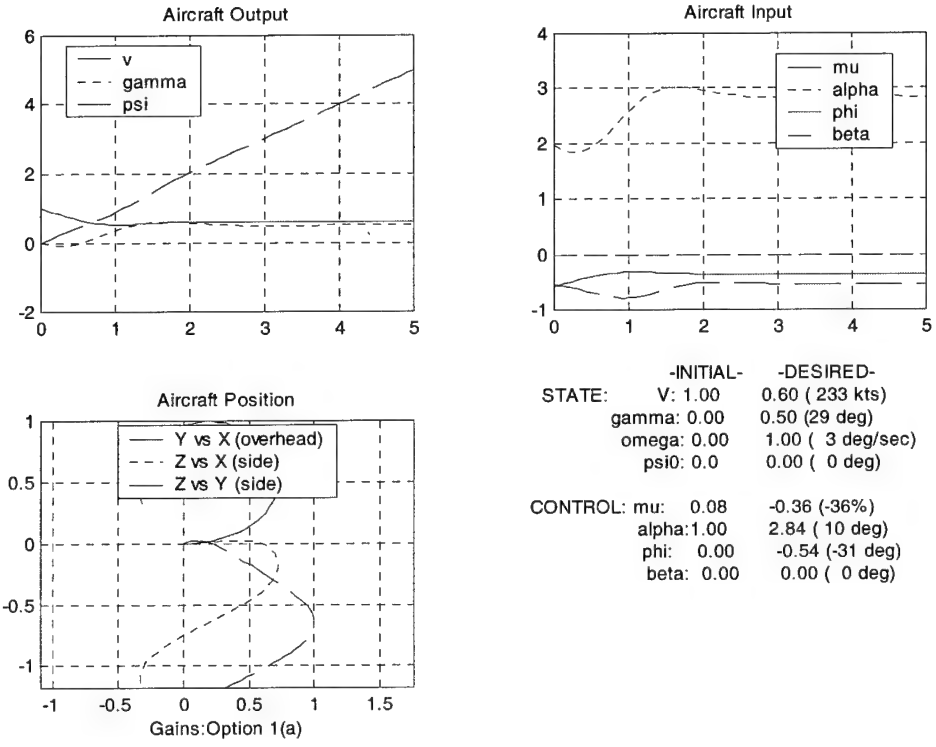

Figure 41: Decelerate, Dive, Turn

For control option 1a, the gains are

$$K_P = \begin{bmatrix} K_{\mu V} & K_{\mu \gamma} \\ K_{\alpha V} & K_{\alpha \gamma} \end{bmatrix} = \begin{bmatrix} -0.5561 & 0 \\ 0 & 1.728 \end{bmatrix}$$

Thus, velocity error is fed back to modify thrust, while flight path angle error is fed back to modify AOA.

In the simulation results, we see that high amplitude set point changes are well handled by the controller.

Figure 22 shows the system behavior when the reference signal $\overline{V}$ is changed to 0.9 . The new trim thrust setting $\overline{\mu}$ is the same as the old one (0.08), and the new trim $\overline{\alpha}$ increases to 1.23. As expected, the aircraft reacts to the new reference by decreasing thrust until the new trim $\overline{V}$ is reached. As the control system applies the new trim $\overline{\alpha}$ to the aircraft still flying at the old $\overline{V}$, the flight path angle γ increases. The compensator reacts by temporarily decreasing α until the velocity state reaches equilibrium. Note that the trim thrust setting $\overline{\mu}$ does not change because, as discussed previously, the aircraft was initially operating "ahead of the power curve", while the new trim puts the system "behind the power curve." See, e.g., Figure 5.

In Figure 23, the commanded velocity decrease to 0.7 is more significant, and the transient is greater as the controller dampens the oscillations.

In Figure 24, the new reference velocity is 0.41. In an effort to reach this state, the aircraft briefly reverses thrust, and then pitches up nearly vertical. The overshoot in V is so great that the velocity dips below V = 0.07. This is outside the flight envelope of the aircraft; the vehicle has stalled. The equations of motion are strongly nonlinear near

V = 0. The high overshoot is due to the low damping ratio near V = 0.5, as shown previously in Figure 9. Decreasing the reference (commanded) velocity further, as shown in Figure 25, causes the flight control system to depart.

Acceleration maneuvers are easier to perform. Figure 26 shows the simulation results for a commanded reference $\overline{V} = 2$, and Figure 27 shows the reference $\overline{V} = 3$ results. Since damping increases with velocity in this region, the plots show over-damped responses during acceleration maneuvers, as expected..

The system response to commanding a dive is shown in Figure 28. The new set point $\bar{\gamma}$ is set to 0.5, while $\overline{V}$ remains at 1.0. The new trim values are $\bar{\mu} = -0.4$ and $\bar{\alpha} = 0.88$. Seeing the instantaneous error in the desired flight path angle, the compensator "unloads" the aircraft, reducing α to approximately 0. Initially, the aircraft continues to travel in a horizontal direction. Given the reduced (reversed) thrust, the aircraft slows to below the reference velocity. In response, the compensator temporarily adds thrust, until the flight path angle reaches equilibrium.

Figure 29 shows a steep dive ($\bar{\gamma} = 1$) maneuver, and Figure 30 shows a vertical dive ($\bar{\gamma} = \frac{\pi}{2}$) maneuver. Despite the obvious success of the controller at achieving the desired state, the system appears to require large control usage. The thrust required in the vertical dive is 0.95 in reverse, nearly equal to the weight of the aircraft. It is unreasonable to expect this from an actual aircraft, even using speed brakes. Actually, however, it is the commanded maneuver that is extreme. A diving aircraft must dissipate energy or accelerate. By maintaining the speed $\overline{V} = 1$, and since the aerodynamic drag is insufficient, the speed brakes must be deployed. In a dive, increased airspeed would be

both expected and acceptable. Given the increased drag brought about by an increase in airspeed, less reverse thrust would be required.

Similarly, Figures 31-33 show the flight control system's response when commanded to perform climbs of $\bar{\gamma}$ = –0.5, -1.0 and $-\frac{\pi}{2}$, respectively. The flight controls system is able to perform the climbs without difficulty. The thrust required for the vertical climb is necessarily greater than the weight of the aircraft. This would generally require the use of afterburners.

A tight right 14°/sec turn maneuver is shown in Figure 34. Because the control variable in the lateral / directional channel is the bank angle ϕ, and because the longitudinal states are unperturbed, there are no associated dynamics. This is not the case in Figure 35. In this simulation, the desired heading (ψ_0) is set to 45°. The aircraft initially rolls left, then levels out as time passes. The roll produces fluctuations in the lift vector, which perturbs the longitudinal states V and γ.

Figure 36 shows the limit of the control system's ability to respond to a heading change command without altering heading rate ω. At a commanded ψ_0 = 74°, the aircraft is able to engage the commanded heading. However, setting ψ_0 = 75° causes the system to fail, as shown in Figure 37. This limit is caused solely by the choice of gain $K_{\phi,\psi}$, chosen in Section 5.3.1. Decreasing this gain would expand the window of allowable commanded ψ_0, but at the expense of performance at smaller values of ψ_0. The other, more reasonable, approach to commanding a new heading is to command a heading rate ω, which does not suffer from the same constraints, being limited only by the maximum turn rate of the aircraft.

The final four figures display results of commanding simultaneous set point changes in velocity, flight path angle, and heading rate. The aircraft performs adequately in all of the simulations.

7.2 Gain Option 1(b)

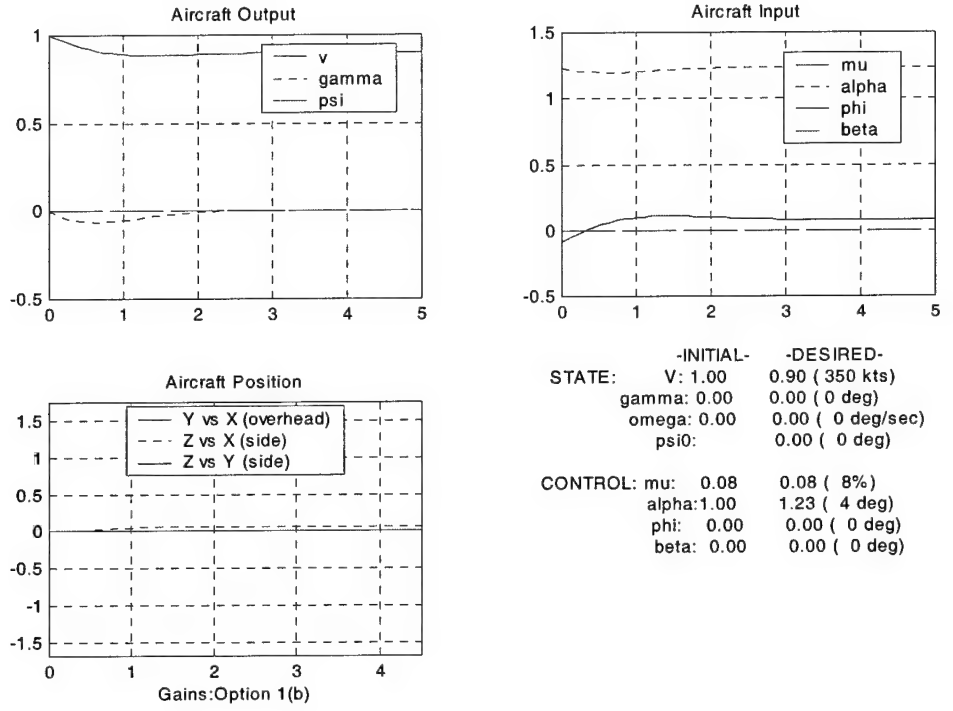

Figure 42: Decrease Speed to 0.9

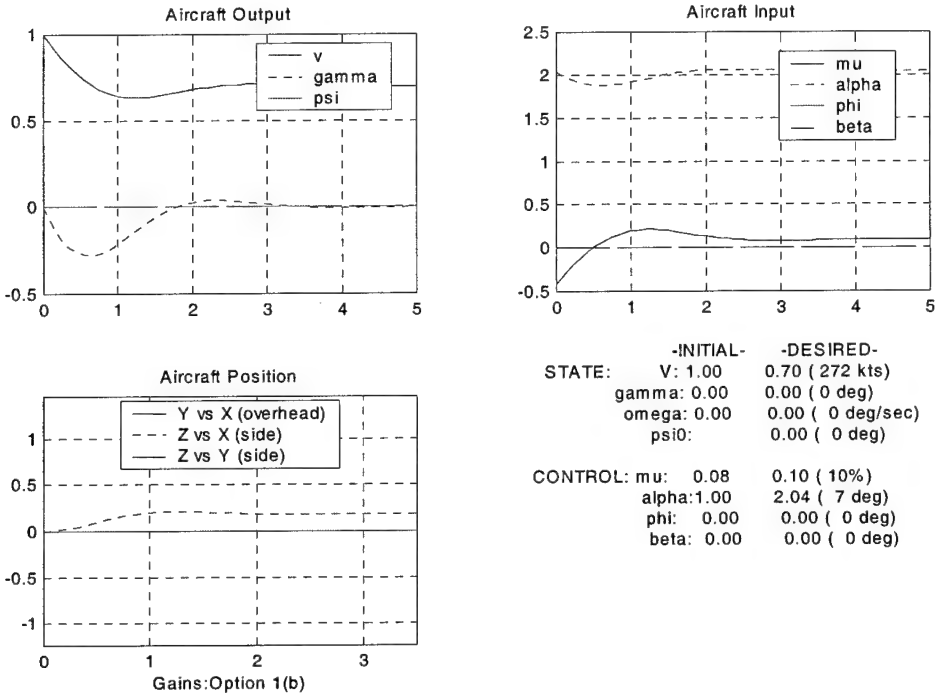

Figure 43: Decrease Speed to 0.7

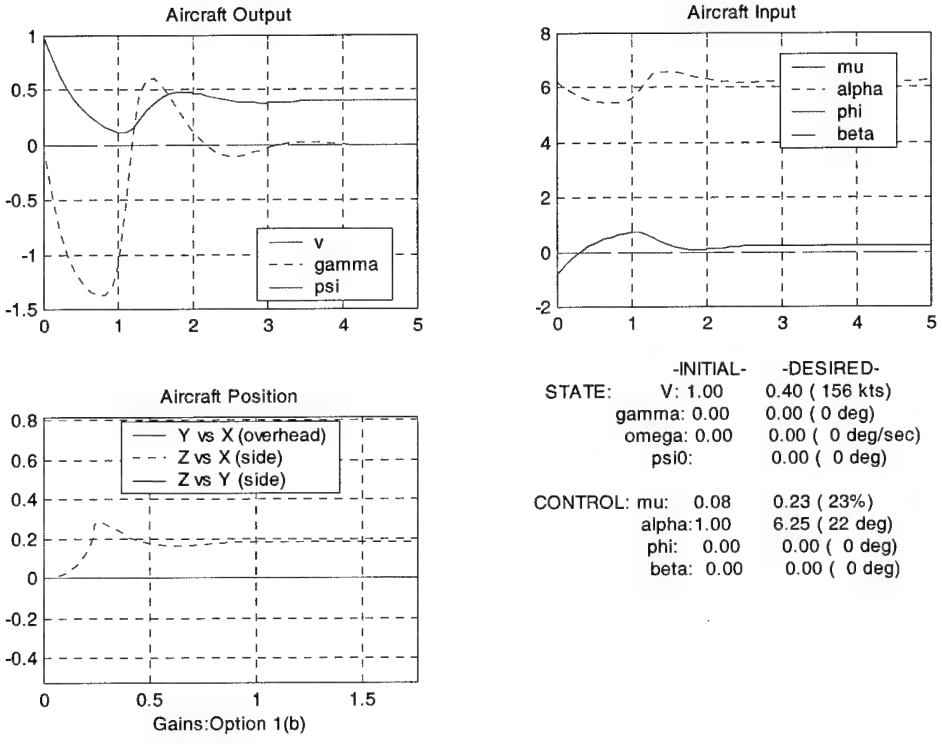

Figure 44: Decrease Speed to 0.40

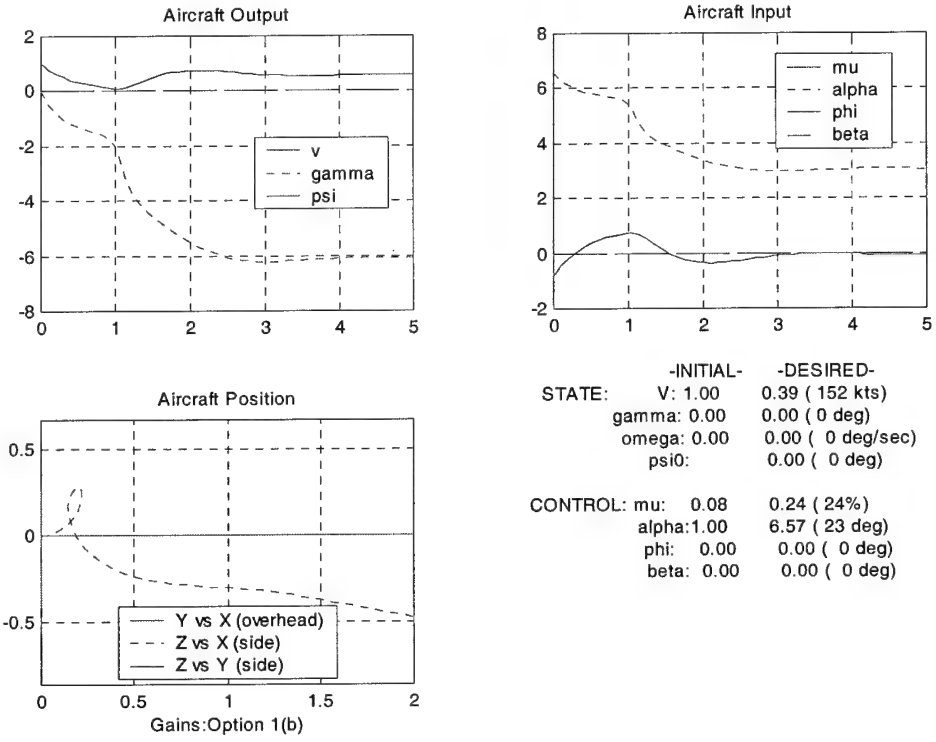

Figure 45: Decrease Speed to 0.39

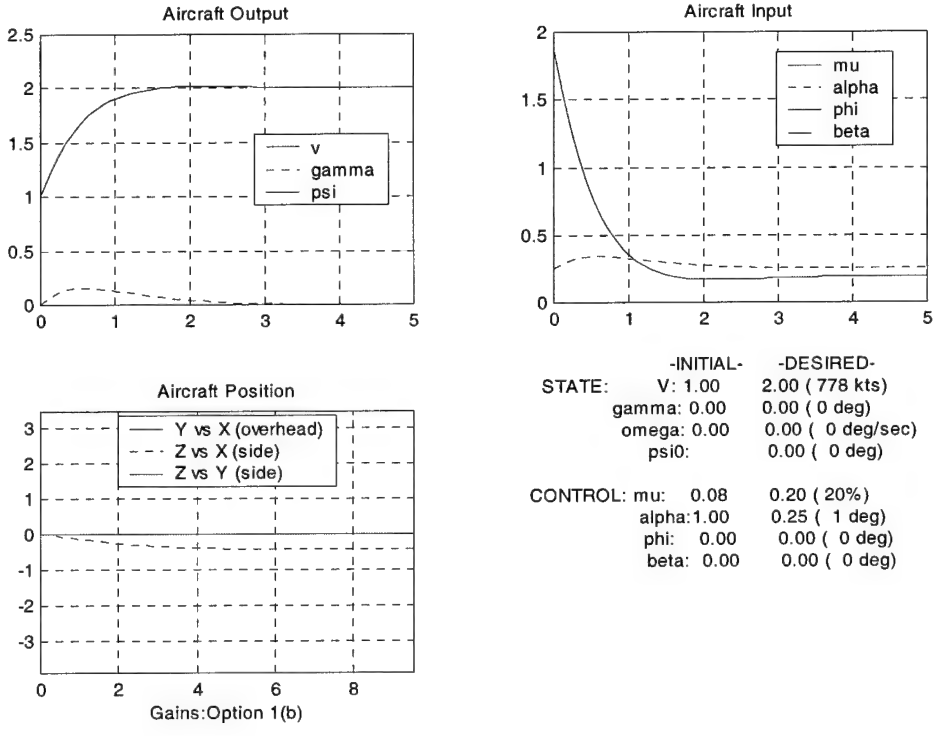

Figure 46: Increase Speed to 2

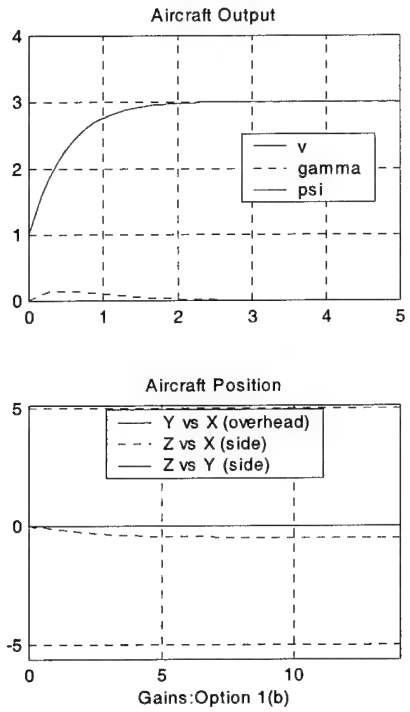

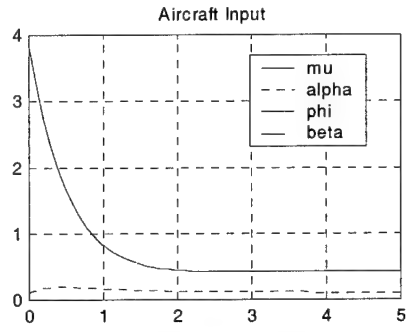

		-INITIAL-	-DESIRED-
STATE:	V:	1.00	3.00 (1166 kts)
	gamma:	0.00	0.00 (0 deg)
	omega:	0.00	0.00 (0 deg/sec)
	psi0:		0.00 (0 deg)
CONTROL:	mu:	0.08	0.43 (43%)
	alpha:	1.00	0.11 (0 deg)
	phi:	0.00	0.00 (0 deg)
	beta:	0.00	0.00 (0 deg)

Figure 47: Increase Speed to 3

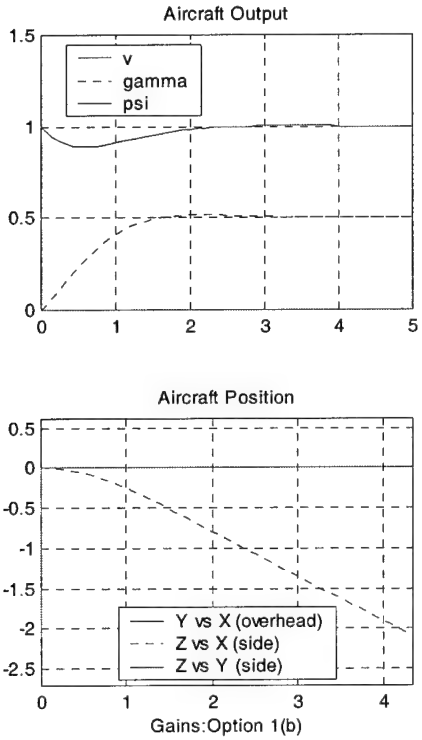

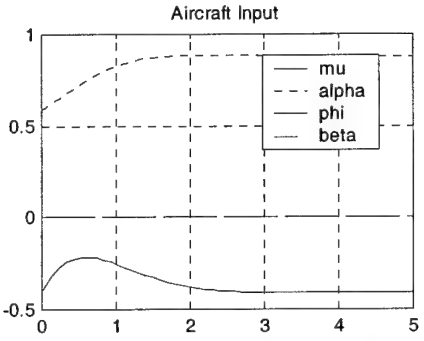

		-INITIAL-	-DESIRED-
STATE:	V:	1.00	1.00 (389 kts)
	gamma:	0.00	0.50 (29 deg)
	omega:	0.00	0.00 (0 deg/sec)
	psi0:		0.00 (0 deg)
CONTROL:	mu:	0.08	-0.40 (-40%)
	alpha:	1.00	0.88 (3 deg)
	phi:	0.00	0.00 (0 deg)
	beta:	0.00	0.00 (0 deg)

Figure 48: Dive

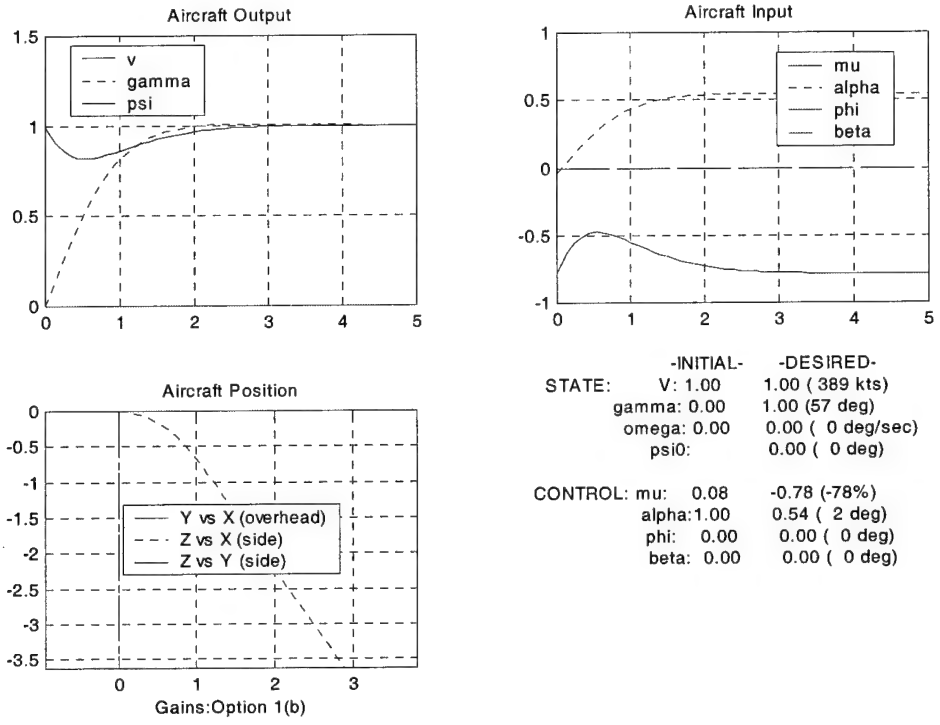

Figure 49: Steep Dive

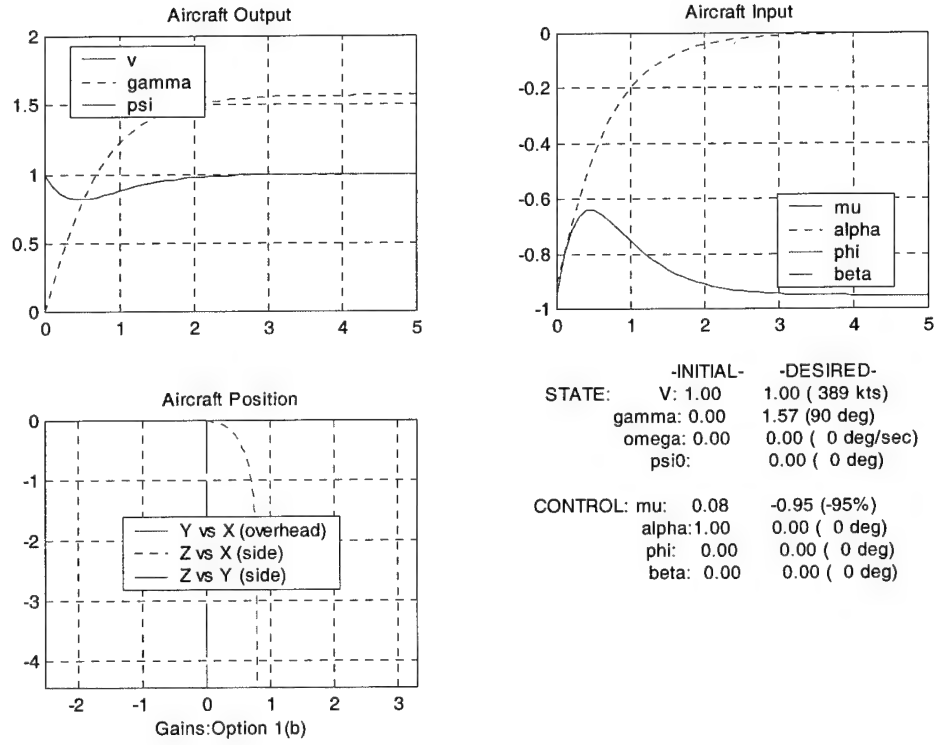

Figure 50: Vertical Dive

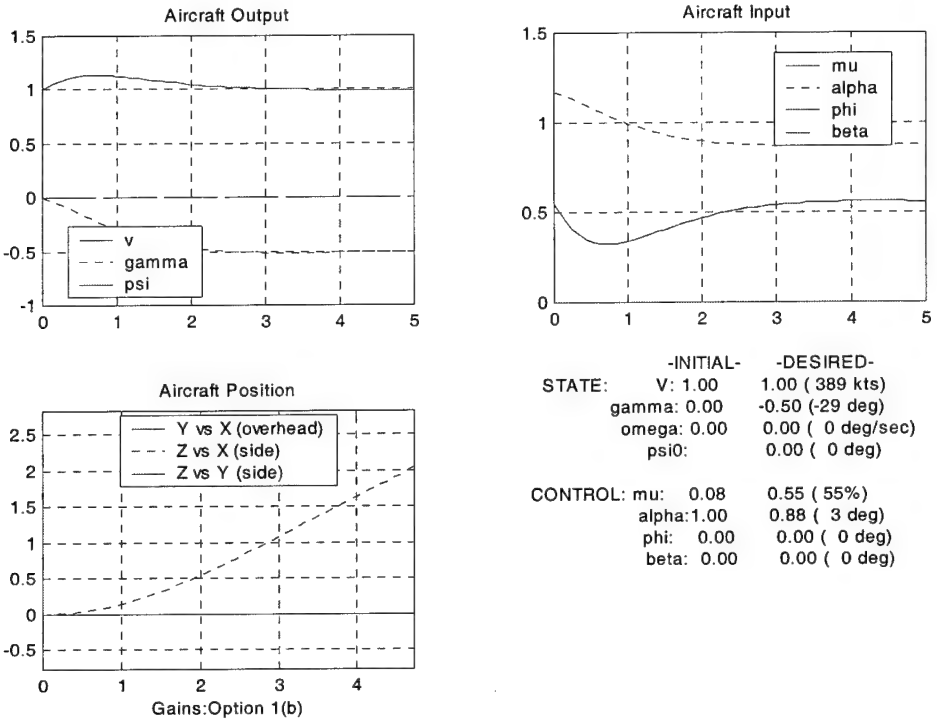

Figure 51: Climb

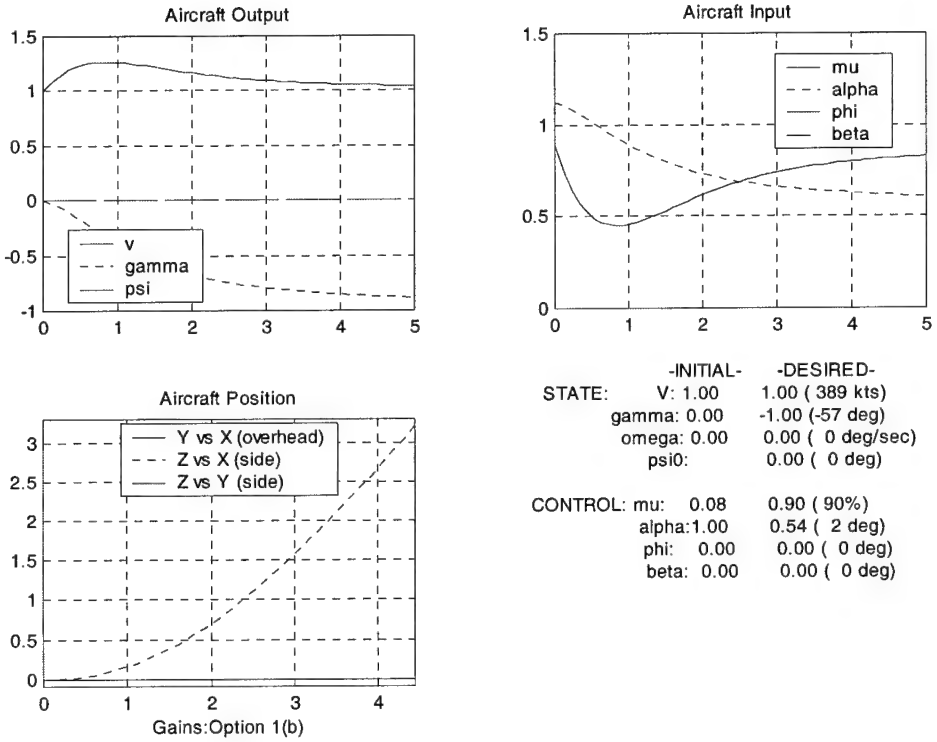

Figure 52: Steep Climb

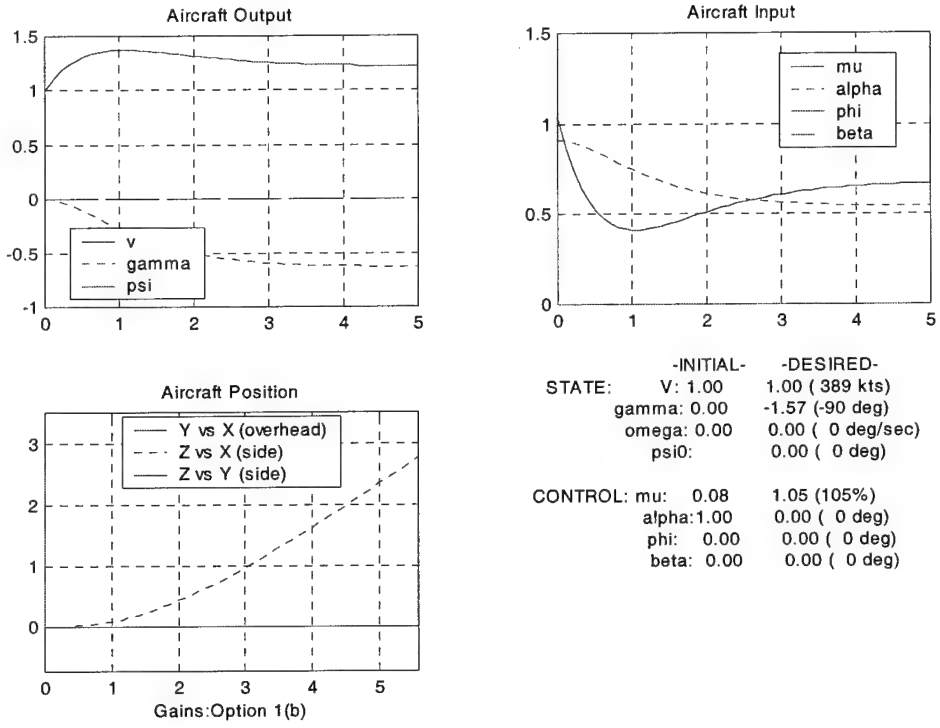

Figure 53: Vertical Climb

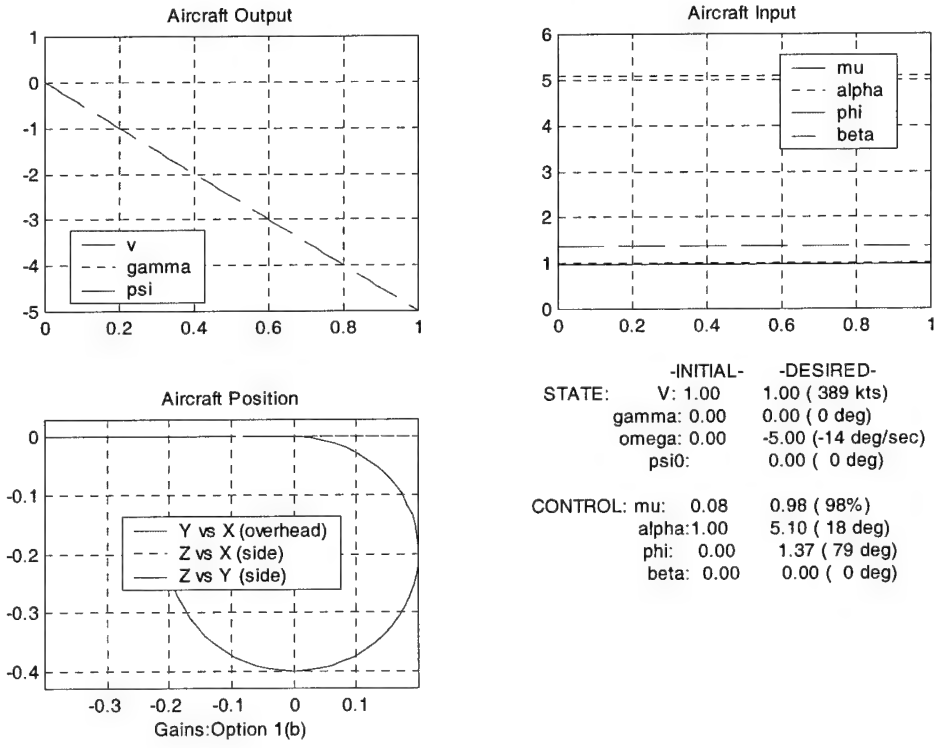

Figure 54: Right Turn

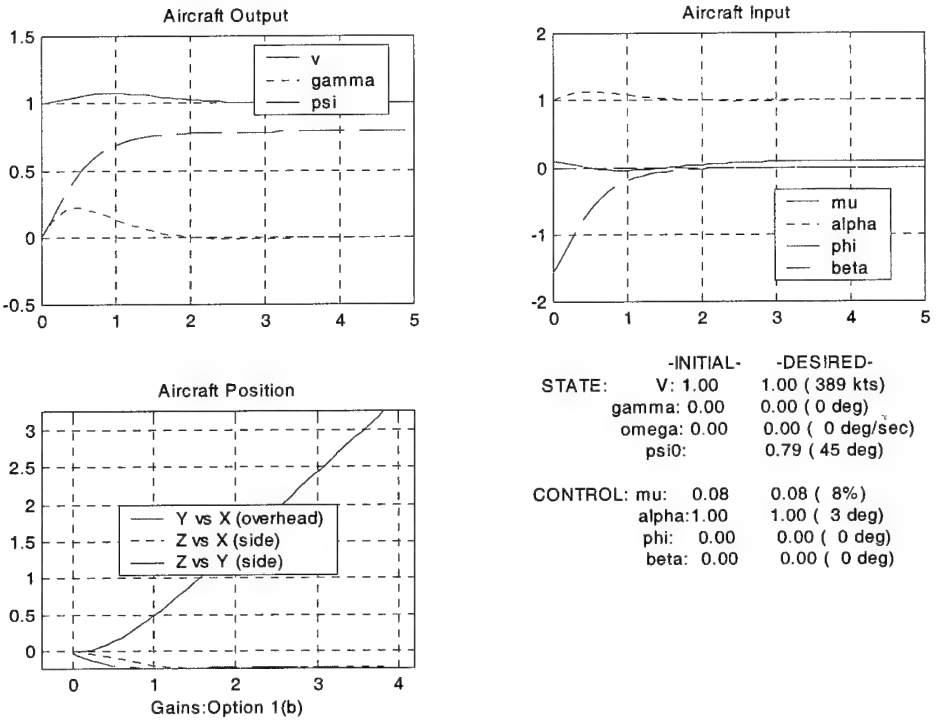

Figure 55: 45 Degree Heading Change

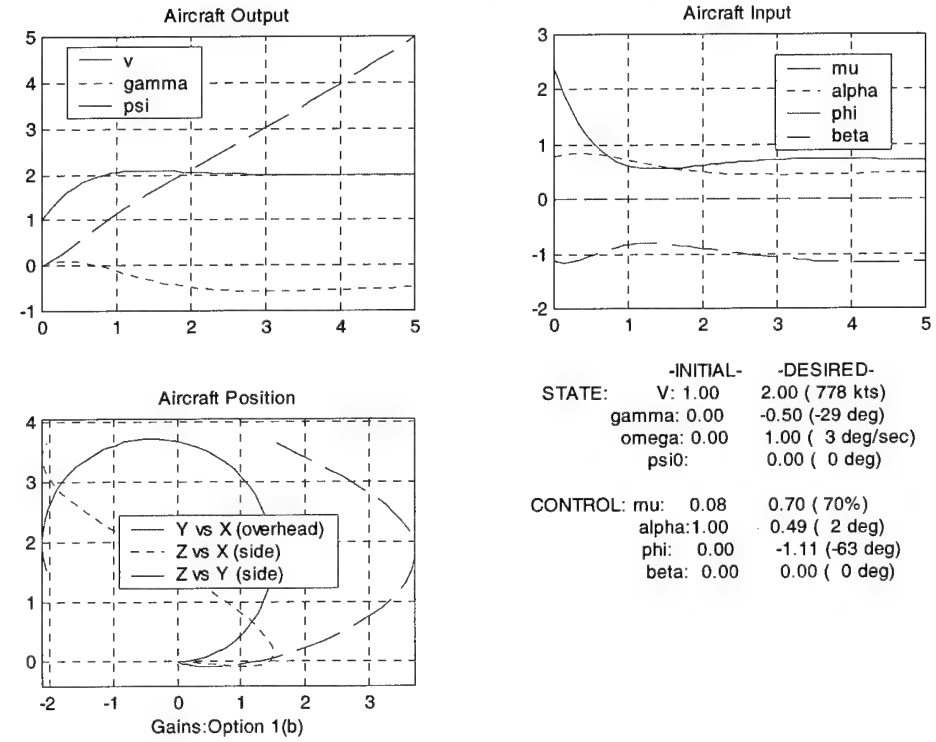

Figure 56: Accelerate, Climb, Turn

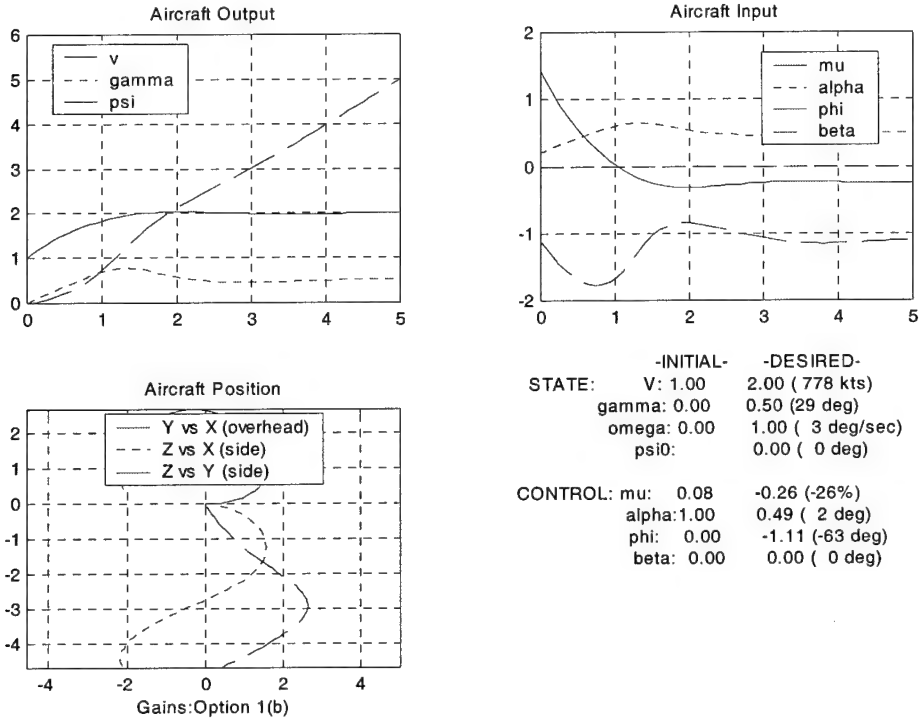

Figure 57: Accelerate, Dive, Turn

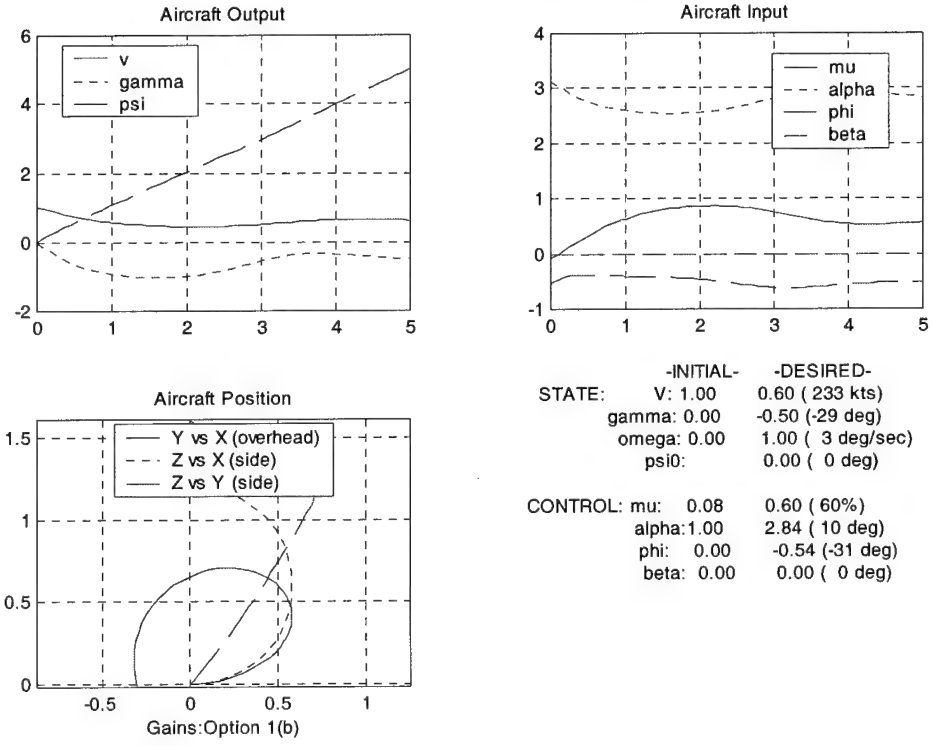

Figure 58: Decelerate, Climb, Turn

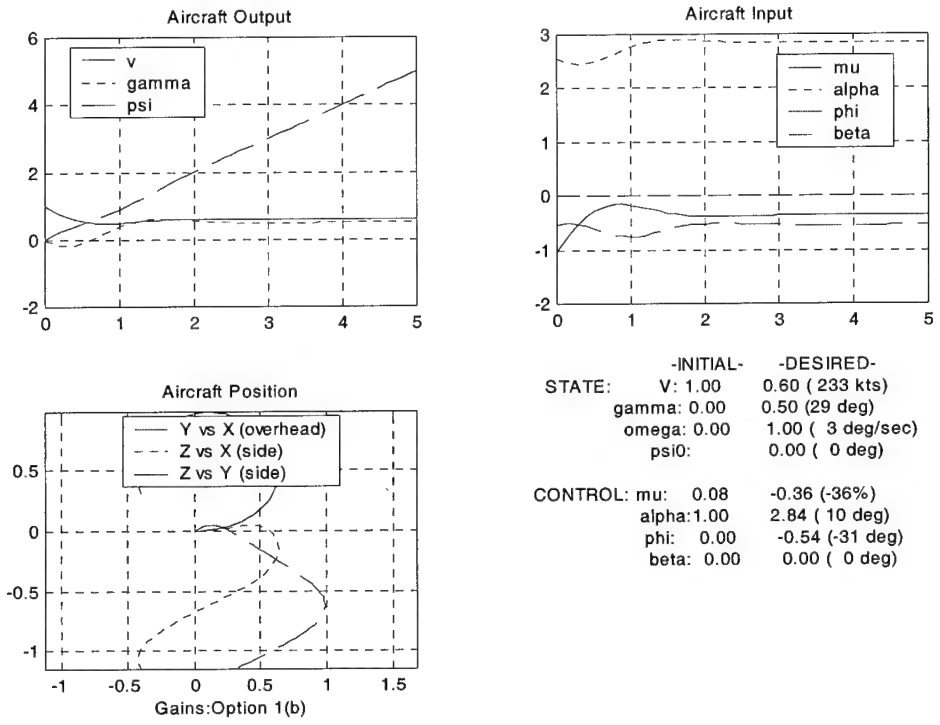

Figure 59: Decelerate, Dive, Turn

For control option 1b, the gains are

$$K_P = \begin{bmatrix} K_{\mu V} & K_{\mu \gamma} \\ K_{\alpha V} & K_{\alpha \gamma} \end{bmatrix} = \begin{bmatrix} -1.7055 & 0 \\ 0 & 0.5787 \end{bmatrix}$$

Again, velocity error is fed back to modify thrust, while flight path angle error is fed back to modify AOA. Note that with these gains, the thrust setting μ is used more heavily to control perturbations, while the AOA α is used less.

The plots in this section are similar to the plots in Section 7.1. The following description serves primarily to highlight the differences between the two control options.

As seen in Figure 44 and Figure 45, the system is again unable to transition to very low velocities. The slightly lower velocity reached by this set of gains can be

attributed to the slightly higher damping ratio at low velocities, when the control law (1b) is used, as shown previously in Figure 11. This produces slightly less overshoot.

As shown in the next figures, the flight control system is able to perform the commanded velocity increases and the commanded dives. However, Figure 52 and Figure 53 show that the system is unable to perform significant climbing maneuvers. Indeed, this was predicted in Section 6.3, where it was shown that the flight control system becomes unstable for $\gamma < -1.0$.

7.3. Gain Option (2)

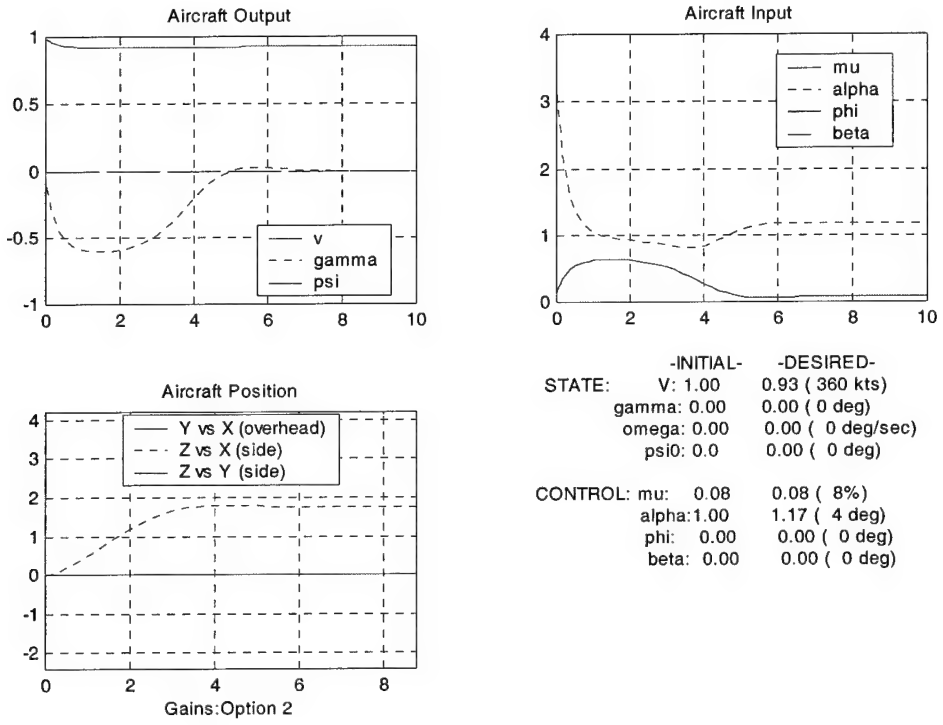

Figure 60: Decrease Speed to 0.925

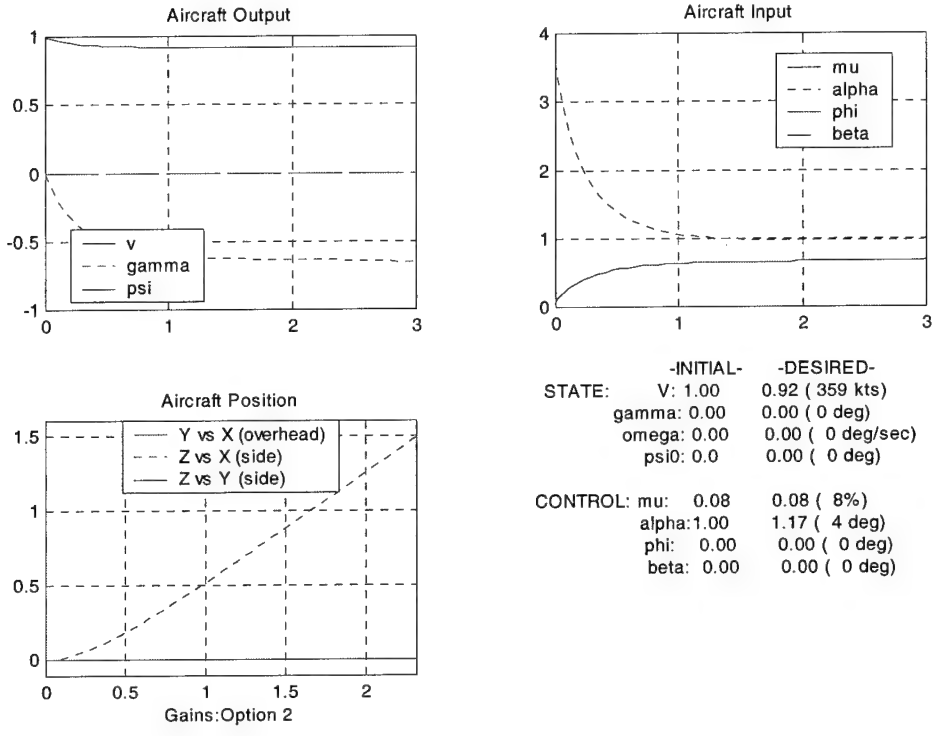

Figure 61: Decrease Speed to 0.924

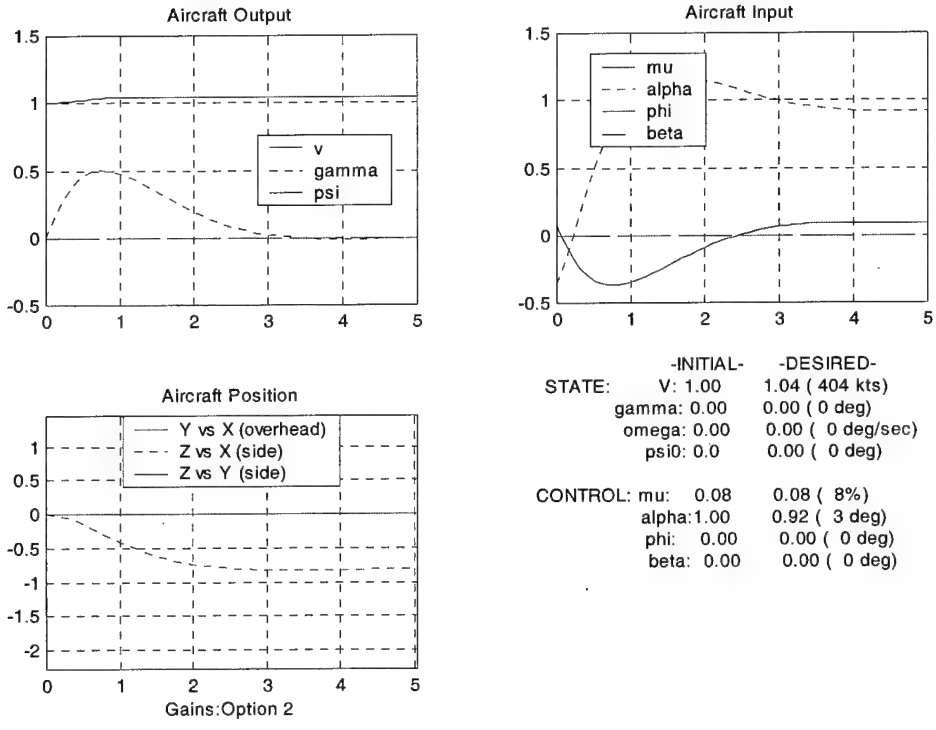

Figure 62: Increase Speed to 1.04

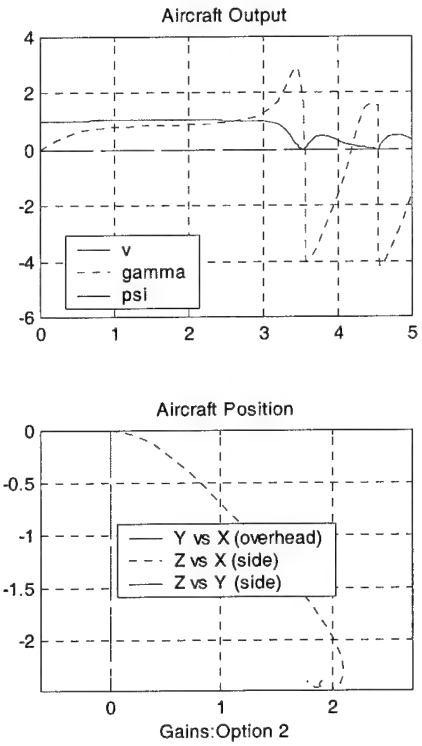

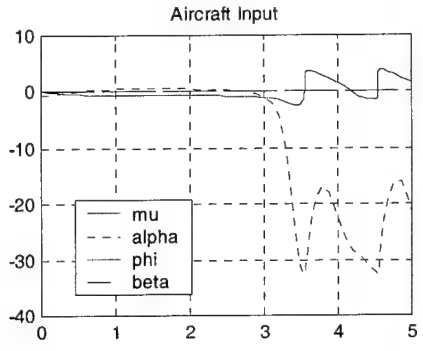

		-INITIAL-	-DESIRED-
STATE:	V:	1.00	1.05 (408 kts)
	gamma:	0.00	0.00 (0 deg)
	omega:	0.00	0.00 (0 deg/sec)
	psi0:	0.0	0.00 (0 deg)
CONTROL:	mu:	0.08	0.08 (8%)
	alpha:	1.00	0.91 (3 deg)
	phi:	0.00	0.00 (0 deg)
	beta:	0.00	0.00 (0 deg)

Figure 63: Increase Speed to 1.05

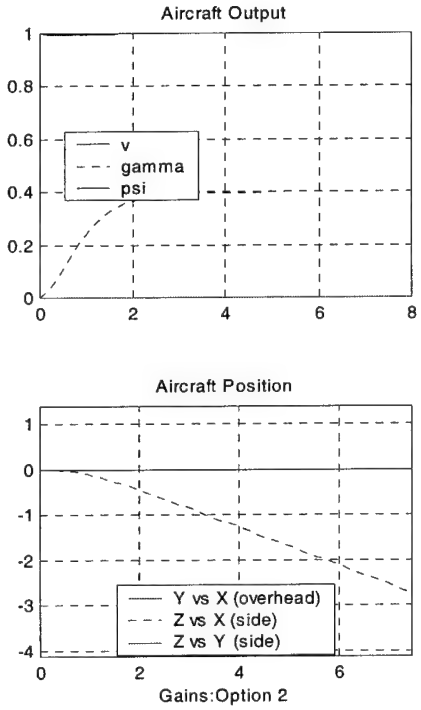

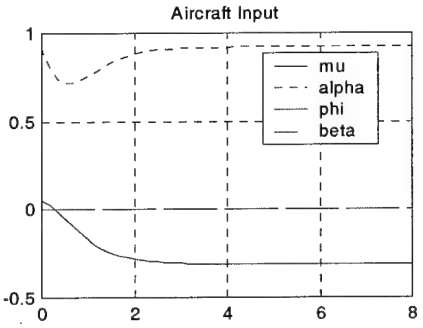

		-INITIAL-	-DESIRED-
STATE:	V:	1.00	1.00 (389 kts)
	gamma:	0.00	0.40 (23 deg)
	omega:	0.00	0.00 (0 deg/sec)
	psi0:	0.0	0.00 (0 deg)
CONTROL:	mu:	0.08	-0.31 (-31%)
	alpha:	1.00	0.92 (3 deg)
	phi:	0.00	0.00 (0 deg)
	beta:	0.00	0.00 (0 deg)

Figure 64: Dive 0.40

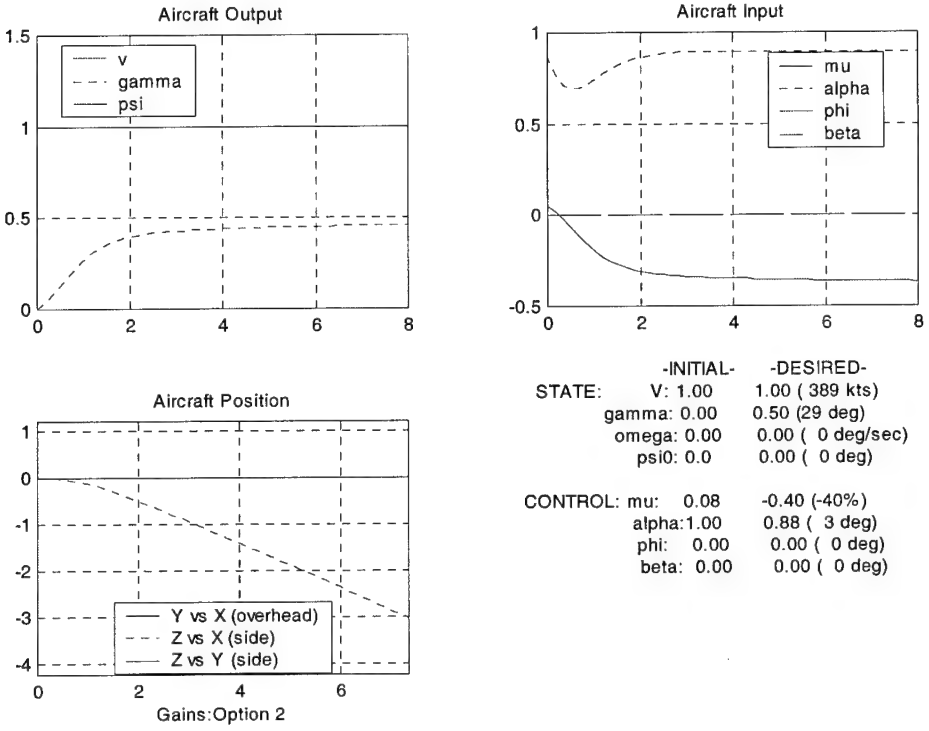

Figure 65: Dive 0.50

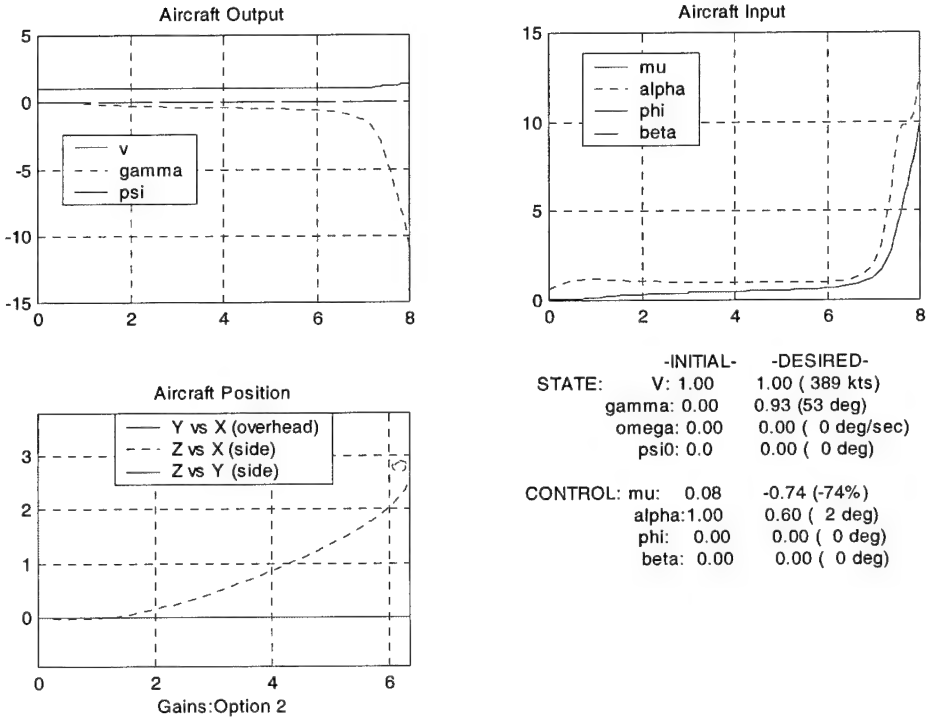

Figure 66: Dive 0.93

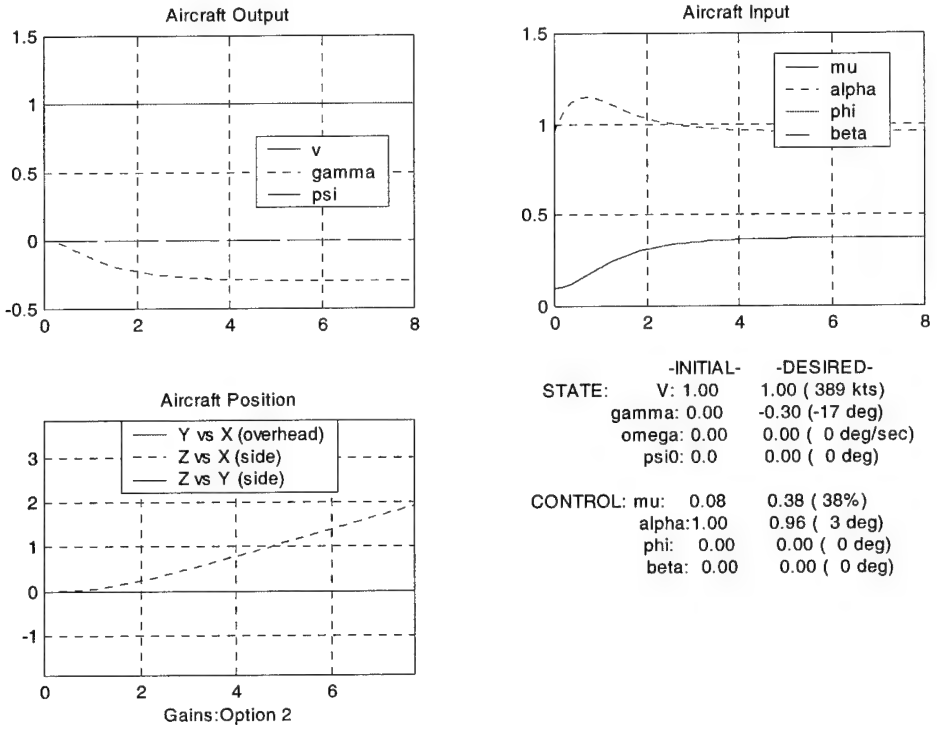

Figure 67: Climb (-0.30)

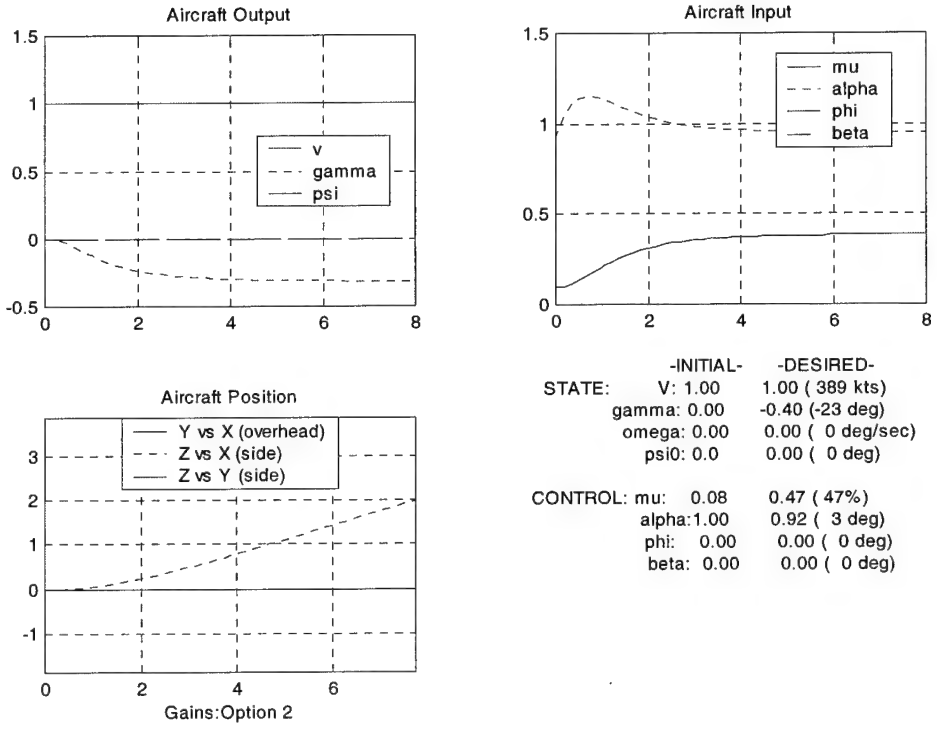

Figure 68: Climb (-0.40)

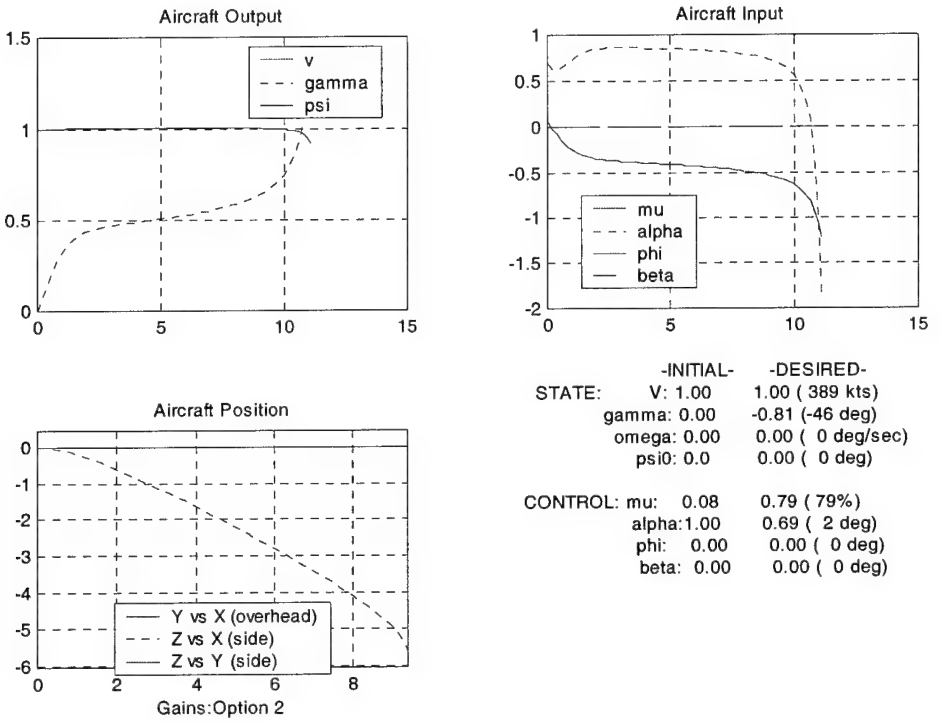

Figure 69: Climb (-0.81)

For control option (2), the gains are

$$K_P = \begin{bmatrix} K_{\mu V} & K_{\mu \gamma} \\ K_{\alpha V} & K_{\alpha \gamma} \end{bmatrix} = \begin{bmatrix} 0 & -0.9118 \\ 31.9955 & 0 \end{bmatrix}$$

This gain set implements and "opposite" control strategy, as compared to the two previous gain sets. Here, velocity error is fed back to modify AOA, while flight path angle error is fed back to modify thrust. This control law was shown in Section 6.3 to have a sharply reduced operating envelope. The simulations verify this. The control system is unable to decrease speed below V = 0.92 or increase speed above V = 1.04. It can accurately track a $\gamma = 0.40$ dive reference, but can not assume a dive angle of $\gamma = 0.50$. Commanding $\gamma = 0.93$ causes the aircraft to depart controlled flight. Similarly, it

can accurately track a $\gamma = -0.30$ climb reference, but cannot climb to $\gamma = -0.40$, and commanding $\gamma = -0.81$ causes the aircraft to depart.

7.4. Lateral Disturbance

In an effort to determine the robustness of the flight control system, a lateral channel disturbance is simulated by adding a right roll disturbance to the aircraft input, viz., $\phi := \phi + \phi_d$. Two disturbance types are input: a constant disturbance, and a ramp. Each disturbance type is simulated at various amplitudes. Since it was determined in previous sections that the gains calculated by option (1a) are superior, all simulations in this section are executed using those gains in the longitudinal channel. Also as calculated previously in section 5.4, integral action is included in the lateral channel. No set point changes are commanded during the disturbance rejection simulations.

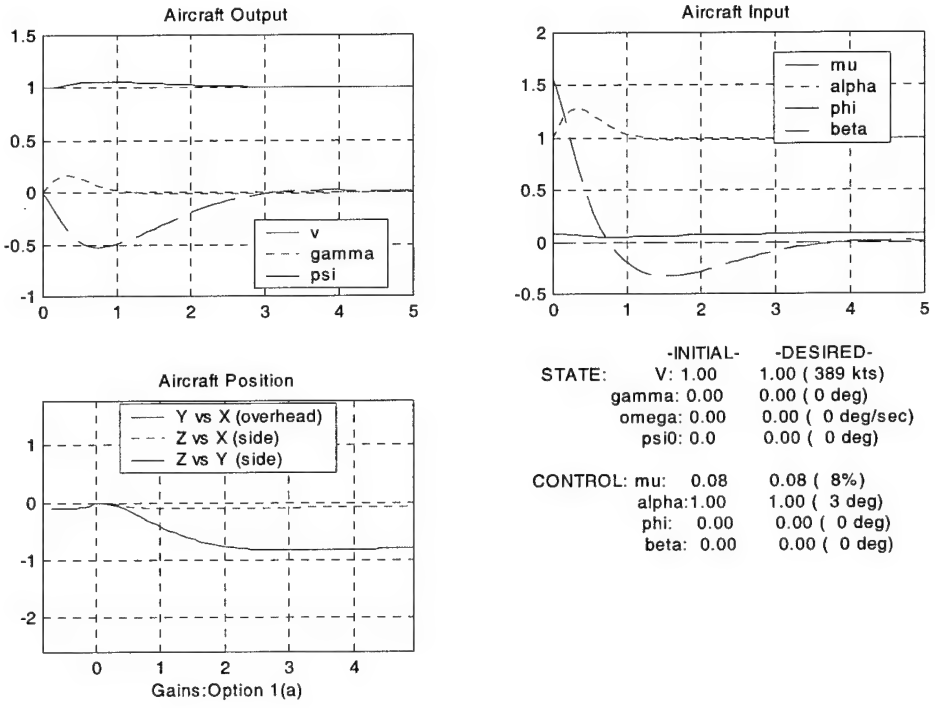

Figure 70: Roll Disturbance = $\pi/2$

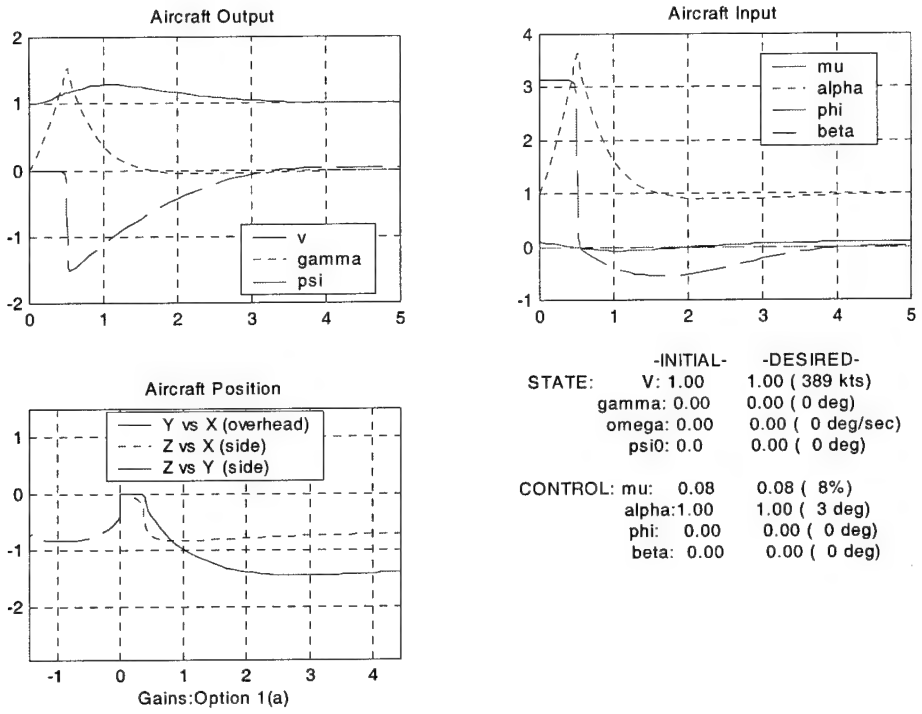

Figure 71: Roll Disturbance = $0.99 \cdot \pi$

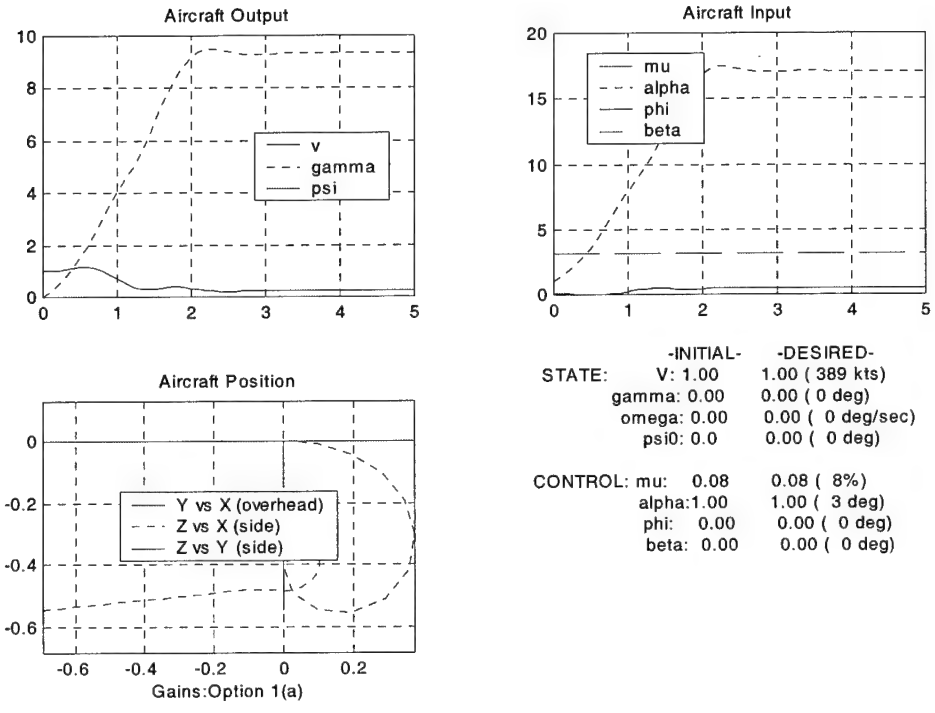

Figure 72: Roll Disturbance = π

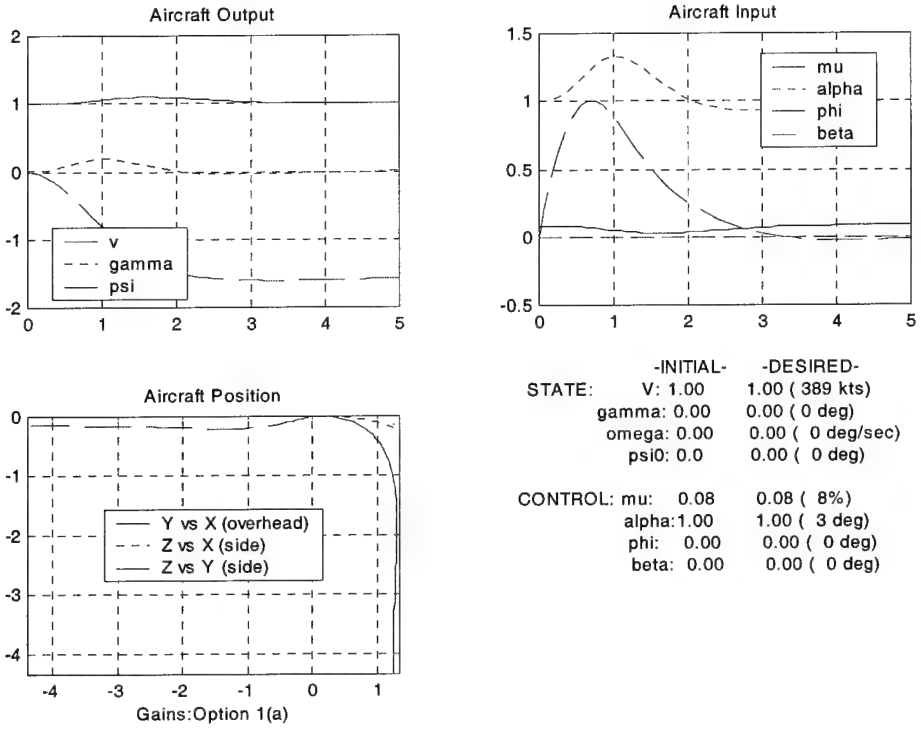

Figure 73: Roll Disturbance = $\pi \cdot t$

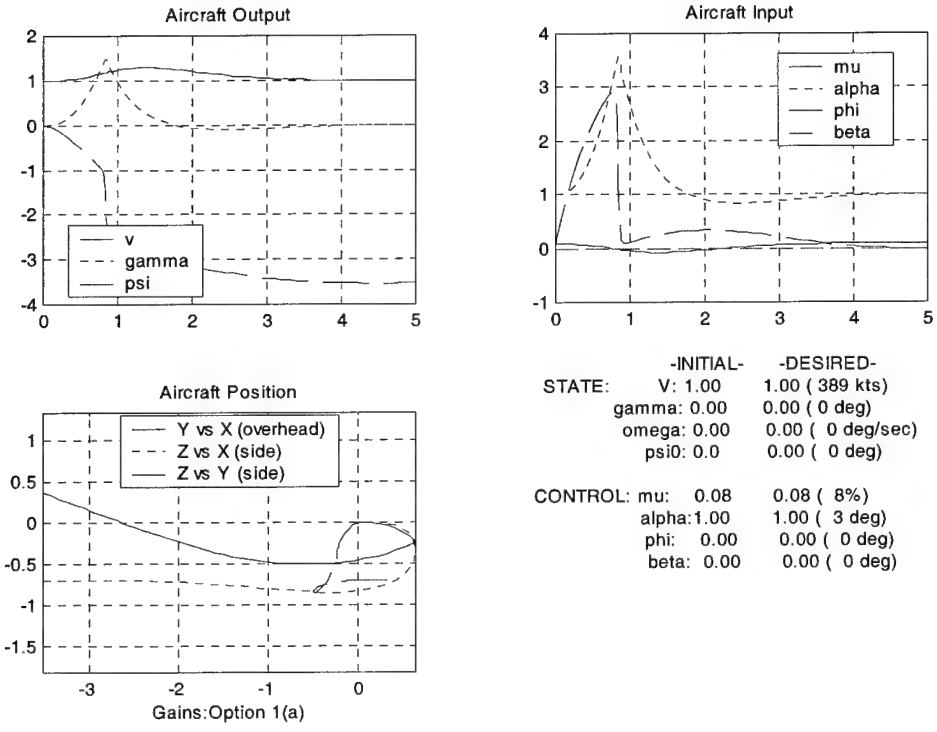

Figure 74: Roll Disturbance = $2.23\pi \cdot t$

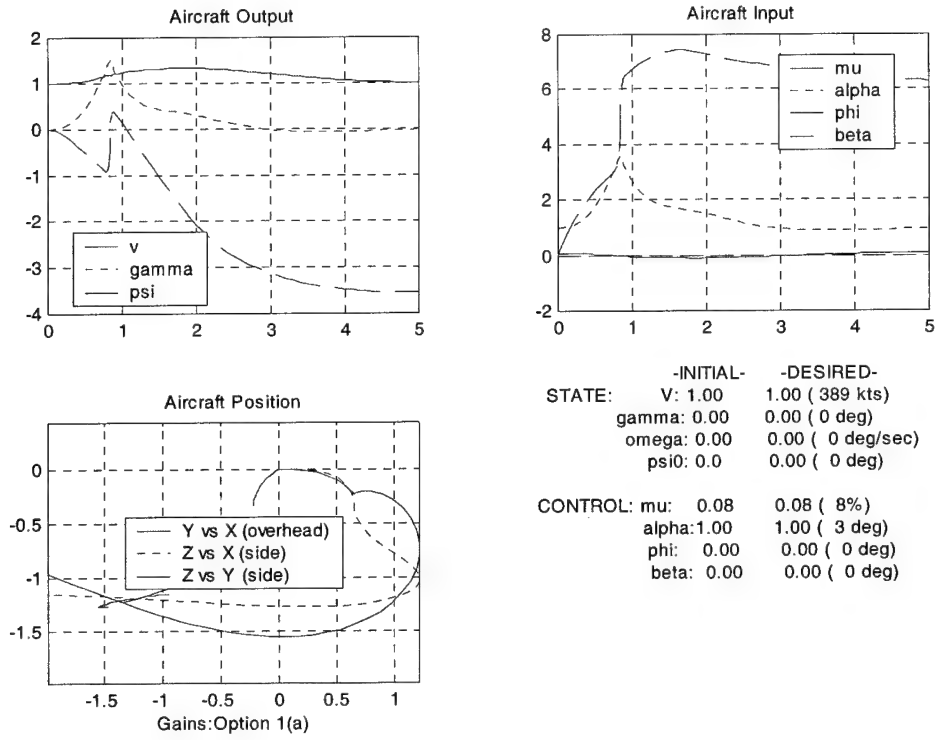

Figure 75: Roll Disturbance = $2.24\pi \cdot t$

Figure 70 shows the simulation results for a high amplitude constant roll disturbance $\phi_d = \pi/2$, applied at t = 0. This large value of ϕ_d is chosen to clearly illustrate the flight control system's behavior under a relatively high disturbance.

Initially, the disturbance can be seen as a nonzero input to the plant. The aircraft's heading changes and the aircraft drifts to the right. The controller reacts, rolling the aircraft to the left until the system returns to the commanded heading; the aircraft's path is displaced in the lateral direction. Figure 71 and Figure 72 show the boundary of the control system's performance capability; if the roll disturbance inverts the aircraft, departure may ensue.

Figure 73 shows simulation results for a dynamic roll disturbance $\phi_d = \pi \cdot t$. Again, given that the goal of this chapter is to determine the limits of system performance, the

simulated disturbance is relatively large. As the disturbance's amplitude increases, the aircraft heading is driven off the commanded heading. The compensator eventually returns the system to wings-level and a recovery is accomplished. Note, however, that the aircraft settles to an undesired heading; a steady-state heading error results. This is characteristic of the ramp response of a first-order system, [8]. Figure 74 shows the boundary of the control system's performance capability, while Figure 75 shows the departure that results when exceeding this boundary.

It is the integral action in the controller's lateral channel that makes this recovery possible. Without it, the constant disturbance would drive the system to an incorrect heading, while the ramp disturbance induced error would be unbounded, causing a loss of control and departure from controlled flight.

7.5. Tracking a Dynamic Reference Signal

In order to test the system's capability to react to dynamic reference signals, and thus exercise "phugoid damping" control, the previously constant reference signals were replaced with sinusoidal ones (in fact, A $\cos(2\pi ft)$). The velocity reference signal amplitude was chosen to swing between the previously simulated levels of 0.41 and 3.0. The flight path angle reference signal amplitude covered the full $\pm\pi/2$ range possible. The yaw rate reference signal was allowed to swing between $\pm$ 5, which was statically simulated previously, and is approximately the aircraft's structural limit. Now, in the simulations experiments, the frequency "f" of the sinusoidal reference signals is increased from 0, which corresponds to a set point change command, to f_{max} , where windup inevitably occurs, viz., the phugoid damping controller breaks down.

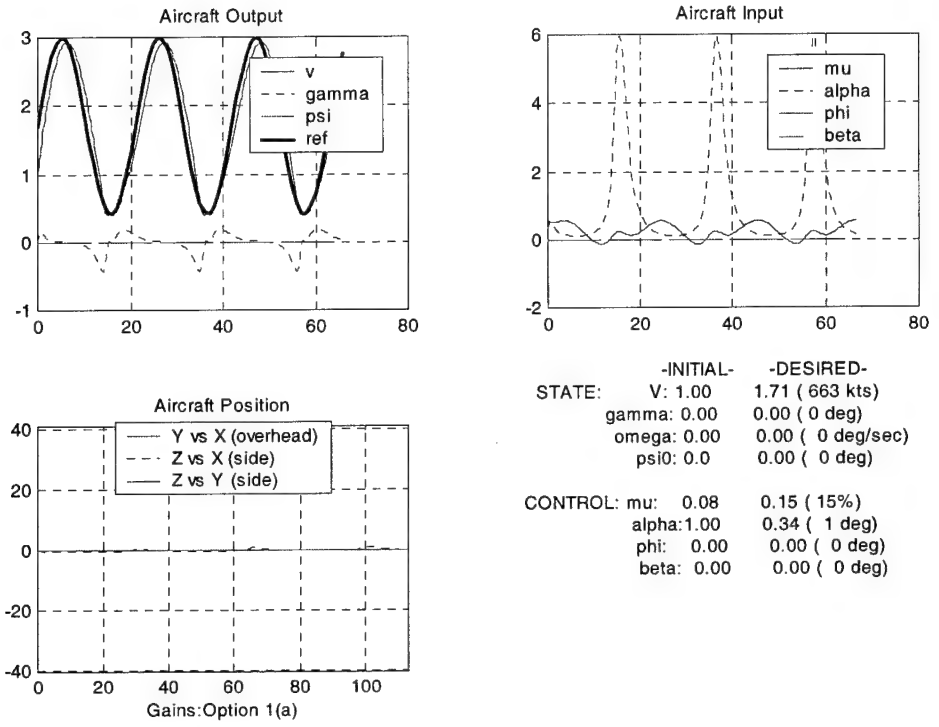

Figure 76: Tracking of V reference = 1.7 + sin(0.3 t)

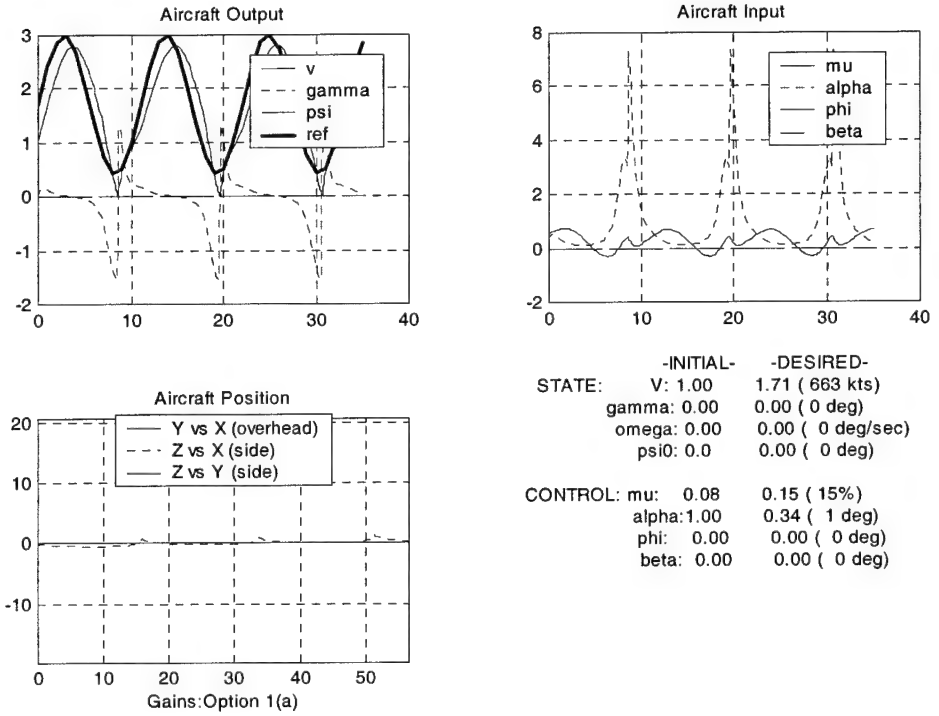

Figure 77: Tracking of V reference = 1.7 + sin(0.57 t)

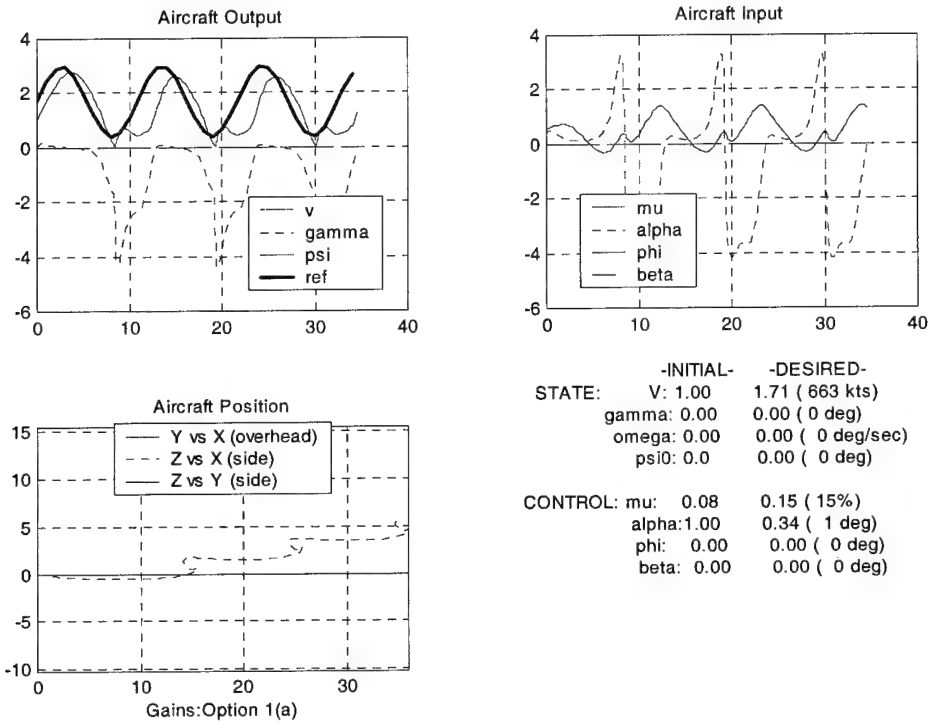

Figure 78: Tracking of V Reference = 1.7 + sin(0.58 t)

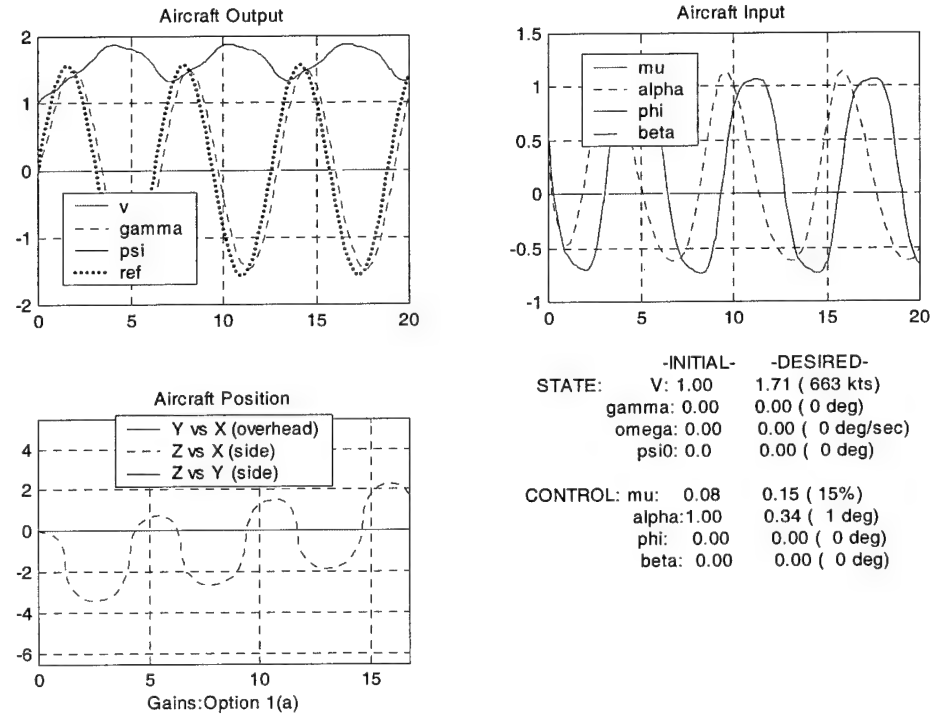

Figure 79: Tracking of Gamma Reference = 1·sin(t)

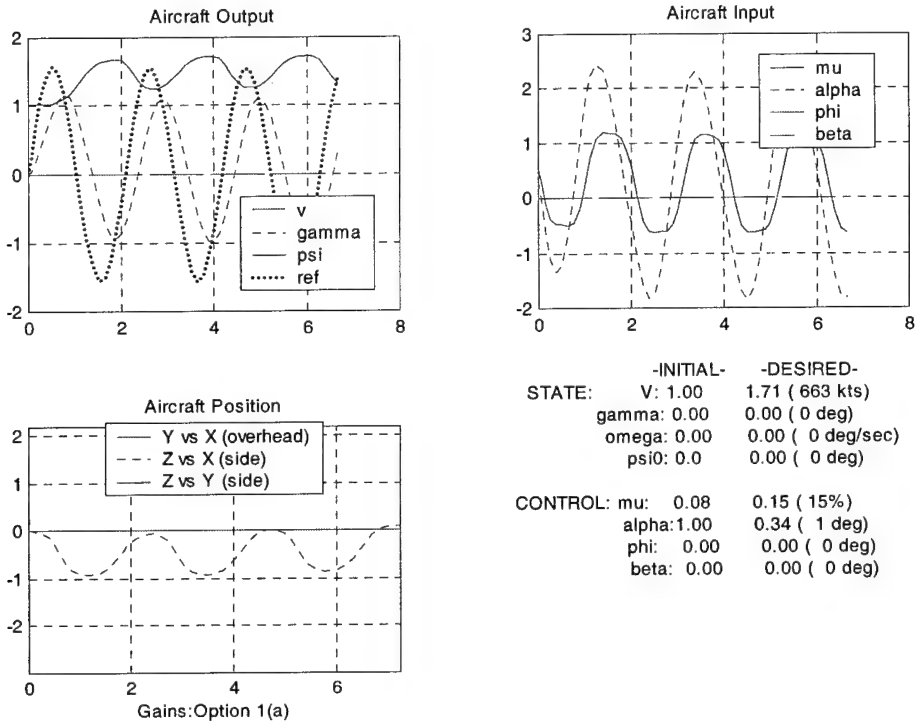

Figure 80: Tracking of Gamma Reference = 3·sin(t)

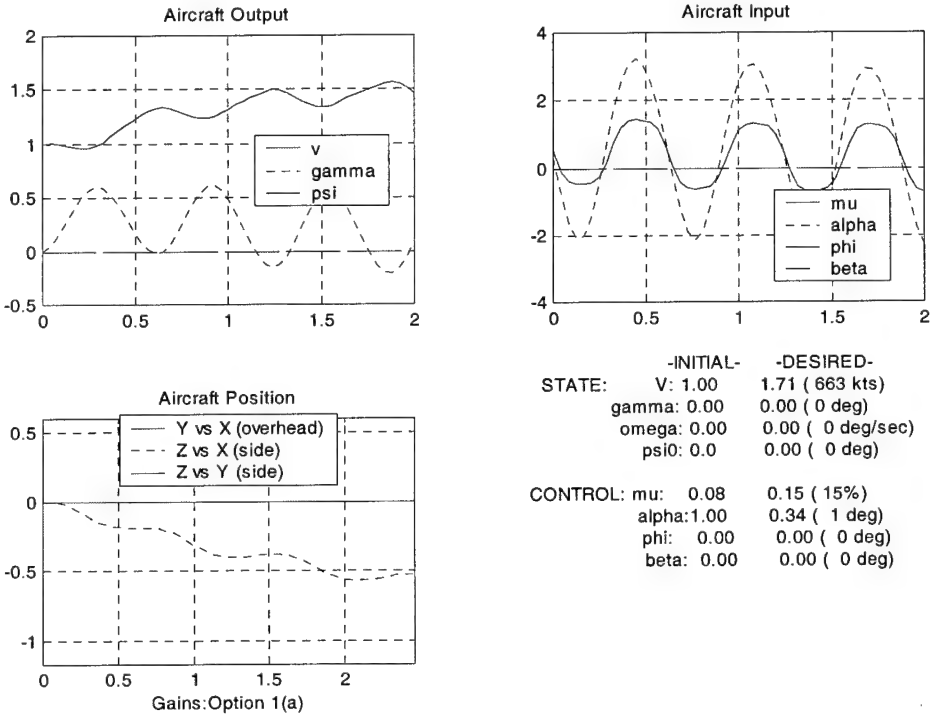

Figure 81: Tracking of Omega Reference = 10·sin(t)

Figure 76 shows the system tracking a velocity (V) reference that changes with a frequency f = 0.3, which is nondimensionalized in keeping with previous analysis. Note that the dimensional frequency is $0.3\frac{g}{V_0}$ Hz = 0.0147 Hz. The aircraft tracks the reference closely. Figure 77 shows the limit of the system's ability to track the changing velocity reference, with V's frequency of 0.57. Figure 78 shows the system breaking down as it attempts to track a reference with a frequency of 0.58. The higher frequency of the reference signal causes the aircraft to repeatedly reverse direction.

Figure 79 shows the system tracking a flight path angle (γ) reference whose frequency is 1.0 ($=\frac{g}{V_0}$ Hz $\approx$ 0.05 Hz). The aircraft tracks the reference closely. Figure 80 shows the limit of system's ability to track the changing flight path angle reference. The γ output sinusoid has decreased by 3 dB, versus a reference signal γ that changes with a frequency of 3.0. A further increase in this frequency causes a decrease in output amplitude, which signals operation beyond the bandwidth of the closed-loop system.

Figure 81 shows the flight control system tracking a yaw rate (ω_c) varying with a frequency of 10 ($=10\frac{g}{V_0}$ Hz $\approx$ 0.5 Hz). The aircraft tracks the reference closely. Increasing the frequency of the yaw rate has no effect on the flight control system. This is so because (i) roll angle is a control variable, so there is no lag in the plant's ability to change yaw rate, as long as the maximum yaw rate is attainable; and (ii) maximum yaw rate is limited in this simulation to an attainable level of 5.

7.5. Chapter Summary

The simulations were performed using Matlab's Simulink, with each gain option being tested and the aircraft going through a variety of multivariable, high amplitude, and dynamic maneuvers. As predicted, gains option (1a) performed better than the others, demonstrating a wide operational envelope. Deceleration maneuvers were shown to be somewhat problematic. At low speed, the velocity dropped below stall speed. Control option (1b) performed adequately in most maneuvers, but could not perform steep climbs. Control option (2) had a narrow operating envelope and therefore frequently caused a departure from controlled flight. All results agreed with the analysis done previously in Chapter 6.

In addition, the flight control system, using gains calculated using option (1a), was tested against lateral disturbances. It withstood a very large roll disturbance before failure. Finally, its ability to track a dynamic reference signal, as in phugoid damping control, was tested. Even with the reference signals having high amplitudes and relatively high frequencies, the control system performed successfully, as long as the (nondimensional) reference signal's frequencies were below 0.57 and 3.0, for V and γ commands, respectively.

8. CONCLUSIONS

A novel phugoid damping control design methodology is developed, based on the use of wind axes and a point-mass aircraft model. A multivariable set point controller is designed which consists of: (i) A trim calculation-based nonlinear feed-forward control computer; thus, given a commanded new trim state (air speed, flight path angle, and yaw rate), the required trim thrust setting and trim angle of attack, roll angle, and sideslip angle inputs are solved for, and, (ii) a small signal linear feedback regulator; the equations of motion linearized about the trim condition of wings level, constant altitude flight, which simplifies the dynamics to allow separation between the lateral and longitudinal control channels, are used, and a small-signal linear multivariable regulator is designed. The linear compensator also entails integral action. Thus, the controller consists of a strongly nonlinear feed-forward module and a linear small signal compensator. The novel proposed multivariable set point controller encompasses full three-axes autopilot functions. The command signals are airspeed, flight path angle, and heading angle or heading rate. Moreover, this controller is used as a tracking controller, a.k.a. a "phugoid damping" controller, provided that the bandwidth of the command signal is substantially less than the bandwidth of the closed loop flight control system. Robust and flexible, the flight control system exhibits the capability to independently control either bank angle or sideslip angle, allowing the air vehicle to perform weapons-pointing tasks. The phugoid damping controller's performance is examined in extensive simulations and its wide operational envelope is demonstrated. It is shown that the controller can accept high amplitude commands. Thus, the speed can be commanded to change between $\overline{V} = 0.41$ and $\overline{V} = 3.0$, the flight path angle can be varied anywhere in

the full range of $\bar{\gamma} = \pm\frac{\pi}{2}$, and heading changes can be offset $\pm 74°$, while heading rate commands are limited only by the maximum turn rate of the aircraft.

REFERENCES

1. Blakelock, John H., Automatic Control of Aircraft and Missiles, John Wiley & Sons, Inc., New York NY, 1991.

2. Chetwyn, Kim. *RAF Page.* 31 Jan. 2001 <http://www.stable.demon.co.uk/raf.htm>.

3. Franklin, Gene F., J. David Powell, and Michael L Workman. Digital Control of Dyanmic Systems, Addison-Wesley Publishing Co, New York NY, 1990

4. Garrison, Peter. "Aftermath." *Flying* Oct. 1986: 22-24.

5. Hall, J. K., and M. Pachter, "Formation Maneuvers in Three Dimensions", Proceedings of the 2000 AIAA Guidance, Navigation, and Control Conference, Denver CO, August 9-11, 2000, AIAA paper no. 00-37128

6. *Lateral vs. Directional Control Authority.* Airline Pilots Association. 31 Jan. 2001 < http://safety.alpa.org/submissions/lateral.htm>

7. Maybeck, Peter S. Stochastic Models, Estimation, and Control, Vol 3, Academic Press, Inc., New York NY, 1982

8. Ogata, Katsihiko, Modern Control Engineering, Prentice-Hall, Inc, Upper Saddle River NJ, 1997.

9. Pachter, M., J. J. D'Azzo, M. Veth, "Proportional and Integral Control of Nonlinear Systems," International Journal of Control, Vol 64, No 4, 1996, pp 679-692.

10. van Dolderen, D.J. *The History of the RNLAF.* 31 Jan. 2001 <http://web.inter.nl.net/hcc/D.vanDolderen/wo2.htm>.

VITA

Lieutenant Nicolas J. Schindeler graduated from King City High School in King City, California . After attending community college, he entered the undergraduate program at the California State University in Chico, California, where he graduated with a Bachelor of Science degree in electrical / electronic engineering in May 1992. He held jobs in accounting, restaurant management, and forestry, and attended graduate courses at the University of Nevada, Reno. Eventually, he joined the US Air Force, attended Officer Training School, and was commissioned in April, 1997.

His first assignment was to Tyndall AFB as an Advanced Missile Analyst, planning, supporting, analyzing, and reporting live-five AIM-120 AMRAAM tests for the 83rd FWS. In August 1999, he entered the Graduate School of Engineering and Management, Air Force Institute of Technology. Upon graduation, he will be assigned to AFRL at Wright-Patterson AFB.

REPORT DOCUMENTATION PAGE

Form Approved
OMB No. 0704-0188

1. REPORT DATE *(DD-MM-YYYY)*	2. REPORT TYPE	3. DATES COVERED *(From – To)*
20-03-2001	Master's Thesis	Aug 1999 – Mar 2001

4. TITLE AND SUBTITLE

PHUGOID DAMPING CONTROL

5a. CONTRACT NUMBER

5b. GRANT NUMBER

5c. PROGRAM ELEMENT NUMBER

6. AUTHOR(S)

Schindeler, Nicolas J., 1Lt, USAF

5d. PROJECT NUMBER

5e. TASK NUMBER

5f. WORK UNIT NUMBER

7. PERFORMING ORGANIZATION NAMES(S) AND ADDRESS(S)

Air Force Institute of Technology
Graduate School of Engineering and Management (AFIT/EN)
2950 P Street, Bldg 640
Wright-Patterson AFB OH 45433-7542

8. PERFORMING ORGANIZATION REPORT NUMBER

AFIT/GE/ENG/01M-19

9. SPONSORING/MONITORING AGENCY NAME(S) AND ADDRESS(ES)

AFRL/VACA
Attn: Capt James K. Hall
2210 8th Street Bldg 146 Rm 305
Wright-Patterson AFB, OH 45433 DSN 785-8275

10. SPONSOR/MONITOR'S ACRONYM(S)

AFRL/VACA

11. SPONSOR/MONITOR'S REPORT NUMBER(S)

N/A

12. DISTRIBUTION/AVAILABILITY STATEMENT

APPROVED FOR PUBLIC RELEASE, DISTRIBUTION UNLIMITED.

13. SUPPLEMENTARY NOTES

14. ABSTRACT

A novel phugoid damping control design methodology is developed, based on the use of wind axes and a point-mass aircraft model. The state variables are air speed, flight path angle, and heading angle, the control variables are thrust setting, angle of attack, bank angle, and sideslip angle, and the command signals are airspeed, flight path angle, and heading angle or heading rate. All the variables and parameters are nondimensionalized. A multivariable set point controller is developed which consists of: (i) a trim calculation-based nonlinear feed-forward control computer; thus, given a commanded new trim state (air speed, flight path angle, and yaw rate), the required trim thrust setting and trim angle of attack, bank angle, and sideslip angle inputs are determined, and, (ii) a small signal linear feedback regulator; the equations of motion linearized about the trim condition of wings level, and constant altitude flight, which simplifies the dynamics to allow separation between the lateral and longitudinal control channels, are used, and a small-signal linear multivariable regulator is designed. The linear compensator also entails integral action. Thus, the controller consists of a strongly nonlinear feed-forward module and a linear small signal compensator. The novel proposed multivariable nonlinear set point controller encompasses full three-axes autopilot functions. Moreover, this controller is used as a tracking controller, a.k.a. a "phugoid damping" controller, provided that the bandwidth of the command signal is substantially less than the bandwidth of the closed loop flight control system. The phugoid damping controller's performance is examined in extensive simulations and its wide operational envelope is demonstrated.

15. SUBJECT TERMS

Flight Control Systems, Outer Loop Control, Phugoid Damping Control

16. SECURITY CLASSIFICATION OF:			17. LIMITATION OF ABSTRACT	18. NUMBER OF PAGES	19a. NAME OF RESPONSIBLE PERSON
a. REPORT	b. ABSTRACT	c. THIS PAGE			Pachter, Meir, Dr.
U	U	U	U	132	19b. TELEPHONE NUMBER *(Include area code)* (937) 255-3636 x 4593

Standard Form 298 (Rev. 8-98)